TASHKENT STATE TECHNICAL UNIVERSITY AFTER ISLAM KARIMOV
NEW UZBEKISTAN UNIVERSITY

On the right of the manuscript
UDC: 530.12:531.51

01.03.01 - Astronomy

01.04.02 - Theoretical Physics

RAKHIMOVA GULZODAXON ISROILJON QIZI

THERMODYNAMIC AND ENERGETIC PROCESSES AROUND COMPACT OBJECTS IN MODIFIED THEORIES OF GRAVITY

DISSERTATION OF THE DOCTOR OF PHILOSOPHY (PhD) IN PHYSICS AND MATHEMATICS

Supervisors:

Prof. Abdujabbarov Ahmadjon Adiljanovich

Ahmedov Bahodir Babomurotovich

Tashkent-2025

List of Abbreviations

BH	Black Hole
GR	General Relativity
MG	Modified Gravity
EHT	Event Horizon Telescope
PFDM	Perfect Fluid Dark Matter
EGB	Einstein–Gauss–Bonnet
4D EGB	Four-dimensional Einstein–Gauss–Bonnet gravity
RN	Reissner–Nordström
KN	Kerr–Newman
SV BH	Simpson–Visser Black Hole
BSW effect	Bañados–Silk–West effect
CM energy / E_{CM}	Center-of-Mass Energy
DM	Dark Matter
ADM mass	Arnowitt–Deser–Misner mass
ISCO	Innermost Stable Circular Orbit
MPD	Mathisson–Papapetrou–Dixon equations
SSC	Spin Supplementary Condition
TD	Tulczyjew–Dixon

Contents

INTRODUCTION

Topicality and demand of the theme of the dissertation.

The theme is highly topical due to the growing interest in alternative theories of gravity, which aim to resolve fundamental issues in General Relativity (GR), such as singularities and incompatibility with quantum mechanics. Recent advancements in astrophysical observations, including gravitational wave detections and black hole imaging by the Event Horizon Telescope, have provided unprecedented opportunities to test these theories.

The demand for such research stems from the need to understand the dark components of the universe, dark matter and dark energy, which remain unexplained within standard GR. Modified gravity theories offer potential solutions, making this dissertation relevant to contemporary astrophysics and cosmology. The work investigates key phenomena like particle acceleration and thermodynamic properties, which are crucial for probing the nature of gravity in extreme environments. For instance, the Banados-Silk-West (BSW) mechanism, which suggests black holes can act as particle accelerators, has implications for high-energy astrophysics and cosmic-ray production.

Furthermore, the dissertation's focus on observable signatures, such as photon orbits and ergosphere dynamics, bridges theoretical predictions with real-world observations. This alignment with current observational capabilities ensures the practical applicability of the research. By examining black holes in modified grav-

ity, the work contributes to the broader quest for a unified theory of gravity and quantum mechanics, making it a timely and valuable addition to the field.

Moreover, the dissertation aligns with the strategic scientific priorities in Uzbekistan and the broader international community. This dissertation work corresponds to the tasks of the following state regulatory documents: Decree of the President of the Republic of Uzbekistan No. UP-4947 "On the Strategy of Actions for the Further Development of the Republic of Uzbekistan" dated February 07, 2017, Decree of the President of the Republic of Uzbekistan No. PP-2789 "On Measures for Further Improvement of Academy of Sciences, Organization, Management, and Financing of Research Activities from 18.02.2017.

Relevance of the research to the priority areas of science and technology development of the Republic of Uzbekistan. Dissertation research has been carried out in accordance with the priority areas of science and technology in the Republic of Uzbekistan: II. “Power, energy and resource-saving”.

Degree of study of the problem

The problem of understanding thermodynamic and energetic processes around compact objects in modified theories of gravity has been extensively studied, yet significant gaps remain. Classical works laid the foundation for black hole shadows and geodesic motion (Bardeen, Luminet , Event Horizon Telescope Collaboration, Abdujabbarov, Ahmedov, Bambi), while later studies introduced the concept of black holes as particle accelerators (Banados, Silk, West, Zaslavskii, Wei, Liu, Atamurotov). Modified gravity theories, such as Einstein-Gauss-Bonnet (EGB) and scalar-tensor models, have been explored in contexts like horizon structure, photon spheres, and particle dynamics. However, most existing research focuses on isolated aspects, such as thermodynamics (Bekenstein, Hawking, Glavan, Lin, Ghosh, Ahmedov, Jamil), without integrating these phenomena into a cohesive

framework. Additionally, while the BSW mechanism is well studied in Kerr and Kerr-Newman spacetimes, its implications in modified gravity, particularly with additional fields like dark matter or nonlinear electrodynamics, remain underexplored.

Recent advancements in observational astronomy, such as the imaging of M87* and Sgr A*, have intensified the need for comprehensive models that account for deviations from GR. Studies on rotating black holes in 4D EGB gravity, Simpson-Visser metrics, and perfect fluid dark matter (PFDM) environments have emerged (Simpson, Visser, Kiselev, Abdujabbarov, Atamurotov, Ghosh), yet systematic comparisons with observational data are still limited. Thermodynamic properties, including Hawking radiation and phase transitions, have been analyzed in simplified scenarios, but the effects of thermal fluctuations and higher-order corrections are not fully understood. The dissertation addresses these gaps by unifying particle dynamics and thermodynamics in modified gravity, providing a more holistic understanding of compact objects. By leveraging both analytical and numerical methods, the work aims to bridge theoretical predictions with observable phenomena, contributing to the ongoing refinement of alternative gravity theories.

Connection of the topic of the dissertation with the scientific research of the higher educational/research institutions, where the dissertation was carried out. The dissertation was done in the framework of the scientific projects funded by the Ministry of Innovative Development: F-FA-2021-510 "Investigations of nuclear matter of neutron stars in modified gravity" (2021-2026).

The aim of the research is the comprehensive analysis of astrophysical processes around rotating black holes in modified theories of gravity.

The tasks of the research:

- to analyze the spacetime structure of rotating and charged black holes in modified gravity theories (Einstein-Gauss-Bonnet, Simpson-Visser, and PFDM models), including horizon configurations, extremality conditions, and ergosphere properties, and to determine how these features depend on additional gravitational parameters;
- to derive and investigate the equations of motion for test particles of rotating black holes in modified gravity, using the effective potential approach;
- to study particle acceleration mechanism near black holes in both extremal and non-extremal regimes;
- to examine the innermost stable circular orbits (ISCOs) and effective potentials for test particles in modified gravity backgrounds;
- to derive the thermodynamic quantities of rotating black holes in modified gravity, such as Hawking temperature, entropy, angular velocity, and Gibbs free energy;
- to examine thermodynamic stability and phase behavior, including the effects of thermal fluctuations and higher-order entropy corrections;

The objects of the research are rotating black holes in modified gravity, charged black holes, horizon and ergosphere structures, Observable characteristics such as distortion, particle dynamics and thermodynamic systems.

The subjects of the research are particle acceleration mechanisms, effective potentials and stability, thermodynamic properties, dark matter and quintessence effects.

The methods of the research are methods of computational mathematics, methods of theoretical astrophysics, modern methods of mathematical physics, analytical and numerical methods of calculating differential equations for field and particle motion. The method of metric analysis and analytical calculations has been used for the derivation of black hole solutions in modified gravity and the computation of horizon and ergosphere structures via metric component analysis. Method of numerical simulations and computational modeling has been used to solve nonlinear field equations numerically for charged/dark matter-modified black holes. Stability analysis have been used for evaluating Hawking temperature, entropy, and Gibbs free energy via surface gravity and Euclidean action methods.

The scientific novelty of the research is the follows:

- The first unified study of dynamics of particles and thermodynamics allowed us to combine particle acceleration (BSW effect), and thermodynamic stability in modified gravity (e.g., 4D EGB, Simpson-Visser) within a single framework, revealing interdependencies previously studied only in isolation.
- Obtained derivations of observable signatures (e.g. ISCO shifts) for black holes in PFDM providing testable deviations from General Relativity.
- The theoretical results incorporate thermal fluctuations and higher-order entropy corrections into modified gravity black holes, addressing gaps in understanding quantum/statistical effects on Hawking radiation and phase transitions.

Practical results of the investigation are as follows:

- The results on particle acceleration processes quantify energy limits for near-

horizon particle collisions in modified spacetimes, with implications for high-energy astrophysics (e.g., cosmic rays, AGN jets).

- Analysis of stability criteria for exotic compact objects identify parameter ranges where black holes in modified gravity remain stable, guiding theoretical models and numerical relativity simulations.

- the results provide a direct, quantitative link between the spin of matter in an accretion disk and the fundamental parameters of a black hole, offering a new method to use astrophysical observations to test for the existence of "hairy" black holes beyond the standard model.

Reliability of the research results provided by applying modern proven methods of mathematical physics, computational mathematics, and relativistic astrophysics. The results were obtained strictly within the mathematical apparatus of general relativity and theoretical physics. Modern numerical and analytical methods of calculation are also used, and the results are compared with available observational data and the results of other authors. The structured conclusions of the thesis correspond to the basic rules of astrophysics of compact objects. All derived solutions strictly adhere to the mathematical frameworks of modified gravity theories (e.g., 4D Einstein Gauss-Bonnet gravity, PFDM). Calculations are cross-verified using established methods like Hamilton-Jacobi formalism for geodesics.

The scientific and practical significance of the research results are follows

- The results of the dissertations integrate particle dynamics, and thermodynamics of compact objects in 4D Einstein-Gauss-Bonnet, Simpson-Visser

spacetimes into a single self-consistent formalism, revealing previously unexplored interconnections between these phenomena.

- The results demonstrate that a black hole's hair – the fundamental parameters describing its deviation from general relativity – directly governs the dynamics of spinning particles, providing a new theoretical framework to observationally test and constrain alternative gravity theories.

- The study in the dissertation extends the Banados-Silk-West particle acceleration mechanism to rotating black holes in modified gravity, deriving critical angular momentum conditions and collision energy limits for spacetimes with additional fields (scalar and PFDM).

- The analysis of thermodynamics with higher-order quantum corrections develops a comprehensive thermodynamic description incorporating logarithmic corrections and thermal fluctuations for modified gravity black holes, resolving ambiguities in their stability and phase transition behavior beyond semiclassical approximations.

Application of the research results.

The results of the study of the dynamics of particles around black holes in modified gravity theories have been applied as follows:

the theoretical research results and methods, published in the scientific paper "G. Rakhimova, F. Atamurotov, F. Javed, A. Abdujabbarov, G. Mustafa, Thermodynamical analysis of charged rotating black hole surrounded by perfect fluid dark matter, Nuclear Physics B, V. 996, 116363 (2023), https://doi.org/10.1016/j.nuclphysb.2023.116363" and presented in the Doctorate (PhD) thesis of Ms. Gulzoda Rakhimova have been used in the framework of the programs supported by the Fudan University (Letter from Prof. Cosimo Bambi)

Approbation of the research results

The dissertation results have been discussed in 4 international conferences.

Publication of the research results

On the theme of the dissertation, 13 scientific works were published, including 6 scientific papers in international scientific journals recommended by the Supreme Attestation Comission of the Republic of Uzbekistan for publishing basic scientific results of PhD dissertations.

Volume and structure of the dissertation

The dissertation is presented on 108 pages and consists of an introduction, three chapters, conclusion, and a bibliography.

List of published papers

1. Rakhimova G., Atamurotov F., Javed F., Abdujabbarov A., Mustafa G. Thermodynamical analysis of charged rotating black hole surrounded by perfect fluid dark // Nuclear physics B 2023, Volume 996, article id.116363 (2023) (№1 Web of Science, IF: 2.8).

2. Nosirov A., Atamurotov F., Rakhimova G., Abdujabbarov A., Particle acceleration and thermodynamics of the rotating Simpson–Visser black hole// The European Physical Journal Plus 2023, Volume 138, article number 846, (№1 Web of Science, IF: 2.9)

3. Nosirov A., Atamurotov F., Rakhimova G., Abdujabbarov A., Ghosh S.G Particle acceleration near a rotating charged black hole in 4D Einstein-Gauss-Bonnet gravity // Nuclear Physics Section B, 2024, Volume 1005, article id. 116583 (№1 Web of Science, IF: 2.8)

4. Rakhimova G., Abdulkhamidov F., Atamurotov F., Abdujabbarov A., Mustafa G. Spinning particle motion around charged black hole from T-duality //

Chinese Journal of Physics, 2025, Vol. 94, p.66-78. (№1 Web of Science, IF: 4.6)

5. Rakhimova G., Atamurotov F., Juraeva N., Abdujabbarov A., Mustafa G., Spinning particle motion around charged decoupled hairy black hole // Physics of the Dark Universe, 2025 Volume. 47, article id. 101721 (№1 Web of Science, IF: 6.4)

6. Tayyab Nasser, Allah Ditta, Asifa Ashraf, Kashif Ammar Yasir, S.K.Maurya, Gulzoda Rakhimova, Farruh Atamuratov, Analyzing QPOs and dynamics with trajectories around charged Horndeski black hole // Nuclear Physics B, Volume 1021, December 2025, 117186(№1 Web of Science, IF: 2.8)

7. Uktamov U., Rakhimova G., Shadow of rotating Bardeen black hole with clouds of string // Journal of Fundamental and Applied Research, 2023 Volume 3, article id. 20230001.

8. Rakhimova G., Abduvokhidov A., Khamidov V., Particle dynamics around charged rotating black hole in perfect fluid dark matter // O'zbekiston Milliy Universiteti xabarlari, 2024 [3/1/1], 503-506 betlar.

9. Mannobova S., Rakhimova G., Juraeva N., A generic study of thin-shell via regular charged black hole // O'zbekiston Milliy Universiteti xabarlari, 2025 [3/1/1], 434-436 betlar.

10. Rakhimova G., Ro'zmetov Q., Atamurotov F., Particle acceleration near charged rotating black hole in PFDM// "Globallashuv davrida O'zbekiston Respublikasi harbiy ta'lim muassasalarida tabiiy fanlarni o'qitishning dolzarb muammolari" Respublika ilmiy-amaliy konferensiya materiallari to'plami, 2023 yil 28-aprel.31-32 betlar.

11. Rakhimova G., Ro‘zmetov Q., Abdujabbarov A., Thermodynamics of charged rotating black hole surrounded by perfect fluid dark matter// “Fizika faning rivojida iste’dodli yoshlarning o’rni” Respublika ilmiy-amaliy konferensiya (RIAK-XVI-2023) materiallari to’plami:O’zMU,28-29-aprel,2024-yil.Toshkent.57-60 betlar.

12. Rakhimova G., Abduvokhidov A., Davletova P., Thermodynamics of the rotating Simpson–Visser black hole// “Fizika fanining rivojida iste’dodli yoshlarning o’rni” Respublika ilmiy-amaliy konferensiya (RIAK-XVII-2024) materiallari to’plami: O’zMU,5-6-aprel,2024-yil. Toshkent.113-115 betlar.

13. Rakhimova G., Ibrokhimov T., Khayitboyev F., Atamurotov F., Particle acceleration of the rotating Simpson–Visser black hole // “Oliy harbiy ta’lim muassasalarida tabiiy va texnik fanlarni o‘qitishda zamonaviy yondashuvlar va innovatsiyalar” mavzusida Respublika ilmiy-uslubiy anjuman. Toshkent. 2024-yil 29-mart.109-111-betlar.

Chapter I

Particle acceleration near a rotating charged black hole in 4D Einstein-Gauss-Bonnet gravity

In this chapter we investigate the horizon structure and ergosphere of a charged rotating black hole within 4D Einstein-Gauss-Bonnet gravity, which introduces additional parameters such as the charge (Q) and Gauss-Bonnet parameter (β), besides the mass (M) and rotation parameter (a). Interestingly, for each value of the parameter Q (β), there is a critical GB parameter $\beta = \beta_E$ ($Q = Q_E$) that corresponds to an extremal black hole with degenerate horizons. For $\beta < \beta_E$ ($Q < Q_E$), it describes a non-extremal black hole with two horizons, and for $\beta > \beta_E$ ($Q > Q_E$), no black hole exists. The extremal value β_E (Q_E) is also affected by the GB parameter β and the ergosphere. We also study the collision of two equal-mass particles near the horizon of this black hole and explicitly show the effect of the parameter β (Q). The innermost stable circular orbits (ISCO) and the effective potential, which governs the motion of particles in spacetime, have been analyzed for different parameter values. The centre-of-mass energy ($E_{\rm CM}$) depends on the rotation parameter a and the parameters β and Q. We investi-

gate the $E_{\rm CM}$ of two colliding particles near the horizon for both extremal and non-extremal cases. It is shown that in extremal cases, when one of the colliding particles has a critical angular momentum, the $E_{\rm CM}$ can be arbitrarily high, suggesting that the charged rotating black hole in 4D Einstein-Gauss-Bonnet gravity can function as a particle accelerator. Despite the complexity of the BH solution, an exact expression for the thermodynamic quantities of black holes, such as the mass, Hawking temperature, and entropy, is derived in terms of the horizon radius. These quantities show significant deviations from the Kerr solution because of the influence of the Gauss-Bonnet parameter and electric charge.

1.1 Introduction

In 2009, Banãdos, Silk and West (BSW) [1] showed that a Kerr black hole could function as a particle accelerator. Specifically, when two particles collide near the event horizon of an extremal Kerr black hole, the center-of-mass energy (denoted as E_{CM}) can . It was observed that the E_{CM} increases even further for an extremal black hole when one of the colliding particles possesses a critical angular momentum. The BSW mechanism has not only captured considerable attention but has also served as a foundation for subsequent research papers [1–22]. These papers have extended the BSW mechanism to various spacetimes, providing insights into new physics and its potential applications in astrophysics. For instance, these studies have proven instrumental in comprehending gamma-ray bursts and active galactic nuclei (AGNs) in galaxies. One notable contribution is the work by Jacobson and Sotiriou [2], delving into the practical limitations of the Kerr black hole in its ability to function as a particle accelerator. A crucial observation shows that infinite E_{CM} for colliding particles is only possible under specific conditions. The black hole must be precisely extremal, and the collision

must occur on the black hole's horizon, and infinite E_{CM} requires an infinitely long time. Lake [3] conducted a study on the BSW mechanism near the Cauchy horizon, revealing that the E_{CM} for colliding particles becomes infinite. Moreover, when extending the BSW mechanism to the case of Kerr-Newman black holes, Wei [4] found that an unrestricted E_{CM} necessitates an additional constraint on the spin parameter a. It was further argued that a similar effect could be observed in nonrotating, charged black holes, even in the simplest scenario of radial particle motion within the Reissner-Nordström background. Zaslavskii demonstrated that the BSW mechanism is a universal property of rotating black holes [5,6]. The BSW mechanism has been successfully extended to various rotating and non-rotating black holes, yielding consistent outcomes [7–11, 23–29]. Recently, Zaslavskii [30] investigated the collision of spinning particles within the event horizon of a black hole, which suggests that even in this scenario, the divergence of the E_{CM} can still be observed (see also, [31, 32]). Interestingly, it has been discovered that the 4D Gauss-Bonnet black hole can function as a particle accelerator, yielding E_{CM} of arbitrary magnitude [25]. The Gauss-Bonnet coupling constant β introduces deviations in the results compared to those obtained for the Kerr black hole. The allowed range of angular momentum and critical angular momentum values are contingent upon the specific value of β [33].

We aim to investigate the collision of particles within the event horizon of an extremal rotating black hole in 4D Einstein-Gauss-Bonnet gravity [34]. The aim is to determine whether a divergent E_{CM} can still be observed in this scenario. We aim to explore phenomena similar to the Kerr or Kerr-Newman black hole to identify a critical angular momentum that results in an infinite E_{CM}. The E_{CM} of two colliding particles in the horizon's vicinity has been investigated for both extremal and non-extremal scenarios. Specifically, the study examines the explicit

impact of the Gauss-Bonnet coupling constant (β) and compares them to those for the Kerr/Kerr-Newman black holes. We also discuss the influence of charge and the Gauss-Bonnet coupling parameter β on the fundamental thermodynamic quantities. It is also worth to note that in [35] authors argued that the black hole solution obtained in Ref. [34] is not consistent with the 4D-Gauss-Bonnet field equations due to that the Einstein-Gauss-Bonnet theory in four dimension becomes general relativity. On the other hand black holes (with GB curvature effects) can be considered in the context of Einstein-scalar-Gauss-Bonnet theory (see, e.g. [36, 37]. In this paper we plan to test the black solution in 4D-Einstein-Gauss-Bonnet model using thermodynamic properties and particle dynamics in the background spacetime.

Here we plan to study the particle dynamics, acceleration process, and thermodynamic properties of charged BH in 4D Einstein-Gauss-Bonnet gravity. The chapter is organized as follows: We briefly describe the charged rotating spacetime metric of 4D Einstein-Gauss-Bonnet gravity in Sect. 1.2. The equations of motion of the test particles have been explored in Sect. 1.3. The acceleration of test particles near the horizon of rotating 4D Einstein-Gauss-Bonnet BH with its charge is studied in Sect. 1.4. Finally, we discuss the thermodynamic properties of the rotating charged BH in Sect. 1.5. We conclude our results in Sect. 1.6.

1.2 Rotating charged black hole

Glavan and Lin [38] proposed a novel approach for dynamics of the Gauss-Bonnet (GB) term in gravity theory in 4D spacetime by rescaling the GB coupling parameter as $\beta \to \beta/(D-4)$ and considering the limit $D \to 4$ in the field equations, they showed that the theory exhibits nontrivial contributions from the GB term in 4D. It has been demonstrated that this theory only possesses the de-

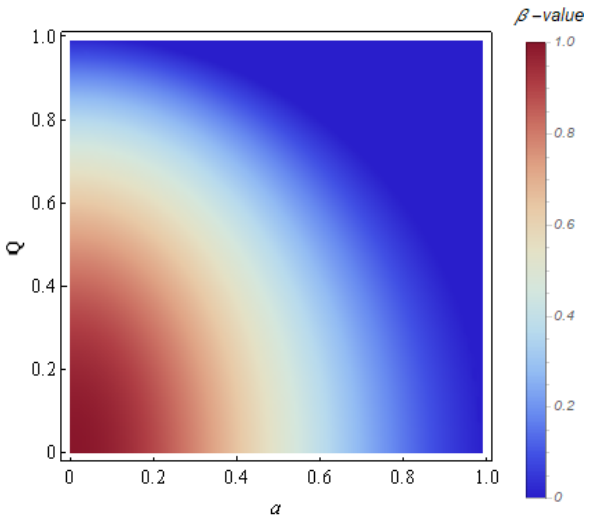

Figure 1.1: Plot showing the correspondence of parameters a, Q and β for extremal BH. For example, when $a = 0.4$ and $Q = 0.4$, it can be seen that the colour of the point whose coordinate is (0.4,0.4) in the plot corresponds to $\beta \approx 0.5$ (precisely $\beta = 0.5236$) in the bar. So, higher values of β for the same a and Q correspond to the non-extremal BH. And smaller values of it for ordinary BH with two horizons.

grees of freedom of a massless graviton, similar to general relativity, thus avoiding ghosts [38]. As a result, the $4D$ Einstein-Gauss-Bonnet (EGB) gravity theory has picked up significant attention and has been extensively investigated including the spherical black holes [39–47]. Kumar and Ghosh [48] derived the rotating EGB black hole metric, using the Newman−Janis algorithm modified by Azreg-Aïnou's non-complexification procedure [49, 50], which has been successfully applied for generating imperfect fluid rotating solutions in the Boyer−Lindquist coordinates from spherically symmetric static solutions obtained by Glavan and Lin [38]. In 4D Einstein-Gauss-Bonnet gravity, the gravitational field of a rotating charged black hole can be described using Boyer-Lindquist coordinates, resulting in the following metric [34, 48]

$$ds^2 = -\frac{\Delta}{\rho^2}(dt - a\sin^2\theta d\phi)^2 + \frac{\rho^2}{\Delta}dr^2 + \rho^2 d\theta^2 + \frac{\sin^2\theta}{\rho^2}\left(adt - (r^2 + a^2)d\phi\right)^2, \quad (1.1)$$

with the metric functions defined as

$$\rho^2 = r^2 + a^2 \cos^2\theta, \tag{1.2}$$

$$\Delta = r^2 + a^2 + \frac{r^4}{2\beta}\left(1 - \sqrt{1 + 4\beta\left(\frac{2M}{r^3} - \frac{Q^2}{r^4}\right)}\right), \tag{1.3}$$

where a, Q and β can be referred to as spin, charge and Gauss-Bonnet (GB) coupling parameters of the BH, respectively. In the original paper, the greek letter α is used instead of β, but we changed it into the Greek letter β not to confuse it with spin parameter a. In addition, this work explored only positive values of the β parameter. If we check the metric to the limiting cases, we will get the Kerr-Newman solution if β approaches zero ($\beta \to 0$). The line element Eq. (1.1) can be written in more convenient form:

$$ds^2 = g_{tt}dt^2 + g_{rr}dr^2 + g_{\theta\theta}d\theta^2 + g_{\phi\phi}d\phi^2 + 2g_{t\phi}dtd\phi, \tag{1.4}$$

where

$$\begin{aligned} g_{tt} =& -\frac{\Delta - a^2\ sin^2\theta}{\rho^2},\ \ g_{rr} = \frac{\rho^2}{\Delta},\ \ g_{\theta\theta} = \rho^2, \\ g_{\phi\phi} =& \frac{\left[\left(r^2 + a^2\right)^2 - \Delta\ a^2\ sin^2\theta\right] sin^2\theta}{\rho^2}, \\ g_{t\phi} =& \frac{a\ sin^2\theta\left[\Delta - \left(r^2 + a^2\right)\right]}{\rho^2}. \end{aligned} \tag{1.5}$$

The metric (1.1), in the limit $\beta,\ Q \to 0$ or large r, goes over to the Kerr black holes [51] and also to the spherically symmetric solution of [38] in the limit $a,\ Q \to 0$. The rotating black hole (1.1), like the Kerr/Kerr-Newman black hole, possesses two linearly independent Killing vectors $\eta^{\mu}_{(t)}$ and $\eta^{\mu}_{(\phi)}$, respectively, related with the isometries along the time translation and rotational invariance, and subsequently for definite-ness, we shall call the rotating black hole (1.1) as rotating black hole in 4D Einstein-Gauss-Bonnet gravity. The charged rotating

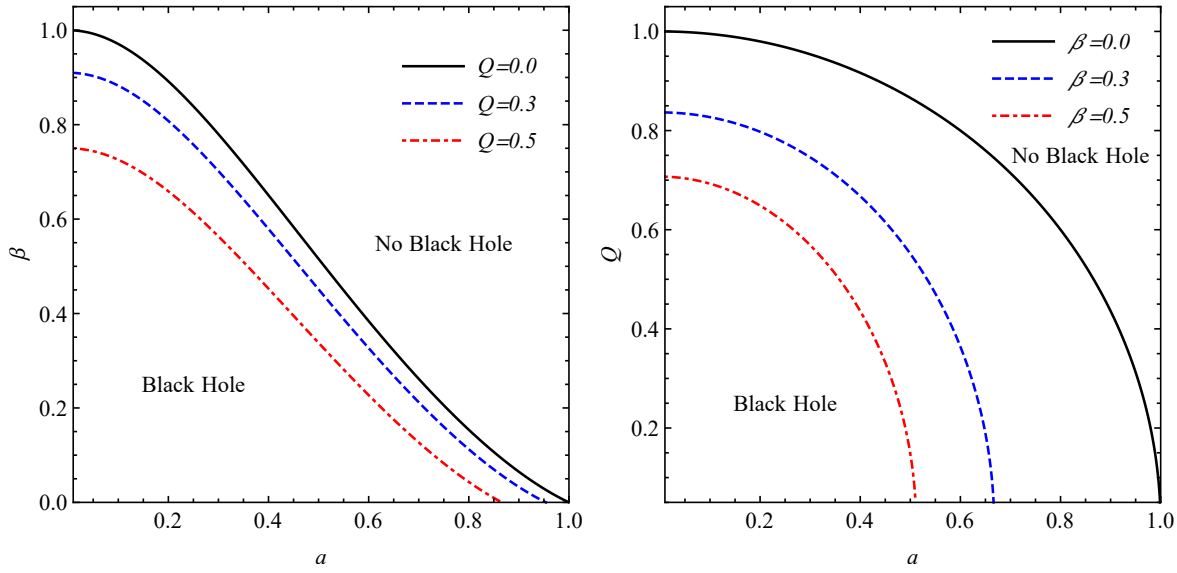

Figure 1.2: Graphs represent black hole and no-black hole regions for different β and Q parameters.

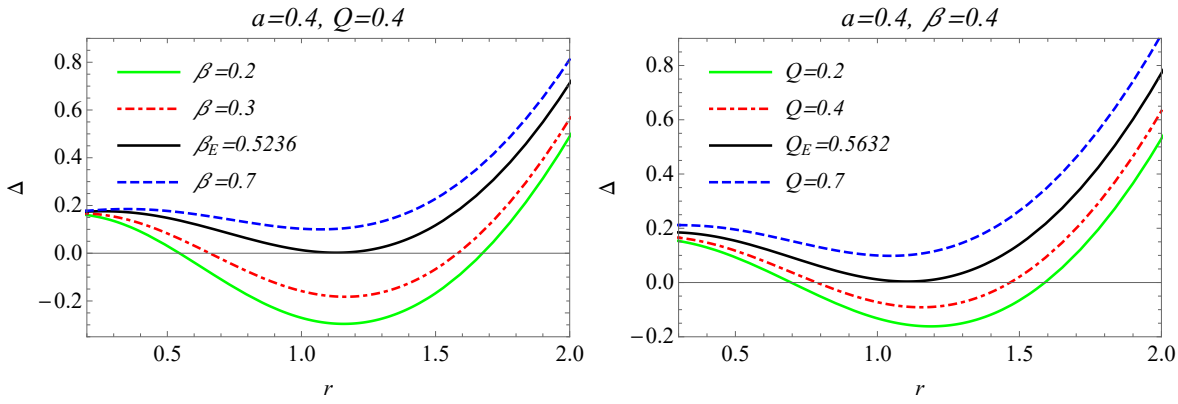

Figure 1.3: Plots show the variation of horizons either change of Q and β parameters.

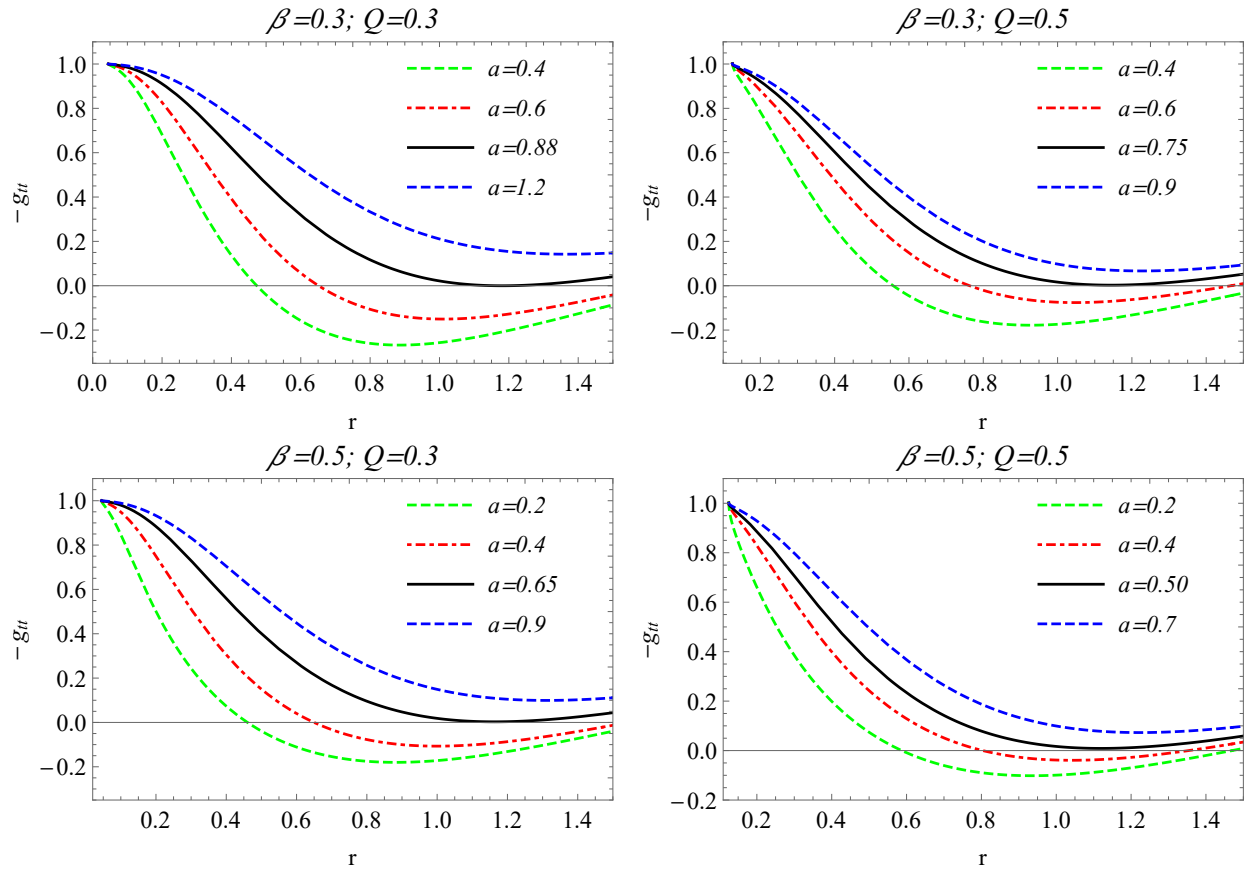

Figure 1.4: Plot showing the variation of infinite redshift surface with different values of the parameters shown in the figure. Here $\theta = \pi/4$ and mass of black hole $M = 1$.

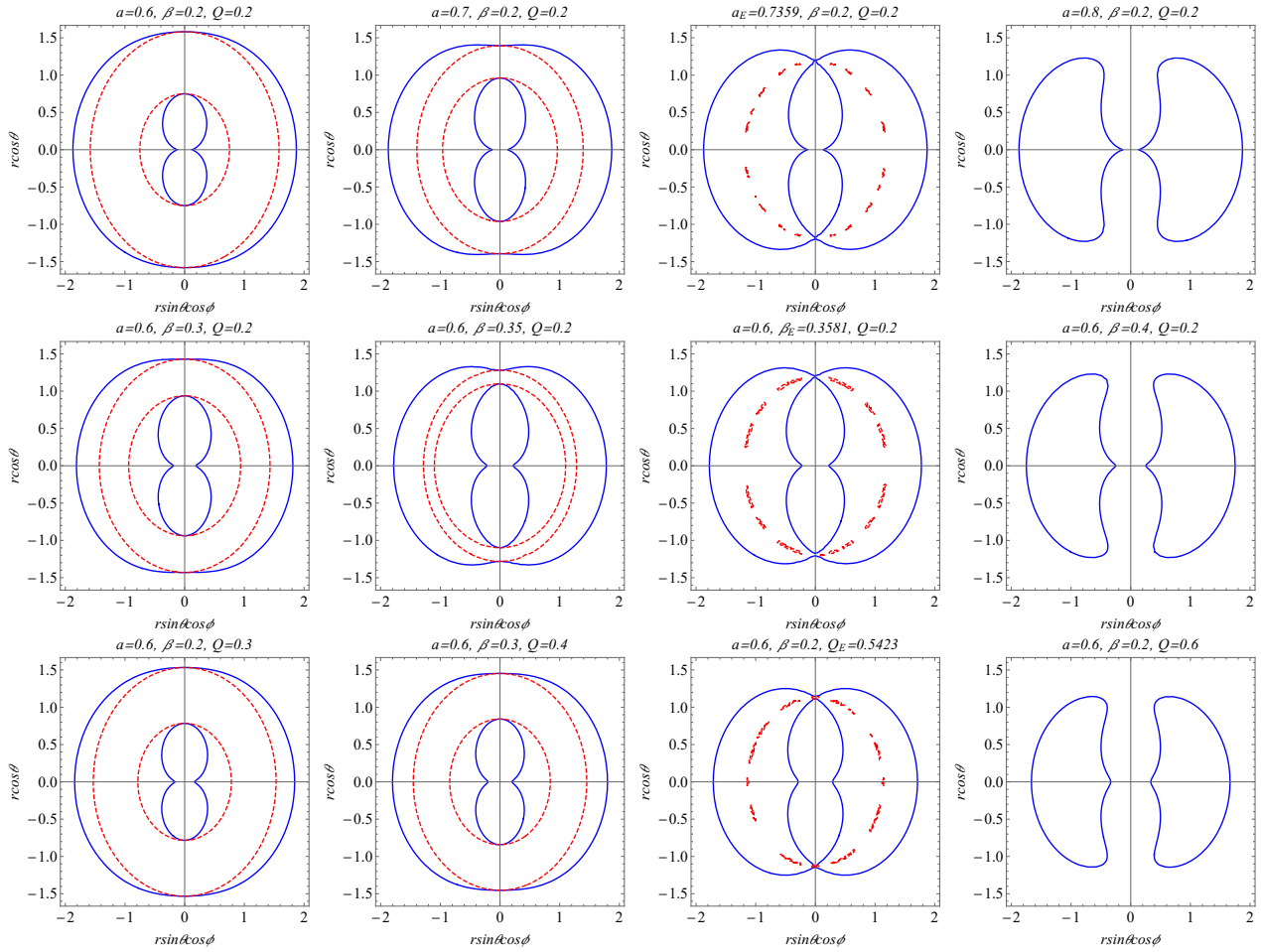

Figure 1.5: Plot showing the variation of the shape of ergosphere for a rotating charged BH in xz-plane for the different values of a, Q and β. The blue and red lines correspond, respectively, to the static limit surfaces and horizons.

Table 1.1: The values of the horizons of a charged rotating BH with the parameter M=1 (δ_e^g= r_H^+ - r_H^-). a_E^*= 0.852804, 0.736012, 0.622437 and 0.501169, which, respectively, corresponds to Q=β=0.1, 0.2, 0.3 and 0.4.

a	$\beta=0.1$ and $Q=0.1$			$\beta=0.2$ and $Q=0.2$			$\beta=0.3$ and $Q=0.3$			$\beta=0.4$ and $Q=0.4$		
	r_H^-	r_H^+	δ_e^g	r_H^-	r_H^+	δ_e^g	r_H^-	r_H^+	δ_e^g	r_H^-	r_H^+	δ_e^g
0.3	0.2975	1.8915	1.5940	0.3928	1.8117	1.4188	0.4931	1.7079	1.2148	0.6224	1.5657	0.9433
0.4	0.3796	1.8487	1.4691	0.4955	1.7608	1.2652	0.6179	1.6429	1.02498	0.7858	1.4672	0.6814
0.5	0.4685	1.7898	1.3212	0.6105	1.6880	1.0775	0.7694	1.5418	0.7723	1.1174	1.1919	0.0745
0.6	0.5697	1.7098	1.1401	0.7502	1.5816	0.8313	1.0085	1.34436	0.3357	-	-	-
a_E^*	1.1488	1.1488	0	1.1820	1.1820	0	1.1805	1.1805	0	1.1549	1.1549	0

BH described by the spacetime metric (1.1) need to be investigated to possess the horizon structure and the ergosphere region, likewise the other rotating BHs. We aim to examine the properties of the above-revealed features depending on the spin parameter a, GB coupling parameter β and charge parameter Q. Fig. 1.1 shows the extremal values of a, β and Q as a density plot. We give a detailed description of this plot in its caption. Also, for a clearer representation of it, Fig. 1.2 shows the variation of β and Q with respect to a for the extremal black hole. The inner region of these plots corresponds to the black hole region, and similarly, the outer region to the no black hole region. With the effect of parameters on the horizons, it is clear from Fig. 1.3 that for the smaller values of GB coupling parameter, there are two horizons, namely Cauchy and event horizons. With the increase of this parameter, they come closer to each other, i.e., the former increases and the latter decreases. Eventually, for the specific beta values (β_E) these two horizons coincide, and BH becomes extremal. There is nothing but naked singularity for $\beta > \beta_E$. The same analysis applies to BH's charge parameter (Q). Table 2.1 gives a numerical representation of the above-given analysis for both extremal and non-extremal cases. It is also convenient to emphasize here that in order to find the radii of horizons by fixing all parameters, we have used the $\Delta = 0$ equation; also, to find an extremal value of a parameter by fixing others, we've utilized the

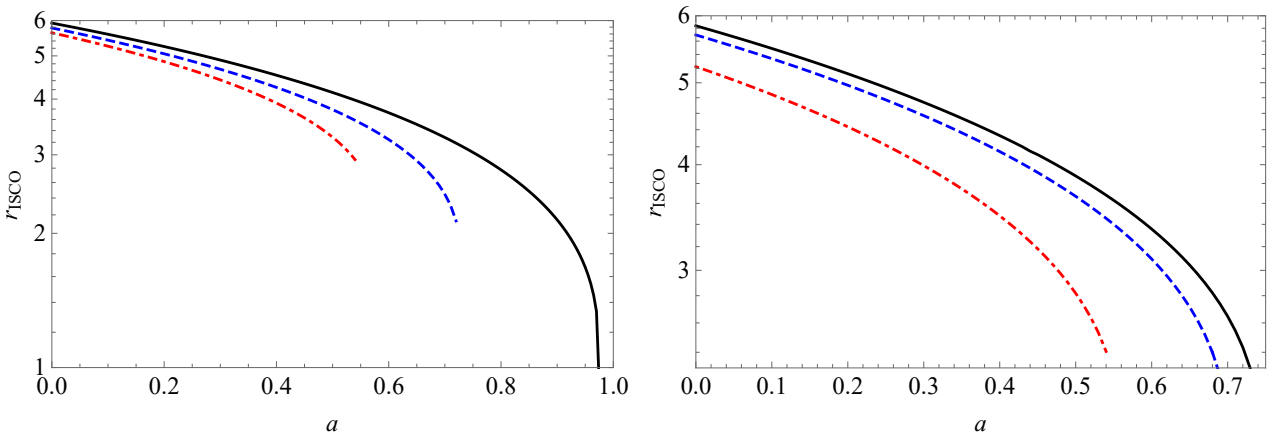

Figure 1.6: The shows the variation of the innermost stable circular orbits with respect to spin parameters for the different values of β and Q. The plot on the left-hand side is for the fixed $Q = 0.2$ and different β, namely $\beta = 0$ (*black*), $\beta = 0.2$ (*blue*) and $\beta = 0.4$ (*red*). Similarly, the figure on the right-hand side is for the fixed $\beta = 0.2$ and different Q, i.e. $Q = 0$ (*black*), $Q = 0.3$ (*blue*) and $Q = 0.6$ (*red*).

following equations:

$$\Delta = 0 \quad \text{and} \quad \frac{d\Delta}{dr} = 0. \tag{1.6}$$

Besides, this BH has two static limit surfaces r^{-}_{sls} and r^{+}_{sls}, which are the positive real roots of equation $g_{tt} = 0$. In Fig. 1.4, we show solutions of this equation with different combinations of the parameters of a, β and Q for $\theta = \pi/4$ only. Plots for other values of θ are like the $\theta = \pi/4$ case. Observing the outer event horizon and the stationary limit surface of this BH, it is verified that the stationary limit surface always lies outside of the event horizon for all values of β and Q. The region between the outer horizon and the static limit surface is called the *ergosphere* region, and its boundary r^{+}_{sls} is called the *quantum ergosphere*. Its shape is that of an oblate spheroid bulging at the equator and flattened at the poles of the rotating BH. In Fig. 1.5, we have studied how the parameters a, β and Q affect the shape of the ergosphere. The first, second and third rows reveal the effect of the increase of a, β and Q parameters, respectively, for the horizons

and static limit surfaces. It can be seen from these plots that an increase of all parameters thickens the ergosphere, and if the parameters are greater than its extremal values, there is no black hole.

1.3 Equations of motion and effective potential in an equatorial plane

Here we consider the motion of a time-like particle with a rest mass m_0 in the equatorial plane $\theta = \pi/2$ where the polar velocity $\dot{\theta}$ becomes zero. The metric and generalized momenta of the particle in the spacetime of a rotating charged BH is expressed in the form

$$P_t = g_{tt}\dot{t} + g_{t\phi}\dot{\phi}, \tag{1.7}$$

$$P_\phi = g_{\phi\phi}\dot{\phi} + g_{t\phi}\dot{t}, \tag{1.8}$$

where P_t and P_ϕ are the constants of motion, corresponding to the particle's energy E and the angular momentum L, respectively. For simplicity, we set the rest-mass of the particle $m = 1$. The overdot denotes differentiation with respect to the proper time. We calculated the equations of motion of a massive particle from Eqs. (1.7)-(1.8) along with the normalization condition $u_\mu u^\mu = -1$, given as below:

$$u_t = \frac{1}{r^2}\left[\frac{(a^2+r^2)}{\Delta}T + a\Big(L - aE\Big)\right], \tag{1.9}$$

$$u_\phi = \frac{1}{r^2}\left[\frac{a}{\Delta}T + \Big(L - aE\Big)\right], \tag{1.10}$$

$$u_r = \pm\frac{\sqrt{T^2 - \Delta\big(r^2 + (L-aE)^2\big)}}{r^2}. \tag{1.11}$$

where $T = E(a^2 + r^2) - aL$ and $+$ and $-$ signs in Eq. (1.11) refer to the outgoing and incoming geodesics, respectively. To evaluate the motion of particles, we have to understand the properties this black hole and its effective potential. An effective potential for a test particle which is at rest at infinity for charged rotating BHs can be calculated with the following formulae:

$$V_{\text{eff}} = -\frac{1}{2g_{rr}}\left(\frac{E^2 g_{\phi\phi} + 2ELg_{t\phi} + L^2 g_{tt}}{g_{t\phi}^2 - g_{tt}g_{\phi\phi}}\right). \tag{1.12}$$

from Eq. (1.12), one can get an explicit form of effective potential easily.

$$V_{\text{eff}} = -\frac{\big(aL - (a^2 + r^2)E\big)^2 - \Delta\big(r^2 + (L - aE)^2\big)}{2r^4}. \tag{1.13}$$

The solution to the simultaneous equations $1)\dot{r} = 0; 2)\partial_r V_{\text{eff}} = 0; 3)\partial_r^2 V_{\text{eff}} = 0$ defines the innermost stable circular orbit r_{ISCO} of the particle. It isn't easy to find an analytic solution for r_{ISCO} here, but in Fig. 1.6, we calculated the r_{ISCO} numerically for the different values of β and Q. Furthermore, it is evident from these figures that an increase in any parameter leads to a decrease in the radius of the innermost stable circular orbit, assuming the other parameters remain constant.

1.4 Particle acceleration

Recently, BSW [1] analyzed the possibility that a Kerr black hole can act as a particle accelerator by studying the collision of two particles near the event horizon of the Kerr black hole. They found that the E_{CM} of the colliding particles in the equatorial plane can be arbitrarily high in the limiting case of an extremal black hole. Thus, the extremal Kerr black hole can be a particle accelerator at the Planck energy scale. In this section, we aim to study the properties of

E_{CM} as r approaches the event horizon r_H of the charged rotating black holes in 4D Einstein-Gauss-Bonnet gravity described by the spacetime metric (1.1). We carefully examine the E_{CM} resulting from a collision between two particles near the BH horizon, considering both extremal and non-extremal BH scenarios.

Our focus lies in a specific scenario where two particles initially in a non-relativistic state are at infinity. These particles gradually fall freely towards the compact object and eventually experience a high-magnitude collision near the horizon. It is important to note that we make a distinct choice for the collision point because of the phenomenon known as infinite blue shift. In this phenomenon, particles approaching from infinity show an infinitely amplified energy at the horizon. As a result, this scenario presents the potential for generating an arbitrarily large amount of energy.

1.4.1 Limiting and critical angular momenta of test particles

The magnitude of the particle's momentum is significant for analyzing its geodesics in curved spacetime.The motion of a test particle in a stationary and axisymmetric black hole spacetime can be described in terms of an effective radial potential $V_{\text{eff}}(r)$. So, physically admissible motion requires: $V_{\text{eff}}(r) \geq 0$.

The limiting values of the angular momentum define the range of angular momenta for which a particle released from infinity can reach the black hole horizon without encountering a turning point. These values are determined by the existence of unstable circular orbits, which act as separatrices between plunging and non-plunging trajectories.

The limiting angular momenta L_{min} and L_{max}, which is depicted in table

1.2 and 1.3, are obtained by imposing the circular-orbit conditions:

$$V_{\text{eff}}(r) = 0 \text{ and } \frac{dV_{\text{eff}}(r)}{dr} = 0. \tag{1.14}$$

Solutions of these equations correspond to unstable circular motion. The associated angular momenta define the boundaries of the allowed interval: $L_{min} < L < L_{max}$.

For angular momenta outside this interval, the effective potential develops a turning point outside the horizon, preventing the particle from reaching the black hole. Therefore, the limiting angular momenta represent a global kinematical condition ensuring horizon accessibility.

The critical angular momentum is defined by the behavior of the particle motion in the immediate vicinity of the event horizon. It is obtained from the condition that the radial velocity vanishes exactly at the horizon, $V_{\text{eff}}(r_h) = 0$. Thus, using Eq. (1.11), one may determine the critical value of the angular momentum. This means that when $r \to r_H^E$ we can get:

$$L_c = \frac{(a^2 + (r_H^E)^2)E}{a}. \tag{1.15}$$

This fine-tuned trajectory plays a central role in the Banãdos–Silk–West (BSW) mechanism, as it leads to an unbounded center-of-mass energy in particle collisions occurring arbitrarily close to the horizon.

Although both the limiting and critical angular momenta are obtained from conditions involving $V_{\text{eff}}(r) = 0$, they have fundamentally different physical meanings. The limiting angular momenta are determined by circular-orbit conditions at radii outside the horizon and impose a global constraint on particle motion from infinity. In contrast, the critical angular momentum is determined by a local horizon condition and does not by itself guarantee that the particle can reach the horizon.

For the BSW effect to be physically realizable, the critical angular momentum must lie within the allowed range: $L \in [L_{min}, L_{max}]$. If L_{cr} exceeds the maximum allowed angular momentum, a particle with $L = L_{cr}$ encounters a turning point outside the horizon and cannot reach it, despite satisfying the horizon condition. In such cases, the formal divergence of the center-of-mass energy is kinematically forbidden.

Near horizon collision

Now we analyse the ultrahigh-energy produced by a two-particle collision near the horizon of charged rotating black holes in 4D Einstein-Gauss-Bonnet gravity. We consider particles with the same mass $m_1 = m_2 = m_0$ and different four-velocities u_1 and u_2. The CM energy E_{CM} of collision between two particles at the radial coordinate r is given by the following expression [1, 26]:

$$E_{CM} = m_0\sqrt{2}\sqrt{1 - g_{\mu\nu}\mathrm{u}_1{}^{\mu}\mathrm{u}_2{}^{\nu}}. \tag{1.16}$$

By substituting Eqs. (1.9)-(1.11) into the Eq. (1.16) we can easily obtain:

$$\frac{E_{CM}^2}{2{m_0}^2} = \frac{-\mathcal{K}}{r^2\Delta}, \tag{1.17}$$

where

$$\begin{aligned}\mathcal{K} = &\left(a^2 - aL_1 + r^2\right)\left(a^2 - aL_2 + r^2\right) + \Delta\left(r^2 - (a - L_1)(a - L_2)\right) \\ &- \sqrt{\left(a^2 - aL_1 + m_0^2 r^2\right)^2 - \Delta\left((a - L_1)^2 + r^2\right)} \\ &\times \sqrt{\left(a^2 - aL_2 + m_0^2 r^2\right)^2 - \Delta\left((a - L_2)^2 + r^2\right)}\end{aligned} \tag{1.18}$$

For easier calculations, let's consider the case of $m_0 = 1$. We assume these particles are initially at rest at infinity and are falling towards black holes with

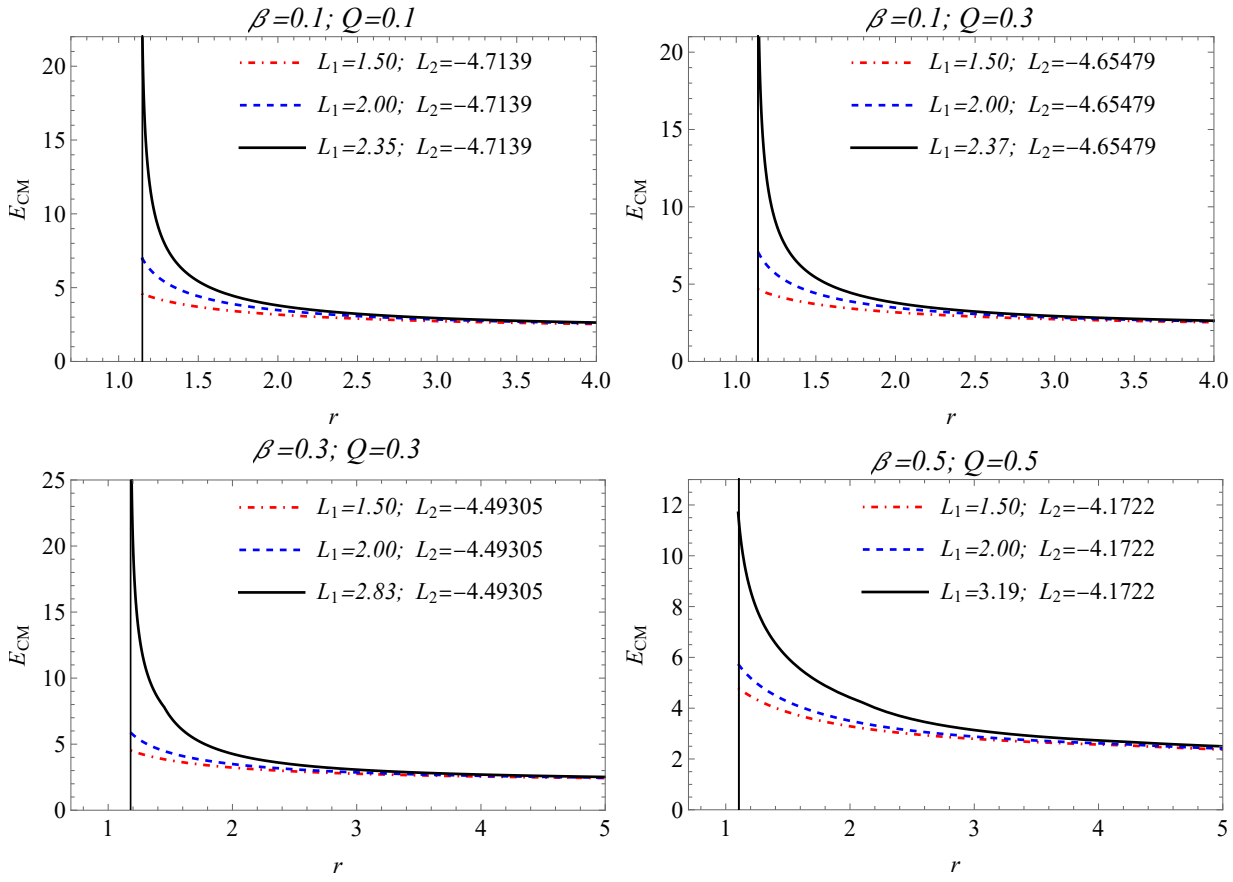

Figure 1.7: The variation of E_{CM} with respect to radial coordinate r for an extremal BH for different values of β and Q. Here $M = 1$.

different angular momenta, L_1 and L_2. We observe that Eq.(1.17) diverges as r approaches r_H^E when we assign numerical values to β, Q, a, and r_H^E. By applying l'Hospital's rule twice, Eq.(1.17) can be expressed in the following form:

$$\begin{aligned}\frac{E_{\rm CM}^2}{2m_0^2}\left(r\to r_H^E\right) &= 7.18-0.07(L_1+L_2)-0.75L_1L_2+\\ &+\frac{L_c-L_1}{L_c-L_2}\left(0.37L_2^2+0.07L_2-0.81\right)+\\ &+\frac{L_c-L_2}{L_c-L_1}\left(0.37L_1^2+0.07L_1-0.81\right),\end{aligned}\tag{1.19}$$

where we choose $\beta = 0.4$, $Q = 0.4$, $a_E = 0.5011694$ and $r_H^E = 1.1549754$. It is easy to see from Eq. (1.19) that if one particle has critical angular momentum,

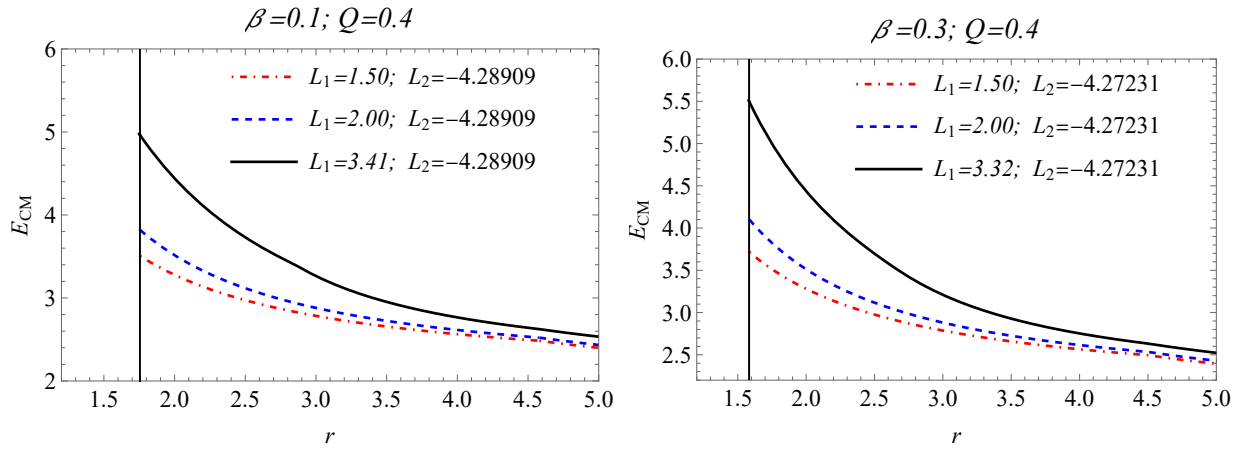

Figure 1.8: Plot showing the behaviour of the $E_{\rm c.m}$ vs. the radial coordinate r for a non-extremal BH. Here $M = 1$.

E_{CM} becomes infinite. The angular momentum's limiting values, along with the BH's corresponding spin, β, Q and radius of the event horizon for the *extremal* case, are presented in Table 1.2. The E_{CM} generated as a result of collision near the horizon of an extremal BH for different values of β and Q is shown in Fig. 1.7. Numerical analyses of E_{CM} show that it is impossible to reach an infinite amount of E_{CM} for all values of β and Q. The reason for this is that the critical angular momentum exceeds the maximum allowed angular momentum determined by unstable circular orbits. Consequently, particles with critical angular momentum encounter a turning point outside the horizon and cannot reach it, suppressing the BSW effect in this spacetime.

Near horizon collision in non-extremal rotating charged BH

We also study the properties of E_{CM} in the limit $r \to r_H^+$ of non-extremal BH. Again after applying l'Hospital's rule twice, the expression of E_{CM} is proportional to

$$\frac{E^2_{\rm CM}}{2m_0^2}\left(r\to r_H^+\right)\sim\frac{(L_1-L_c')}{(L_2-L_c')^3}+\frac{(L_2-L_c')}{(L_1-L_c')^3}++\frac{1}{(L_1-L_c')\,(L_2-L_c')}. \tag{1.20}$$

The Eq. (1.20) tells us that E_{CM} can be infinite if L_1 or L_2 is equal to L_c'. But the critical value of angular momentum is not in the acceptable range in non-extremal BH case. And we do not also notice any peculiar cases like in extremal BH for non-extremal BH. The limiting values of the angular momentum along with the corresponding spin, charge, GB parameter and the horizons for the *non-extremal* are presented in the Table 1.3. From Table 1.3, one can conclude that a particle with critical angular momentum cannot reach the horizon, and this means that E_{CM} is finite for non-extremal BH. If we consider a collision in a non-extremal space-time background, we attain a limited E_{CM} irrespective of the event's location (see Fig. 1.8).

A rotating black hole can act as a natural particle accelerator, using the frame-dragging effect to accelerate particles to high speeds. The total energy of the system, comprising both kinetic and gravitational potential energy, plays a crucial role in understanding the dynamics of particles near rotating black holes. The total energy of a system is the sum of its kinetic energy, potential energy, and any other forms of energy present. Their total energy comprises several components for particles orbiting or falling into a rotating black hole. Firstly, there's the kinetic energy, which is associated with the particle's motion as the particle accelerates due to the gravitational pull and the frame-dragging effect of the black hole, its kinetic energy increases. Secondly, the gravitational potential energy arises from the gravitational attraction between the particle and the black hole. As the particle moves closer to the black hole, its gravitational potential energy decreases, and its kinetic energy typically increases. Understanding the total energy of particles near a rotating black hole is crucial for predicting their behaviour, including whether

Table 1.2: The limiting values of angular momentum for different extremal cases.

β	Q	a_E	r_H^E	L_{min}	L_{max}	L_{cr}
0.1	0.1	0.852804	1.14881	-4.71391	2.35980	2.40035
0.1	0.2	0.838440	1.14423	-4.69208	2.36291	2.40001
0.1	0.3	0.813929	1.13654	-4.65479	2.36996	2.40094
0.3	0.3	0.622437	1.18055	-4.49305	2.83298	2.86155
0.4	0.4	0.501169	1.15498	-4.35397	3.00904	3.16288
0.5	0.5	0.358248	1.10509	-4.17220	3.19564	3.76714

they will escape the black hole's gravitational pull or eventually fall into it.

The energy in the centre-of-mass frame of two colliding particles has contributions from their rest masses, kinetic energies, and potential energies. This center-of-mass energy diverges when a collision occurs at the horizon of an extremal black hole. This infinite energy boost, despite energy conservation, which might seem counter-intutive but has deeper origins.

Firstly, it is consistent with the infinite blue-shift a static observer observes at the black hole horizon. Furthermore, in the frame of a distant observer, the observed collision energy would be highly redshifted and bounded. Secondly, for an extremal black hole, one of the colliding particles' orbits asymptotically approaches the extremal horizon. As a result, its four-velocity becomes nearly tangent to the null direction, leading to an unbounded centre-of-mass energy when colliding with another particle.

$E_{\rm CM}$ is the total energy in the CM frame, it is not a part of the total energy. Hence, other components of the total energy may not be minus infinity.

Table 1.3: The limiting values of angular momentum for different non-extremal cases.

β	Q	a	r_H^+	r_H^-	L_{min}	L_{max}	L_{cr}
0.1	0.3	0.4	1.79992	0.40315	-4.32006	3.45952	8.49932
0.1	0.4	0.4	1.75454	0.42731	-4.28909	3.40803	8.09605
0.2	0.3	0.4	1.72661	0.51472	-4.31206	3.42612	7.85292
0.2	0.4	0.4	1.67569	0.54524	-4.28079	3.37120	7.41985
0.3	0.3	0.4	1.64295	0.61796	-4.30389	3.38812	7.14819
0.3	0.4	0.4	1.58352	0.65778	-4.27231	3.32845	6.66883

1.5 Thermodynamics

The study of black hole thermodynamics unveiled a fundamental relationship between gravitation, thermodynamics, and quantum theory. This insight has been achieved through classical and semiclassical analysis, significantly enhancing our understanding of quantum phenomena in strong gravity [52, 53]. Advancements in quantum field theory on curved surfaces have established a direct link between surface gravity and temperature [54], and between the area of the event horizon and entropy [55].

Next, we explore the thermodynamic properties of charged rotating black holes in 4D Einstein-Gauss-Bonnet gravity. To simplify the calculations, we focus on the equatorial plane. We begin by examining the angular velocity of the event horizon. Specifically, the angular velocity of a test particle at the event horizon, with vanishing angular momentum, can be calculated using the formula $\Omega_H = -g_{t\phi}/g_{\phi\phi}$ for charged rotating black holes in 4D Einstein-Gauss-Bonnet gravity. By substituting the expression from Eq. (1.5), our equation for the angular momentum becomes:

$$\Omega_H = \frac{a\ R^2\left(\sqrt{1-\frac{4\beta(Q^2-2MR)}{R^4}}-1\right)}{2\beta R^2+a^2\left[2\beta+R^2\left(-1+\sqrt{1-\frac{4\beta(Q^2-2MR)}{R^4}}\right)\right]}. \tag{1.21}$$

The radius of the event horizon is labelled with $R = r_H^+$. To find the Hawking temperature of this black hole, we use the well-known formula $T = \frac{\kappa}{2\pi}$, where κ is the surface gravity of rotating BH, and we can calculate it with the following expression [56]

$$\kappa = \frac{1}{2}\partial_r f\left(r\right)|_{r_H^+}, \tag{1.22}$$

where

$$f\left(r\right) = \frac{\Omega_H \Delta}{a}. \tag{1.23}$$

Eq. (1.21), (1.22) and (1.23) give the following expression for Hawking temperature of BH

$$T = \frac{5\beta MR - R^4(X-1) - 2\beta Q^2 - \beta R^2 X}{\pi R\left(-8\beta MR + R^4(X-1) + 4\beta Q^2\right)}, \tag{1.24}$$

where

$$X = \sqrt{1-\frac{4\beta\left(Q^2-2MR\right)}{R^4}} \ \text{ and } \ R = r_H^+\,. \tag{1.25}$$

It can be seen from Eq. (1.24) and (1.25) that if $Q = \beta \to 0$, expression for Hawking temperature takes the following form

$$T = \frac{r_H^+ - M}{4\pi M r_H^+} \ \text{ or } \ \frac{(r_H^+)^2 - a^2}{4\pi r_H^+\left((r_H^+)^2 + a^2\right)}, \tag{1.26}$$

which is the Hawking temperature formula for the Kerr black hole in GR. Now, one can calculate the area and entropy of Ker-like BH using the following general expression [57]

$$A = \int_0^{2\pi} \int_0^{\pi} \sqrt{g_{\theta\theta}\left(r_H^+\right) g_{\phi\phi}\left(r_H^+\right)} d\theta d\phi = 4\pi \left[a^2 + \left(r_H^+\right)^2\right], \tag{1.27}$$

and by using Bekenstein-Hawking formula we obtain [58]

$$S = \frac{A}{4} = \pi \left[a^2 + \left(r_H^+\right)^2\right]. \tag{1.28}$$

From Eq. (1.28), we can conclude that the entropy of a black hole explicitly depends on the radius of the event horizon r_H^+. We have previously observed that r_H^+ decreases as all parameters increase. Perhaps this decrease could cause a decrease in the system's entropy (both the black hole and the particles around it), violating the Second Law of Thermodynamics. However, this is not the case. The GB parameter is merely a constant value, so considering the growth of the β parameter as a violation of this law is illogical. Only the collision of a particle with a specific spin and charge can increase the spin and charge of a black hole, but it also increases its mass. The area of the event horizon (and the entropy) of a black hole increases as the universe's entropy can never decrease.

1.6 Conclusion

We have investigated the particle motion, BSW mechanism and thermodynamic properties of charged rotating black holes in 4D Einstein-Gauss-Bonnet gravity are explored, and we highlight several results obtained.

For the smaller values of parameters, this black hole has two horizons, and with the increase of these parameters, these horizons come closer. Eventually, for the specific values (these are called *extremal values*) of these parameters, horizons

collide, and there will be one horizon and black hole called *extremal black hole*. For the greater values than extremal ones, there is no black hole.

BSW demonstrated that the E_{CM} of two colliding particles can reach arbitrarily high levels in the case of extremal Kerr black holes. By extending the BSW analysis to the charged rotating black hole in 4D Einstein-Gauss-Bonnet gravity, it is impossible to achieve arbitrary high E_{CM} when the collision occurs near the horizon of an extremal charged rotating black holes in 4D Einstein-Gauss-Bonnet gravity due to the exceeding the values of the critical angular momenta than maximum allowed value of angular momentum. Also, it is impossible to achieve infinite amount of E_{CM} in non-extremal BH case.

Hawking temperature of this black hole is derived and limiting cases of it are discussed. Despite the intricacy of the black hole solution, a precise formulation for the thermodynamic properties of black holes, including parameters like mass, Hawking temperature, and entropy, is obtained with the horizon radius. These quantities exhibit notable deviations from the Kerr solution due to the influence of GB parameters and electric charge.

Chapter II

Particle acceleration and thermodynamics of the rotating Simpson–Visser black hole

In this chapter, we have considered a time-like geodesics in the background of rotating Simpson-Visser (SV) black hole (BH) to examine structure of the horizon and ergosphere. The innermost stable circular orbits (ISCO) and the effective potential, which controls the particle's motion in spacetime, have been studied for different values of parameters in SV BH. Centre-of-mass (CM) energy of two colliding particles near the horizon has been investigated for both extremal and non-extremal cases. Furthermore, thermodynamic properties of SV black hole have been also investigated in detail.

2.1 Introduction

The general relativity (GR) is a part of standard model describing the gravitational interaction. GR has been justified via the observation of gravitational lensing of photons near the Sun detected during the solar eclipse in 1919 [59, 60] just after its proposal by Einstein in 1915 [61]. Later GR has been several times well tested in weak (e.g. using solar system tests [62]) and strong field

regimes (e.g. gravitational wave observation [63] and observation of shadow of black holes (BHs) [64, 65]). At the same time GR meets some fundamental problems related to, for example, the existence of the singularity at the origin of vacuum solutions, etc. There is strong belief that these issues may be resolved by introducing the modifications or alternatives to the standard theory of gravity.

Any modifications/alternates to standard theories have to be probed using experimental and observational data. However, the big number of modified and alternative theories of gravity create additional degeneracy problem: the effects due to parameters of different models may mimic each other. In order to resolve one may consider several independent experiments/observations [66, 67] or use the parameterization [68, 69].

Authors of Ref. [70] have proposed very interesting approach to generalize the Kerr BH solution into regular rotating Kerr-like (or rotating SV) one. This new regular Kerr-like solution contains asymptotically Minkowski core. Optical properties of this Kerr-like regular spacetime has been studied in [71]. The non-rotating case of this regular BH solution has been analyzed in [72]. The geodesic properties of spherical-symmetric regular spacetime containing asymptotically Minkowski core have been explored in Ref. [73]. Particularly, gravitational lensing effect in the weak field regime around Schwarzschild-like BH has been studied in Ref. [74] in the presence of plasma. Here we plan to explore the thermodynamics, energetic properties and dynamics of rotating SV BH.

One of the most prominent way to test the metric theory of gravity is exploration of particle dynamics [75–80]. Especially, the dynamics of the charged test particles become very sensitive to external electromagnetic field [81–83]. One may find interesting works where test particles with nonvanishing electric and/or magnetic charges dynamics have been explored in detail [84–98]. Authors of Ref. [75]

have shown that extreme rotating Kerr BH can play a role of accelerator of particles. Particularly, for the fine tuned value of the particle's angular momentum the center of mass energy diverges at the horizon. The effect of other parameters of rotating BH in different gravity models have been discussed in Refs. [99–104]. Magnetic field around no-rotating BH may mimic the effect of rotation and accelerate the charged particles [105–109].

The study of the BH thermodynamics is directly related to the properties of the entropy of the BH. The pioneering works on thermodynamic properties of BH can be found in Refs. [55, 110, 111]. Surely, the simplest BH solution is described by the Schwarzschild spacetime metric and the entropy and related thermodynamic properties of this type of BH have been explored in [52, 54, 112]. Particle spectrum and some thermodynamical properties of Reissner-Nordström BH have been studied in [113]. The thermodynamics of a magnetically charged regular BH obtained using the action of general relativity and nonlinear electromagnetics has been studied in [114]. The effects of quintessence on thermodynamics of BH have been analyzed in [115]. The thermodynamic properties of BH in Hořava-Lifshitz gravity have been explored in Refs. [116, 117]. Thermodynamic properties and Joule-Thomson expansion for conical or BTZ-like BH is investigated in [118].

In this chapter we study the particle dynamics, acceleration process, and thermodynamic properties of rotating SV BH. The current work is organized as follows: We start with a short description of the Kerr-like spacetime metric in Sect. 2.2. The equations of motion of the test particles have been explored in Sect. 2.3. The acceleration of test particles near the rotating SV BH horizon is studied in Sect. 2.4. Finally, we discuss the thermodynamic properties of the rotating SV BH in Sect. 2.5. We conclude our results in Sect. 2.6.

Table 2.1: The values of the horizos of a rotating SV BH with the parameter M=1 (δ_e^g= r_{sls}^+ - r_H^+). a_E^*= 1, 0.7986107603743899, 0.6950554457736542 and 0.5872962339024399, which, respectively, corresponds to l=0, 0.2, 0.3 and 0.4.

a	$l=0$			$l=0.2$			$l=0.3$			$l=0.4$		
	r_H^-	r_H^+	δ_e^g	r_H^-	r_H^+	δ_e^g	r_H^-	r_H^+	δ_e^g	r_H^-	r_H^+	δ_e^g
0.4	0.0834	1.9165	1.8331	0.2481	1.6804	1.4323	0.3334	1.5428	1.2094	0.4385	1.3813	0.9427
0.5	0.1339	1.8669	1.7321	0.3289	1.6114	1.2824	0.4382	1.4558	1.0175	0.5882	1.2548	0.6666
0.6	0.2	1.8	1.6	0.43487	1.5151	1.0801	0.5875	1.3213	0.7337	-	-	-
0.7	0.2858	1.7141	1.4282	0.5863	1.3712	0.7848	-	-	-	-	-	-
a_E^*	1	1	0	0.9818	0.9818	0	0.9602	0.9602	0	0.9302	0.9302	0

2.2 Rotating Simpson-Visser black hole

The gravitational field of a rotating Simpson-Visser compact object in Boyer–Lindqu coordinates can be expressed through the following line element [70, 71]

$$ds^2 = -\frac{\Delta}{\rho^2}(dt - a\sin^2\theta d\phi)^2 + \frac{\rho^2}{\Delta}dr^2 + \rho^2 d\theta^2 + \frac{\sin^2\theta}{\rho^2}\left(adt - (r^2+a^2)d\phi\right)^2, \quad (2.1)$$

with the metric functions defined as

$$\rho^2 = r^2 + a^2\cos^2\theta, \quad (2.2)$$

$$\Delta = r^2 + a^2 - 2Mre^{-l/r}, \quad (2.3)$$

where a and l can be referred as spin and deviation parameters of SV BH, respectively. This metric is derived from regularisation procedure in Kerr metric like did in Schwardchild metric before where $M \to M(r) = Me^{-l/r}$ modification is done. Here, l can be viewed as quantifying the deviation from Kerr. The spacetime around this black hole behaves as one around typical rotating and the limit $l \to 0$ corresponds to Kerr BH. Furthermore, matematically there is still a discontinuity at $r = 0$ and it maintains asymptotically flatness as $r \to +\infty$.

The Kerr-like BH described by the spacetime metric (2.1) need to be investigated to possess the horizon structure and the ergosphere region, likewise the other rotating BHs. We aim to examine the properties of the above indicated

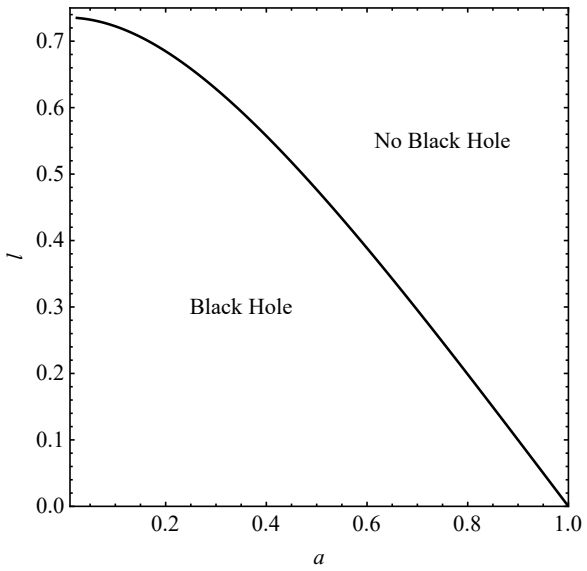

Figure 2.1: Plot showing the behavior of the spin parameter a and a deviation parameter l of Kerr-like BH. The *solid line* is the boundary which separates the BH region from the no BH region. Here $M = 1$.

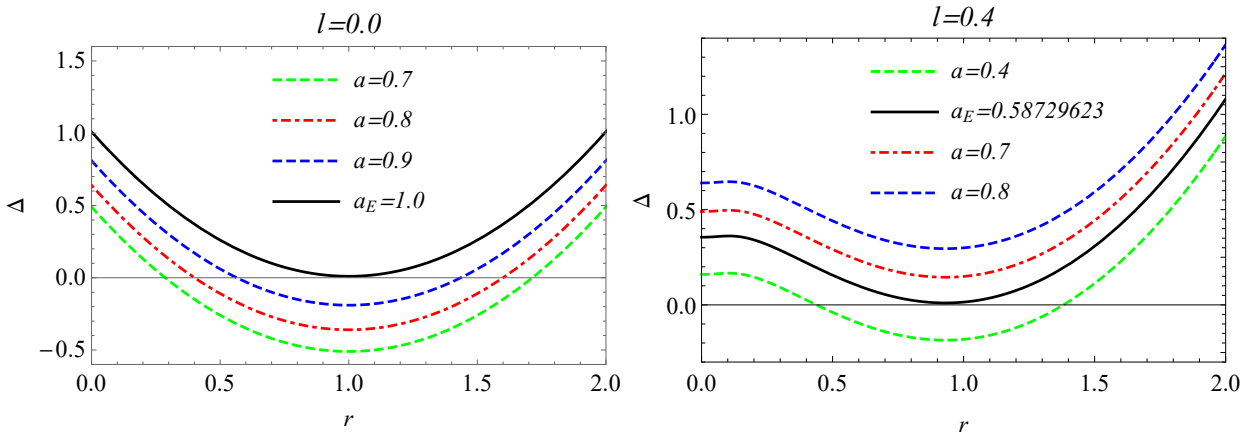

Figure 2.2: Plot showing the behavior of Δ with respect to r for different values of l. The case $a = a_E$ corresponds to an extremal BH. Here $M = 1$.

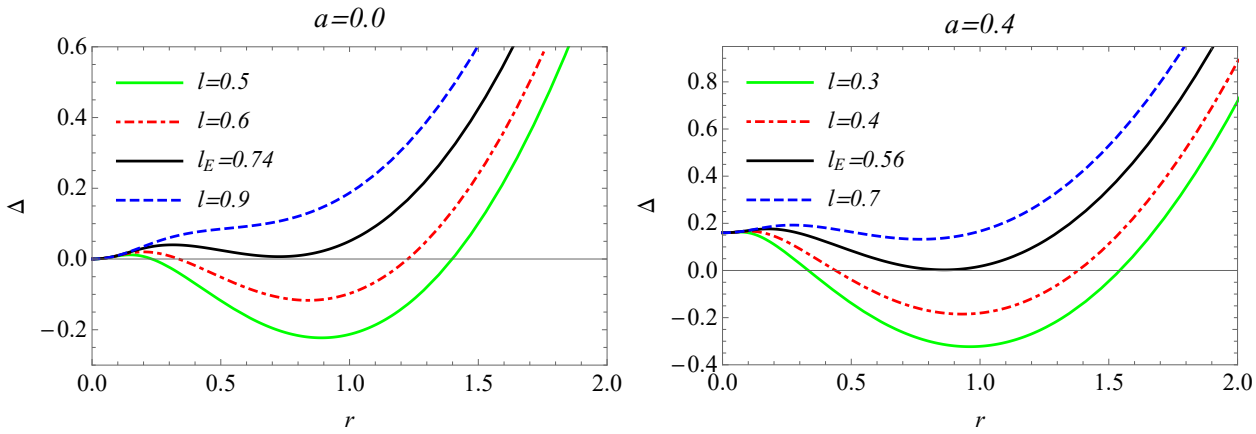

Figure 2.3: Plot showing the behavior of Δ with respect to r for different values of a. Here $M = 1$.

features depending on the spin parameter a and the deviation parameter l. Figure 2.1 clearly shows the regions in $a - l$ plane corresponding to BH and No black hole cases. The radii of the *Cauchy horizon* r_H^- and the *event horizon* r_H^+ are attained by $\Delta = 0$ corresponding to the coordinate singularity. The BH turns out to be an *extremal* BH when the two horizons coincide for a specific critical spin parameter (deviation parameter) $a = a_E$ $(l = l_E)$, whereas $a < a_E$ $(l < l_E)$ refers to a *non-extremal* BH with two distinct horizons. Figures 2.2 and 2.3 show the behaviour of horizons by varying the spin parameters a and l. These figures implies that for $a < a_E$ or $l < l_E$ there exit a set of values of parameters for which one can get two horizons and when $a = a_E$ or $l = l_E$ these horizons collide, i.e. we have an extremal BH with degenerate horizons (cf. Table 2.1). Particularly, in Table 2.1 we have presented the numerical values of the radius of horizons and their difference for different values of l and a. It can be noticed that with the rise of these two parameters, horizons come closer to each other. In the case of $a > a_E$ or $l > l_E$ there is no BH because no horizon appears in that particular case. Moreover, the BH admits two static limit surfaces r_{sls}^- and r_{sls}^+, which are the positive real roots of equation $g_{tt} = 0$. In Fig. 2.4, we depict possible solu-

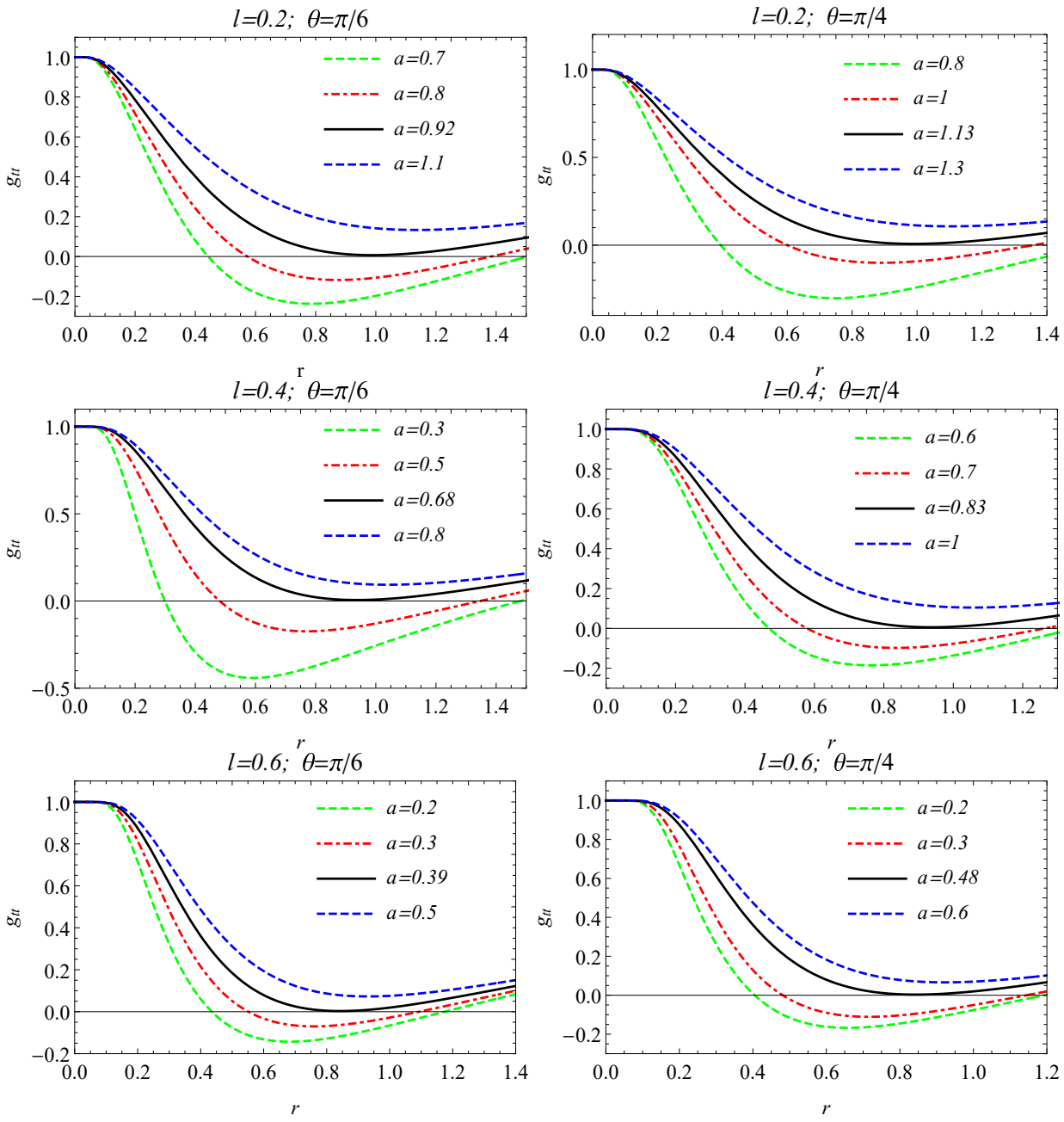

Figure 2.4: Plot showing the variation of infinite redshift surface with different values of l, a and θ. Here $M = 1$.

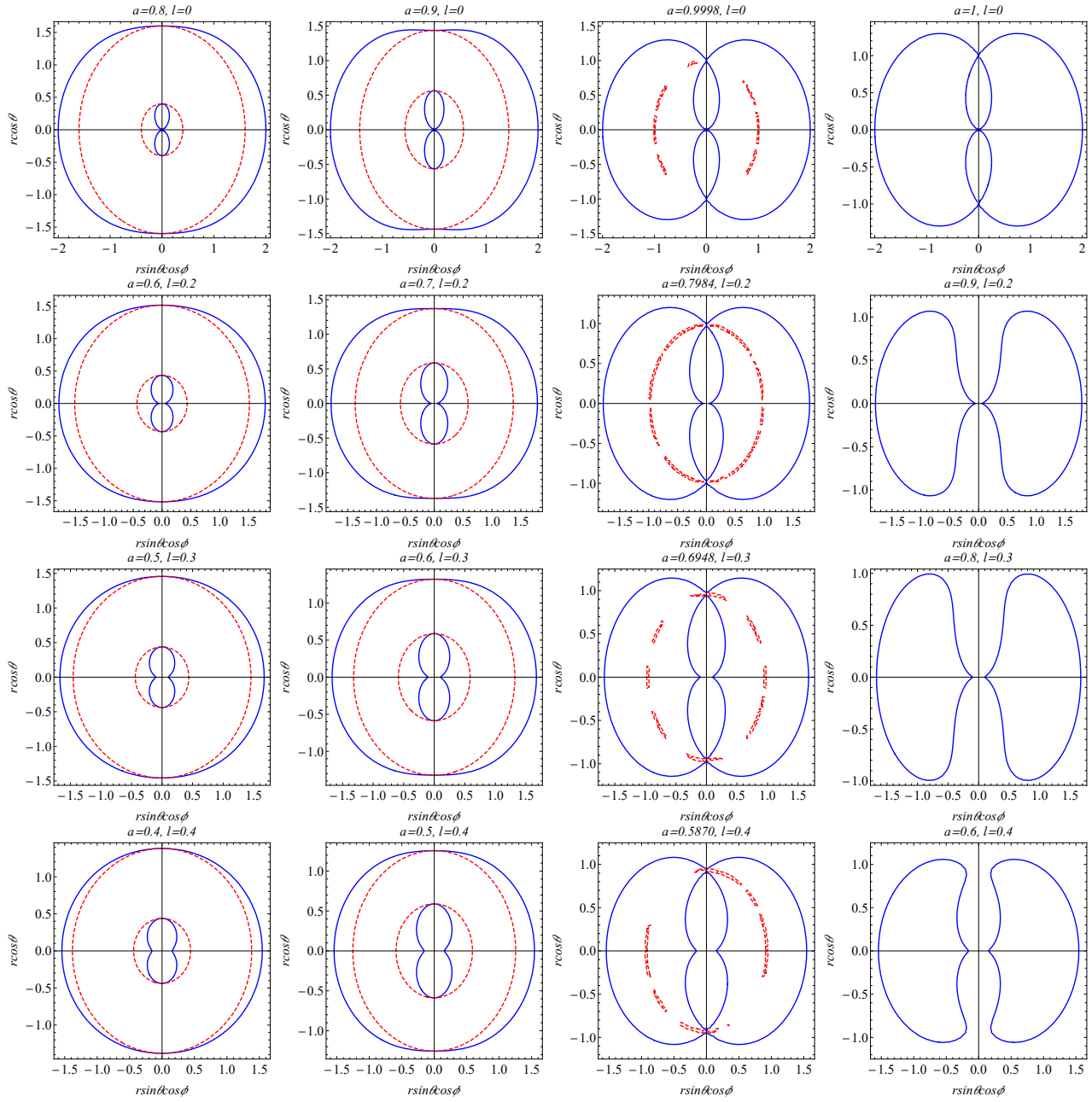

Figure 2.5: Plot showing the variation of the shape of ergosphere for a rotating SV BH in xz-plane for the different values of a and l. The blue and the red lines correspond, respectively, to the static limit surfaces and horizons. The third row illustrates the merging of two event horizons. Here $M = 1$.

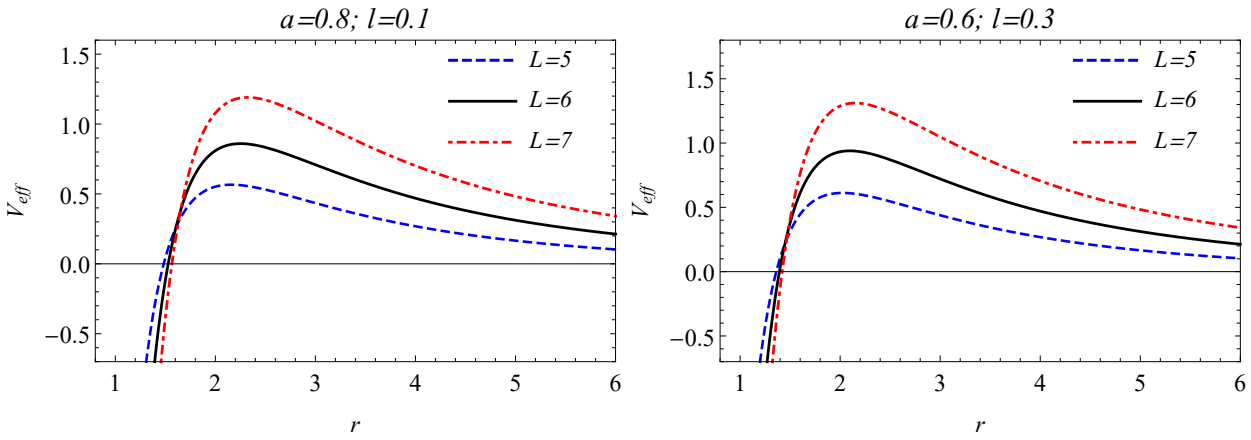

Figure 2.6: Plot shows the behaviour of V_{eff} vs. r for different values of angular momentum, where $M = 1$.

tions of this equation with different combinations of the parameters of a and l and different values of θ . Observing the outer event horizon and the stationary limit surface of this BH, it is verified that the stationary limit surface always lies outside of event horizon for all values of l. The region, i.e, $r_H^+ < r < r_{sls}^+$ connotes the *ergosphere* region and its boundary r_{sls}^+ is called the *static limit surface*. Its shape is that of an oblate spheroid-bulging at the equator, and flattened at the poles of the rotating BH. We have studied how the parameters a and l affect the shape of the ergosphere. The behaviour of ergospheres for $a < a_E$ and $a \approx a_E$ are shown in Fig. 2.5. It can be seen that the ergospere is sensitive to the parameter l, meaning that with the increase of parameter l, the thickness of ergosphere also increases. The same is true for spin parameter a, as well.

2.3 Equations of motion and effective potential in an equatorial plane

Here we consider motion of a time-like particle with a rest mass m_0 in the equatorial plane $\theta = \pi/2$ where the polar velocity $\dot{\theta}$ becomes zero. The metric and

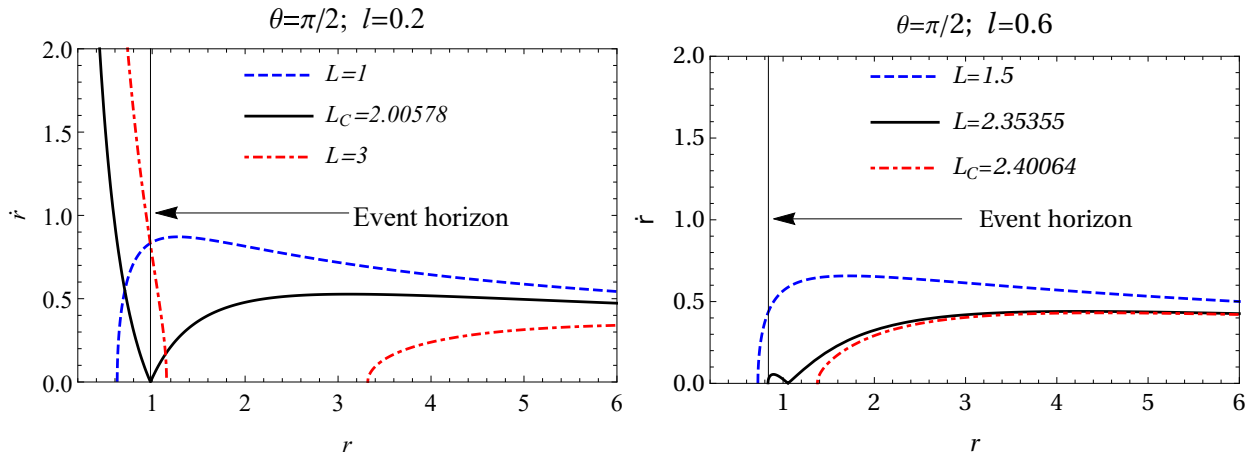

Figure 2.7: The variation of $\dot{r}$ with respect to the radial coordinate for an extremal BH. In the left panel $a_E = 0.7986107603$ and in the right panel $a_E = 0.5872962339$. Here $M = 1$.

generalized momenta of the particle in the spacetime of a rotating BH is expressed in the form,

$$P_t = g_{tt}\dot{t} + g_{t\phi}\dot{\phi}, \tag{2.4}$$

$$P_\phi = g_{\phi\phi}\dot{\phi} + g_{t\phi}\dot{t}, \tag{2.5}$$

where P_t and P_ϕ are the constants of motion. Basically, the two quantities P_t and P_ϕ correspond to the particle's energy $-E$ and the angular momentum L, respectively. The overdot denotes differentiation with respect to the proper time. The equations of motion of a massive particle are calculated from Eqs. (2.4)-(2.5) along with the normalization condition $u_\mu u^\mu = -1$, given as below

$$\dot{t} = \frac{1}{r^2}\left[\frac{(a^2+r^2)}{\Delta}\big(E(a^2+r^2) - aL\big) + a\Big(L - aE\Big)\right], \tag{2.6}$$

$$\dot{\phi} = \frac{1}{r^2}\left[\frac{a}{\Delta}\big(E(a^2+r^2) - aL\big) + \Big(L - aE\Big)\right], \tag{2.7}$$

$$\dot{r} = \pm\frac{\sqrt{\big(aL - (a^2+r^2)E\big)^2 - \Delta\big(m_0^2 r^2 + (L-aE)^2\big)}}{r^2}. \tag{2.8}$$

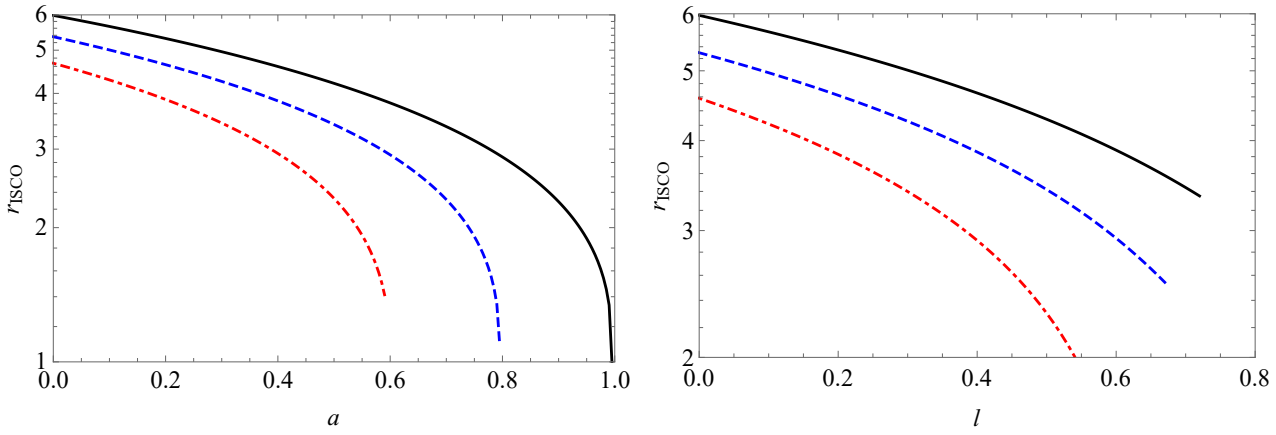

Figure 2.8: The inner most stable circular orbits by varying a and l for various values of l and a. In the left-hand side, for the deviation parameter $l = 0$ (*black*), $l = 0.2$ (*blue*) and $l = 0.4$ (*red*). In the right-hand side, for the spin parameter $a = 0$ (*black*), $a = 0.2$ (*blue*) and $a = 0.4$ (*red*). Here $M = 1$.

The + and − signs in Eq. (2.8) refer to the outgoing and incoming geodesics, respectively. In order to understand the motion of the test particle around SV BH one needs to evaluate the effective potential, which is straightforwardly worked out using Eq. (2.8). We can use the following equation to calculate the effective potential:

$$\frac{1}{2}\dot{r}^2 + V_{\rm eff} = 0, \tag{2.9}$$

$$V_{\rm eff} = -\frac{\big(aL - (a^2 + r^2)E\big)^2 - \Delta\big(m_0^2 r^2 + (L - aE)^2\big)}{2r^4}. \tag{2.10}$$

The range of angular momentum for free falling particle which is depicted in Table 2.2 and 2.3 is calculated by following equations:

$$V_{\rm eff}(r) = 0 \text{ and } \frac{dV_{\rm eff}(r)}{dr} = 0. \tag{2.11}$$

In Fig. 2.6 the effective potential is shown by varying the angular momentum of the incoming test particle for a fixed a and l. It is observed that the potential

barrier rises for greater values of L which means a boosted particle can easily begin circling around the BH.

When observing a particle's geodesics in curved spacetime, the value of the particle's momentum is crucial. Thus one may get the critical value of the angular momentum from Eq. (2.8) by demanding $u_r = 0$ at the horizon. When $r \to r_H^E$, the above condition reduces to

$$E - \Omega_H L \geq 0, \tag{2.12}$$

where $\Omega_H = \frac{a}{r_h^2 + a^2}$ is the angular velocity of the black hole at the horizon and it is derived in Eq. (2.19). The critical angular momentum of the particle is defined by $L_c = E/\Omega_H$.

Fig. 2.7 gives a comprehensible demonstration of the geodesics in this BH. It is numerically calculated that for the values of $l < l_*$ (where $l_* = 0.53948$), the particle with $L < L_c$ is always captured by the BH gravity and falls exactly at the horizon if $L = L_c$, however, when $L > L_c$ the geodesics never fall into the BH. But for the cases of $l > l_*$, the particle which is equipped with L_c can not reach to the horizon. Meaning that turning points of this cases do not corresponds to the event horizon.

The solution to the simultaneous equations $1)\dot{r} = 0; 2)\partial_r V_{\text{eff}} = 0; 3)\partial_r^2 V_{\text{eff}} = 0$ defines the innermost stable circular orbit r_{ISCO} of the particle. It is difficult to find analytical solution of the radius of ISCO, but numerical analysis is given in Fig. 2.8, i.e. it illustrates the variation of r_{ISCO} with respect to a and l for the different cases. Furthermore, it can be easily noticed from these figures that the radius of the innermost stable circular orbit is sensible to the value of l and a. To be more precise, r_{ISCO} shows downward trend for both parameters.

Table 2.2: The limiting values of angular momentum for different extremal cases. Here $l_* = 0.53948$ and $M = 1$.

l	a_E	r_H^E	L_{min}	L_{max}	L_{cr}
0	1.0	1.00000	-4.82843	2.00000	2.00000
0.2	0.79861076037439	0.98186	-4.52868	2.00578	2.00578
0.3	0.69505544577365	0.96026	-4.36208	2.02172	2.02172
0.4	0.58729623390243	0.93023	-4.17874	2.06069	2.06069
l_*	0.47204473678589	0.871887	-3.97046	2.15248	2.15248
0.6	0.34180530576217	0.83888	-3.71893	2.35355	2.40064
0.7	0.16598902588924	0.76850	-3.35378	2.66542	3.72407

Table 2.3: The limiting values of angular momentum for different non-extremal cases. Here $M = 1$.

l	a	r_H^+	r_H^-	L_{min}	L_{max}	L_{cr}
0	0.9	1.43589	0.56411	-4.75680	2.63246	3.19115
0.2	0.6	1.51505	0.43488	-4.36638	2.89374	4.42563
0.3	0.5	1.45583	0.43828	-4.19068	2.89207	4.73888
0.4	0.4	1.38133	0.43857	-3.99933	2.88869	5.17018
0.5	0.3	1.28554	0.44231	-3.78700	2.88276	5.80871
0.6	0.2	1.15506	0.46592	-3.54427	2.87306	6.87081

2.4 Particle acceleration

In this section we do an inclusive analysis to probe the acceleration of particles in the SV BH described by the spacetime metric (2.1). We accurately consider the center of mass (CM) energy produced due to a two-particle collision near the horizon considering an extremal and a non-extremal BHs in the Kerr-like spacetime. We put forth the scenario where two non-relativistic particles initially located at infinity at rest fall freely towards compact object and ultimately encounter a massive collision near the horizon. Here, we do a unique choice for the collision point because particles falling in from infinity appear with an infinite

blue-shift at the horizon and hence are considered to produce an arbitrarily large amount of energy.

2.4.1 Near horizon collision

Now we analyse the ultrahigh energy produced as a result of a two-particle collision near the horizon of SV BH. We consider particles with the same mass m_0 and different four-velocities u_1 and u_2. CM energy E_{CM} of collision between two particles at the radial coordinate r is given by the following expression [75, 102]

$$E_{CM} = m_0\sqrt{2}\sqrt{1 - g_{\mu\nu}\mathrm{u}_1{}^{\mu}\mathrm{u}_2{}^{\nu}}. \tag{2.13}$$

By substituting Eqs. (2.6)-(2.8) into the Eq. (2.13) we can easily obtain

$$\frac{E_{CM}^2}{2{m_0}^2} = \frac{e^{l/r}\mathcal{K}}{r^2\Delta}, \tag{2.14}$$

where $\mathcal{K}$ is defined in the following form

$$\begin{aligned}\mathcal{K} =& 2Mr(a-L_1)(a-L_2) - 2Mr^3 + r^2e^{l/r}\left(2a^2 - L_1L_2 + 2r^2\right) \\ & - e^{l/r}\sqrt{(a^2 - aL_1 + r^2)^2 - \left(a^2 + r\left(r - 2Me^{-\frac{l}{r}}\right)\right)\left((a-L_1)^2 + m_0^2r^2\right)} \\ & \times\sqrt{(a^2 - aL_2 + r^2)^2 - \left(a^2 + r\left(r - 2Me^{-\frac{l}{r}}\right)\right)\left((a-L_2)^2 + m_0^2r^2\right)}.\end{aligned} \tag{2.15}$$

In our discussion, the participating particles have the same intrinsic identities and are mainly distinguished by their angular momenta L_1 and L_2. Here, for the sake of simplicity, we shall take the conserved energies $E_1/m_0{=}E_2/m_0{=}1$. Obviously as $r \to r_H^E$, Eq. (2.14) has indeterminate form when we choose numerical values of M, a, l and r_H^E. After applying l'Hospital's rule twice, it can be seen

that if one of the particles has the critical angular momentum L_c, E_{CM} become infinite as $r \to r_H^E$. The expression of E_{CM} is too lengthy to write it here, but in general it is proportional to

$$\frac{E_{\rm CM}^2}{2m_0^2}\left(r \to r_H^E\right) \sim \frac{1}{\left(L_1 - L_c\right)^{3/2}\left(L_2 - L_c\right)^{3/2}}. \tag{2.16}$$

It is worth to mention that an arbitrarily high amount of energy is obtained when the test particle approaching the black hole has the critical angular momentum L_c. The limiting values of the angular momentum along with the corresponding spin of the BH, deviation parameters l and radius of the event horizon for the *extremal* case are presented, in the Table 2.2. The E_{CM} generated as a result of collision near the horizon of an extremal BH for different values of l is shown in Fig. 2.9. From the Table 2.2 and fig. 2.9, we can conclude that for the smaller values of deviation parameter, the CM energy instantaneously diverges near the horizon whenever the incoming particle is equipped with the critical parameters of the motion. And for the larger values of l ($l > l_*$), particles which has critical angular momentum cannot reach to the horizon and infinite amount of CM energy cannot be produced. Additionally the particles admitting $L < L_c$ contribute only a finite E_{CM} too.

2.4.2 Near horizon collision in non-extremal Simpson-Visser black hole

We also study the properties of E_{CM} in the limit $r \to r_H^+$ of non-extremal BH. Again after applying l'Hospital's rule twice, the expression of E_{CM} is proportional to

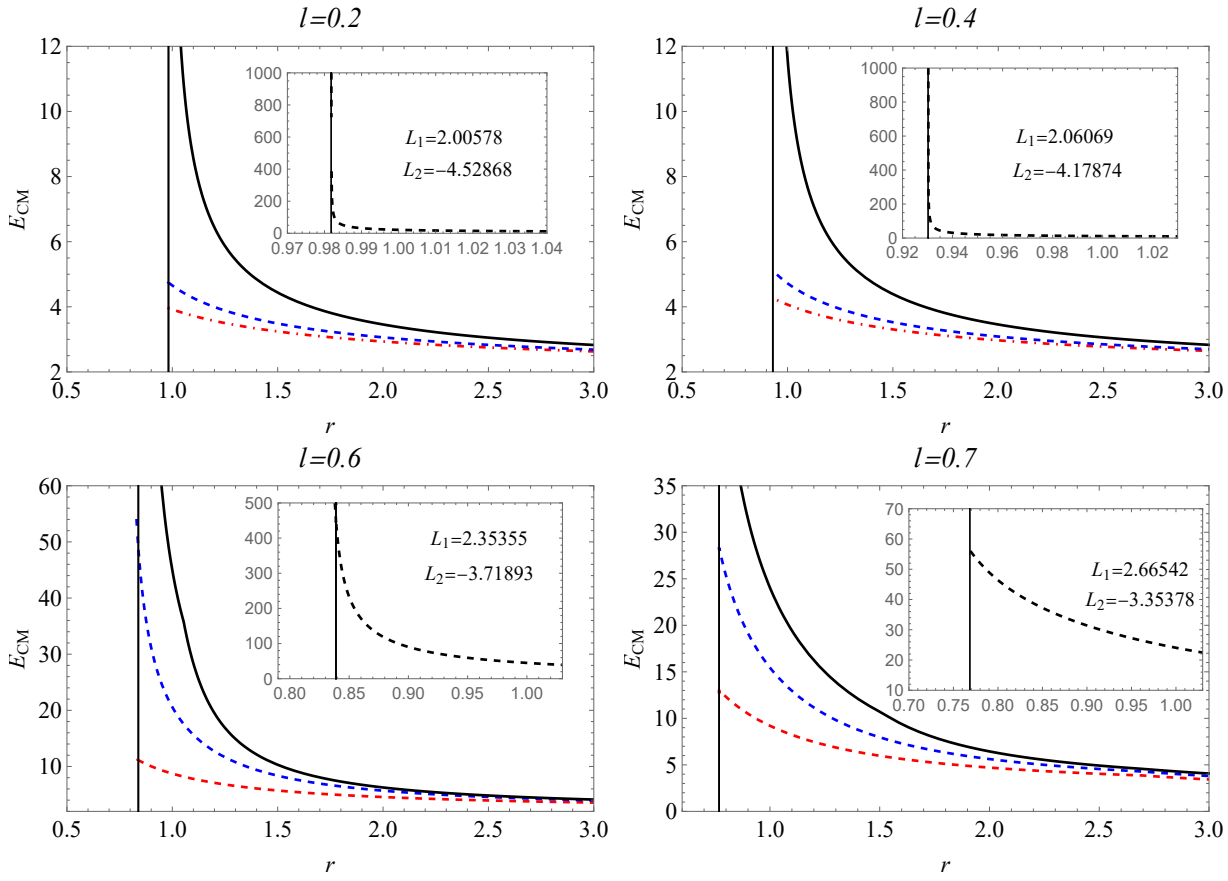

Figure 2.9: Plot shows dependence of the center-of-mass energy $E_{\rm c.m}$ to radial coordinate r for an extremal BH in different values of l. In the top left-hand corner, for the deviation parameter l=0.2, spin $a_{\rm E}$=0.798610, angular momentum L_1=2.00578 (*black*), 1.3 (*blue*), 1 (*red*) and L_2=-4.52868. In the top right-hand corner, for the deviation parameter l=0.4, spin $a_{\rm E}$=0.58729, angular momentum L_1=2.06069 (*black*), 1.3 (*blue*), 1 (*red*) and L_2=-4.17874. In the bottom left-hand corner, for the deviation parameter l=0.6, spin $a_{\rm E}$=0.341805, angular momentum L_1=2.40064 (*black*), 2.35355 (*blue*), 1 (*red*) and L_2=-4.52868. In the bottom right-hand corner, for the deviation parameter l=0.7, spin $a_{\rm E}$=0.165989, angular momentum L_1=3.72407 (*black* which is stopped before 5 radial coordinate), 2.66542 (*blue*), 1 (*red*) and L_2=-4.17874. Here $M = 1$.

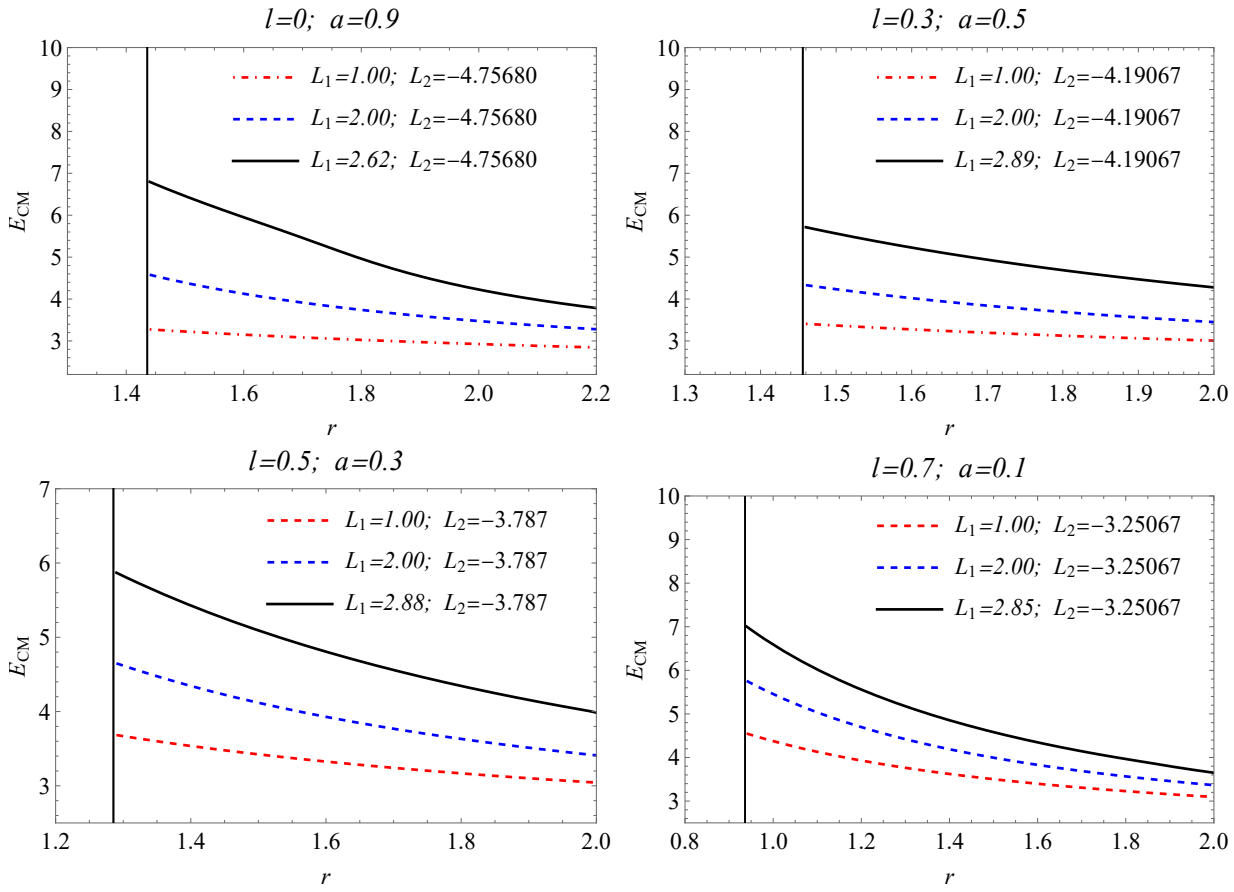

Figure 2.10: Plot showing the behaviour of the center-of-mass energy $E_{\rm c.m}$ vs. the radial coordinate r for a non-extremal BH. Here $M = 1$.

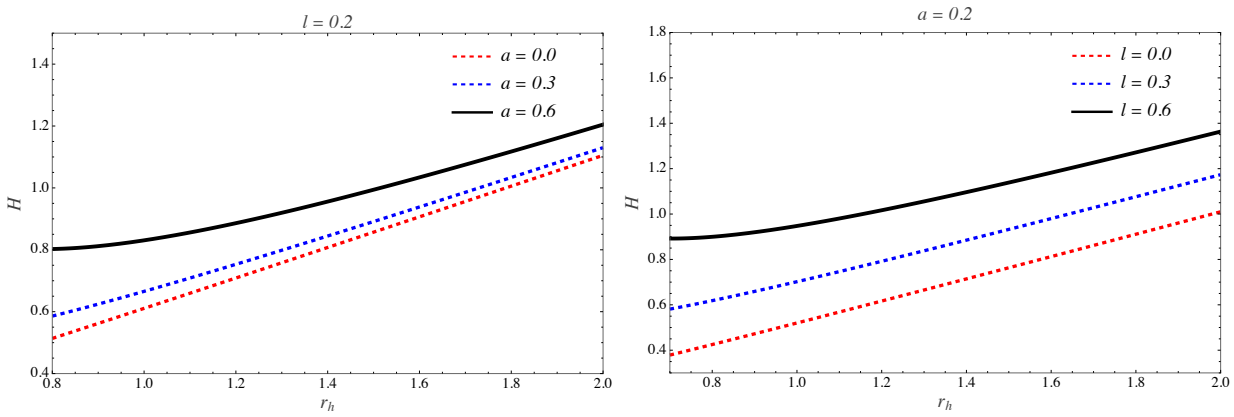

Figure 2.11: Plot shows the variation of enthalpy with respect to horizon radius for different values of$a$ and l.

$$\frac{E^2_{\rm CM}}{2m_0^2}\left(r \to r_H^+\right) \sim \frac{1}{\left(L_1 - L_c'\right)\left(L_2 - L_c'\right)}. \tag{2.17}$$

The Eq. (2.17) tells us that E_{CM} can be infinite if L_1 or L_2 is equal to L_c'. But critical value of angular momentum is not in the acceptable range in non-extremal BH case. For example in the case of $l = 0.2$, $a = 0.6$ and $r_H^+ = 1.51505$, the critical value of angular momentum is calculated as $L_c' = 4.4256$ which is not in the acceptable range. The limiting values of the angular momentum along with the corresponding spin, deviation parameters and the horizons for the *non-extremal* are presented in the Table 2.3. From the Table 2.3 one can conclude that angular momentum of free falling particle can never be equal to the critical value of it for non-extremal BH which means in non-extremal cases the center of mass energy is finite. Fig. 2.10 shows a visualization of this process. In general, if we consider a collision in a non-extremal space-time background, we attain a limited E_{CM} irrespective of the event's location (see Fig. 2.10).

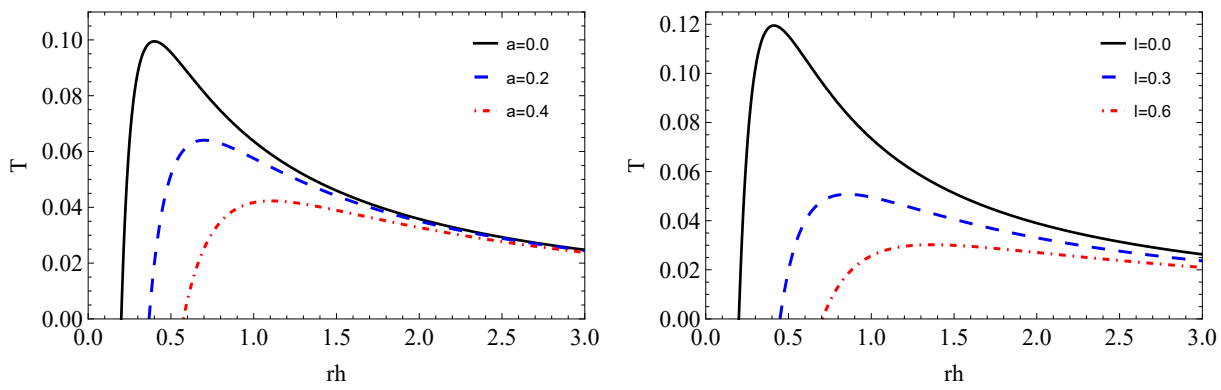

Figure 2.12: Plot shows the variation of Hawking temperature on the horizon radius. Here in the left panel: $l = 0.2$; in the right panel:$a = 0.2$. Here we have taken mass of the bh as a function of radius horizon:$M = M(r_h)$

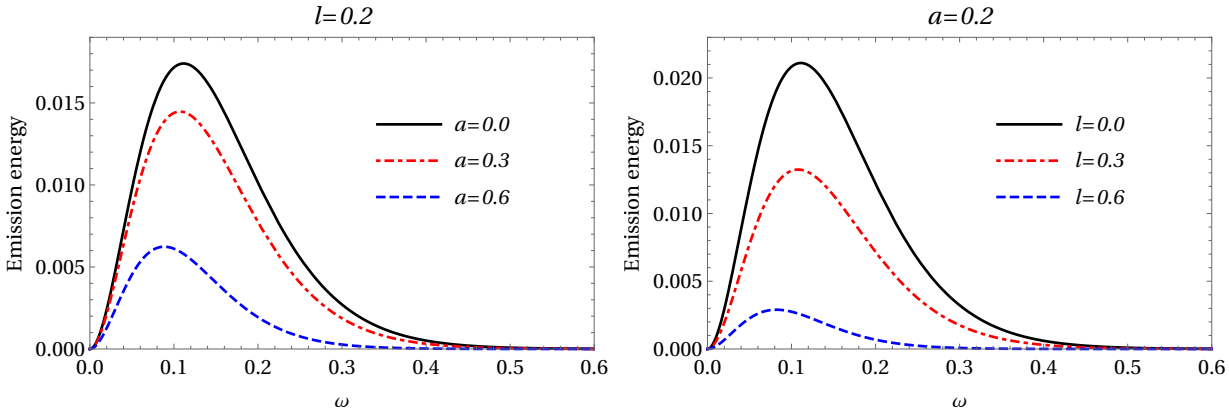

Figure 2.13: Plot shows the variation of temperature with horizon radius. Here $M = 1$.

2.5 Thermodynamics of Simpson-Visser black hole

In this section, we analyze thermodynamics of the Simpson-Visser black hole. General form of metric can be written as:

$$ds^2 = g_{tt}dt^2 + g_{rr}dr^2 + g_{\theta\theta}d\theta^2 + g_{\phi\phi}d\phi^2 + 2g_{t\phi}dtd\phi. \tag{2.18}$$

The angular velocity of a test particle at the event horizon, with vanishing angular momentum, can be calculated using the formula $\Omega_H = -g_{t\phi}/g_{\phi\phi}$ for the rotating Kerr-like BH

$$\Omega_H = \frac{a}{r_h^2 + a^2}. \tag{2.19}$$

We will use the expression (2.19) for our further calculations. Now we turn to calculate thermodynamical quantities of SV BH.

In the standard formulation of black hole thermodynamics for asymptotically flat spacetimes ($\Lambda = 0$), the black hole's mass (M) is commonly identified with its internal energy (U). The corresponding first law of thermodynamics is $dM = TdS + VdP + \Omega dJ + \Phi dQ$. However, in the context of asymptotically Anti-de Sitter (AdS) spacetimes a positive pressure (P) is defined in terms of the negative cosmological constant:$P = -\frac{\Lambda}{8\pi G}$. Varying this pressure introduces a new work term (VdP) into the first law, where V is the thermodynamic volume conjugate to P. The first law in the extended phase space precisely mirrors the differential form of enthalpy ($H = U + PV$) in classical thermodynamics:$dM = TdS + VdP + \cdots = dH$Consequently, the ADM mass (M) of the AdS black hole is identified as the enthalpy (H) of the spacetime. The BH mass (M, which is equal to enthalpy (H))

can be derived by making Eq. (2.3) equals to zero. As a result one may obtain:

$$H = \frac{\left(a^2 + r_h^2\right) e^{\frac{l}{r_h}}}{2r_h}. \tag{2.20}$$

Figure 2.11 demonstrates the enthalpy as a function of r_h. One may see that an increase in the parameters a and l corresponds to greater mass (enthalpy) for fixed r_h. And also using well-known formula $T = \frac{\kappa}{2\pi}$, one can get Hawking temperature for this type of BH, where κ is the surface gravity of rotating BH and we can calculate it with following expression [57, 119]

$$\kappa = \frac{1}{2}\sqrt{(g^{rr})'(G_{tt})'}, \tag{2.21}$$

where

$$G_{tt} = -g_{tt} - 2g_{t\phi}\Omega_H - g_{\phi\phi}\Omega_H^2, \tag{2.22}$$

and $(g^{rr})'$, $(G_{tt})'$ means derivative of g^{rr}, G_{tt} with respect to r, respectively. Eventually the final expression for temperature looks

$$T = \frac{\left(r_h - l\right) r_h^2 - \left(l + r_h\right) a^2}{4\pi \mathrm{r}_h^2 \left(a^2 + r_h^2\right)} \ . \tag{2.23}$$

It is easy to see that one can recover temperature formula for Kerr BH by taking $l = 0$, and also can recover temperature formula for Schwarzschild BH by taking $l = 0$, & $a = 0$. With the help of Eq. (2.23), one can depict this result visually. Figure 2.12 shows temperature dependency on the radius of event horizon for different values of l and a in Kerr-like spacetime. We can notice from this picture that deviation parameter 'cools down' BH. Precisely speaking, an increase of l causes temperature to decrease like spin parameter a if keep radius of horizon unchanged. Now one calculate area and entropy of Ker-like BH using the following general expression [57]

$$A = \int_0^{2\pi} \int_0^{\pi} \sqrt{g_{\theta\theta} g_{\phi\phi}} d\theta d\phi = 4\pi \left(a^2 + r_h^2\right), \tag{2.24}$$

and obtain [58]

$$S = \frac{A}{4} = \pi \left(a^2 + r_h^2\right). \tag{2.25}$$

Although area of outer event horizon and entropy doesn't depend on the deviation parameter explicitly, radius of event horizon depends on it. It means that deviation parameter somehow reduces the area, as well as the entropy. We will use Eqs. (2.23)-(2.20) and (2.25) to define the expression of Gibbs free energy as [58, 120]

$$G = M - TS = \frac{a^2 \left[r_h \left(e^{\frac{l}{r_h}} + 2\right) + 2l\right] + r_h^2 \left[r_h \left(e^{\frac{l}{r_h}} - 2\right) + 2l\right]}{2r_h^2}. \tag{2.26}$$

From Eq. (2.26) one can observe that Gibbs energy is positive in the vicinity of $r_h = 0$ i.e. for small black holes are stable but the black holes are unstable at larger horizon radius. Furthermore, it is clear that both parameters (l an a) cause Gibbs energy to increase.

The phenomenon characterized by the creation and annihilation of an abundant quantity of particles in immediate proximity to the black hole's event horizon is denoted as emission energy. Quantum fluctuations transpiring within the internal regions of black holes constitute the fundamental origin of this energy manifestation. The main reason for the BH evaporation within a certain period is due to the positive-energy particles that tunnel out of the BH in the core area where Hawking radiation occurs. Now we consider the energy emission rate BH with SV parameter. The absorption cross-section often oscillates around a limiting constant value σ_{lim}. The limiting value of cross-section σ_{lim} is depended to the the event horizon's radius as following

$$\sigma_{lim} \approx \pi r_h^2. \tag{2.27}$$

The expression of the emission energy rate from the BH as

$$\frac{d^2\mathcal{E}}{d\omega dt} = \frac{2\pi^2\sigma_{lim}}{e^{\frac{\omega}{T}} - 1}\omega^3, \tag{2.28}$$

where T is the Hawking temperature. The energy emission rate is represented in Fig. 2.13 as a function of ω for different values of the deviation parameter (right panel) and the spin parameter (left panel). From this figure, one can see that there exists a peak of the energy emission rate for the black hole. When these parameters are increased, the peak decreases and is shifted to a low frequency. Also, one can notice that the variation of l has a stronger effect on the emission of particles around the black hole.

2.6 Conclusion

In this chapter, we constructed an insightful discussion regarding the rotating BH's structure, circular orbits, center-of-mass energy, and thermodynamics in rotating SV spacetime. So, we have obtained the following results:

First, we have obtained the border between BH and no BH using their parameters in Fig. 2.1.

If the values of the parameters are lower than their extremal values, there exist Cauchy and event horizon in Fig. 2.2 and 2.3. When these two parameters l and a of the spacetime reach their extremal values, these two horizons merge, and also there is no horizon for $a > a_E$ and $l > l_E$.

The growth of parameters l and a in SV gravity positively affects the thickness of the ergosphere of the BH, meaning that it becomes thicker.

Within this work the radius of ISCO are also discussed in SV spacetime with its parameters l and a. An increase in these parameters makes the ISCO radius smaller, and it is represented in Fig. 2.8.

Using masssive particle orbits, we checked energy extraction from BH for extremal and non-extremal case through the BSW effect. The center of mass energy can be arbitrarily high for the extremal SV BH, which is not true for the nonextremal SV BH.

Properties of thermodynamics are studied for different cases: enthalpy, hawking temperature, entropy, and Gibbs free energy. To be more precise, an increase of BH's parameters l and a also cause Gibbs free energy to increase. An opposite is true for the temperature of this type of BH.

Chapter III

Thermodynamical analysis of charged rotating black hole surrounded by perfect fluid dark matter

This chapter is devoted to studying thermodynamics and particle acceleration around charged rotating BHs surrounded by perfect fluid dark matter. We discuss BH horizons, ergosphere and inner stable circular orbits in the framework of perfect fluid dark matter. It is observed that perfect fluid dark matter effects Hawking's temperature, Gibbs free free energy, and other physical quantities related to thermodynamics. Some different aspects of thermodynamics are discussed within the scope of different values of the involved parameters. Further, we discuss the thermal fluctuations of considered BH solutions, which refer to the random motion of particles around a BH due to temperature fluctuations. Specifically, thermal fluctuations are affecting the entropy and Hawking radiation of a BH, which are crucial for understanding the behavior of physical quantities. It is found that corrected thermodynamical quantities of charged rotating perfect fluid dark matter BHs are smaller than the charged rotating BH without perfect fluid dark matter. We emphasize that the assumptions made in the literature and the

thermodynamics of the previous BH solutions are well consistent with our results.

3.1 Introduction

Several independent experiments and observations have shown that normal matter is only 4% of the Universe. The best part of the Universe consists of dark matter ($\sim 21\%$) [121] and dark energy ($\sim 75\%$) [122]. These new forms of matter are not observed directly but through gravitational interaction. In the astrophysical scenario when one considers the processes around compact objects the effect of dark energy could be neglected. On the other hand, there is strong observational evidence of the existence of dark matter in the environment of giant elliptical and spiral galaxies [123]. Thus the theoretical study of the effect of dark matter on different astrophysical processes around compact gravitating objects becomes one of the key problems of modern relativistic astrophysics.

The different models of dark matter (light bosons, neutrinos, weakly interacting massive particles, self-interacting dark matter, macroscopic models, modified theories of gravity, etc) have been suggested by various authors. One of the most promising models is the quintessence with the property of the perfect fluid. The static spherically symmetric exact solutions of the Einstein equations for quintessential matter surrounding a black hole (BH), charged or uncharged [124]. Quasinormal modes of gravitational perturbation around a static BH surrounded by quintessence have been analyzed in [125]. The derivation of the geometry of quintessential rotating BHs as a generalization of the Kerr spacetimes has been presented in [126]. The effect of an external magnetic field on particle acceleration around BH in the presence of quintessence has been studied in [127]. A discussion regarding the M87 object was done by using the BH surrounded by quintessence and identified using the shadow observation in [128]. Some different kind of BHs

solutions have been calculated by the several authors [129–135] under the effect of dark matter hols. They investigated shadows and other interesting aspects of BHs solutions within the scope of different dark matter halos. They also constrained the involved parameters by using the observational values of dufferent BHs models.

Any modification to standard theory has to be tested/probed using experiments/observations. Metric theories of gravity are usually tested using the dynamics of test particles around the BH horizon. The equation of motion and physical processes connected with the dynamics of test particles (particle orbits, oscillations, acceleration, etc.) can be used to construct different tests of the gravity theories and their modifications [75–80]. One needs to take into account the effect of electromagnetic interaction while considering the charged particle motion around BH in the presence of external electric and magnetic fields [81–83]. The dynamical configurations of thin-shell in the framework of various charged and uncharged BH with massless and massive scalar field are explored in Refs. [136–141]. The particle dynamics with nonvanishing electric charge and/or magnetic dipole momentum around a compact object in the presence of electromagnetic field have been explored in Refs. [84–98, 106].

One of the interesting subjects of BH astrophysics is its thermodynamic properties. One needs to analyze the entropy of the event horizon of BH in order to explore the thermodynamics of the latter. Thermal fluctuations, also known as Hawking radiation, are a proposed phenomenon associated with black holes. According to Stephen Hawking's theory of black hole radiation [142], black holes are not entirely black but instead emit radiation at a temperature that is inversely proportional to their mass. This radiation is thought to be caused by the quantum mechanical processes that occur near the event horizon, where virtual particles are created and annihilated continually. Due to the effects of gravitational fields,

sometimes these particles can become real and escape the black hole in the form of radiation, causing the black hole to slowly lose mass. The first attempts to construct the entropy of the BH event horizon using phenomenological models have been performed in Refs. [55,110,111]. BH entropy and thermodynamical properties in Schwarzschild spacetime have been analyzed in [52, 54, 112]. In Ref. [113] one may find the analysis of particle spectrum and some thermodynamical properties of Reissner-Nordström BH. The thermodynamic properties of regular BH with nonlinear magnetic charge have been studied in [114]. The thermodynamics of BH surrounded by quintessence is considered in [115]. The similar analysis for the BH described by Hořava-Lifshitz gravity have been performed in Refs. [116,117]. Very recently, Faisal and his coauthors [143, 144] discussed the thermal fluctuations and other thermal analysis in the background of modified theories of gravity. The studies of thermodynamic properties of rotating and non-rotating BH can be found in Refs. [57, 58, 118–120, 145–147]. Recently, thermodynamics and Joule-Thomson expansion of BH exhibiting metric-affine gravity are explored in Ref. [148]. Also, the affects of gravitational decouplings on the thermodynamical properties of BH geometries are discussed in [149].

The chapter is organized as follows: In Sect. 3.2 we review the spacetime around rotating BH with electric charge and in the presence of perfect fluid dark matter. We consider the particle acceleration mechanism and explored the center of mass energy of colliding article around rotating charged BH surrounded by PFDM in Sect. 3.3. The thermodynamic properties of rotating charged BH surrounded by perfect fluid dark matter (PFDM) modeled by quintessence have been explored in Sect. 3.4. In Sec. 3.5, Thermal fluctuation and phase transition are considered in PFDM gravity. We have concluded our results in Sect. 3.6.

3.2 Charged black hole in perfect fluid dark matter

In order to incorporate the gravitational effects of dark matter into the black hole spacetime, we adopt the phenomenological framework of perfect fluid dark matter (PFDM). In this approach, dark matter is modeled as a classical gravitational source described by an effective matter Lagrangian, which captures the large-scale influence of a surrounding dark matter halo without specifying its microscopic nature.

The action for the gravity theory minimally coupled with gauge field in PFDM reads as [150, 151]

$$\mathcal{I} = \int dx^4 \sqrt{-g} \left(\frac{1}{16\pi G} R + \frac{1}{4} F^{\mu\nu} F_{\mu\nu} + \mathcal{L}_{DM} \right). \tag{3.1}$$

Here, $g = \det(g_{ab})$ is the determinant of the metric tensor, R is the Ricci scalar, G is Newton's gravitational constant, $F_{\mu\nu} = \partial_\mu A_\nu - \partial_\nu A_\mu$ (A_μ is the gauge potential) is the Maxwell field strength and $\mathcal{L}_{DM}$ is the Lagrangian density for PFDM.

Varying the action with respect to the metric tensor yields the Einstein field equations,

$$G_{\mu\nu} = 8\pi T_{\mu\nu}, \tag{3.2}$$

where the energy–momentum tensor of the PFDM is defined as

$$T_{\mu\nu} = -\frac{2}{\sqrt{-g}} \frac{\delta(\sqrt{-g}\, \mathcal{L}_{\text{PFDM}})}{\delta g^{\mu\nu}}. \tag{3.3}$$

In the PFDM model, the dark matter distribution is described by an effective anisotropic fluid with energy–momentum tensor of the form

$$T^{\mu}{}_{\nu} = \text{diag}\left(-\rho,\, p_r,\, p_\theta,\, p_\phi\right), \tag{3.4}$$

where $\rho(r)$ is the energy density, while p_r, p_θ, and p_ϕ represent the radial and tangential pressures, respectively.

Following the phenomenological construction of perfect fluid dark matter, the equation of state is chosen such that

$$\rho(r) = \frac{\gamma}{8\pi r^3}, \qquad p_r = -\rho, \qquad p_\theta = p_\phi = -\frac{1}{2}\rho, \tag{3.5}$$

where γ is the PFDM parameter characterizing the strength of the dark matter contribution. Physically, it plays the role of an effective dark matter density parameter and is directly related to the mass contribution of the dark matter halo.This choice satisfies the conservation equation $\nabla_\mu T^{\mu\nu} = 0$ and leads to logarithmic corrections in the metric function of the resulting black hole solution.

The adopted Lagrangian formulation provides an effective description of the gravitational influence of dark matter halos on black hole spacetimes and allows one to consistently investigate the impact of dark matter on horizon structure, particle dynamics, and thermodynamic properties.

Charged rotating BH in PFDM is [150, 151]:

$$\begin{aligned} ds^2 &= -\frac{1}{\rho^2}\Big(\Delta - a^2\sin^2\theta\Big)dt^2 - \frac{2a\sin^2\theta}{\rho^2}\Big[2Mr - Q^2 - \gamma r\ln(\frac{r}{\gamma})\Big]dtd\phi + \rho^2 d\theta^2 \\ &\quad + \sin^2\theta\Big[r^2 + a^2 + \frac{a^2\sin^2\theta}{\rho^2}\Big(2Mr - Q^2 - \gamma r\ln(\frac{r}{\gamma})\Big)\Big]d\phi^2 + \frac{\rho^2}{\Delta}dr^2, \end{aligned} \tag{3.6}$$

Here Δ and ρ are defined as

$$\begin{aligned} \Delta &= r^2 + a^2 - 2Mr + Q^2 + \gamma r\ln(\frac{r}{\gamma}), \\ \rho^2 &= r^2 + a^2\cos^2\theta, \end{aligned} \tag{3.7}$$

where M is the mass of the BH, a is the rotational parameter, Q is the charge of the BH.

In the next subsections, we will discuss particle orbits around BH under PFDM and BH parameters.

Horizons and ergosphere

Now we want to briefly discuss the horizons of the charged rotating BH within the scope of perfect fluid dark matter (PFDM). Like all rotating BHs, the metric by (3.6) has two horizons: the inner horizon r_h^- and the outer horizon r_h^+ which are the solutions of the condition $\Delta = 0$. We get an extremal BH for a certain critical value of the rotational parameter $a = a_E$, where the two radii of horizons coincide. The extremal values for the spin parameter at different values of the charge Q has been given in the Tab. 3.1.

It is of great interest to look at the ergosphere of the rotating BH in PFDM and see how the PFDM parameter affects the shape of the ergosphere. Similarly, the condition $g_{tt} = 0$ gives us two static limit surfaces: r_{sls}^- and r_{sls}^+. The region between r_{sls}^+ and r_h^+ corresponds to the ergosphere region. With the help of numerical computation of $\Delta = 0$ and $g_{tt} = 0$ we can easily evaluate the horizon and static limit surfaces of the charged rotating BH in PFDM. The Fig. 3.1) shows the behavior of the regions of the horizon and ergosphere of the charged rotating BH in PFDM for non-extremal BH for different values of charge Q and spin parameter a at fixed PFDM parameter $\gamma = 0.1$. It is clear from the plot that by increasing the charge Q gradually the regions of the ergosphere and horizon are converging and merging into one region, taking an almost spherical shape. To see the influence of the presence of perfect fluid dark matter on the regions of horizon and ergosphere the Fig. (3.2) illustrates the same plot for $\gamma = 0.2$. Considering these figures, it is obvious that the PFDM parameter decreases in both regions.

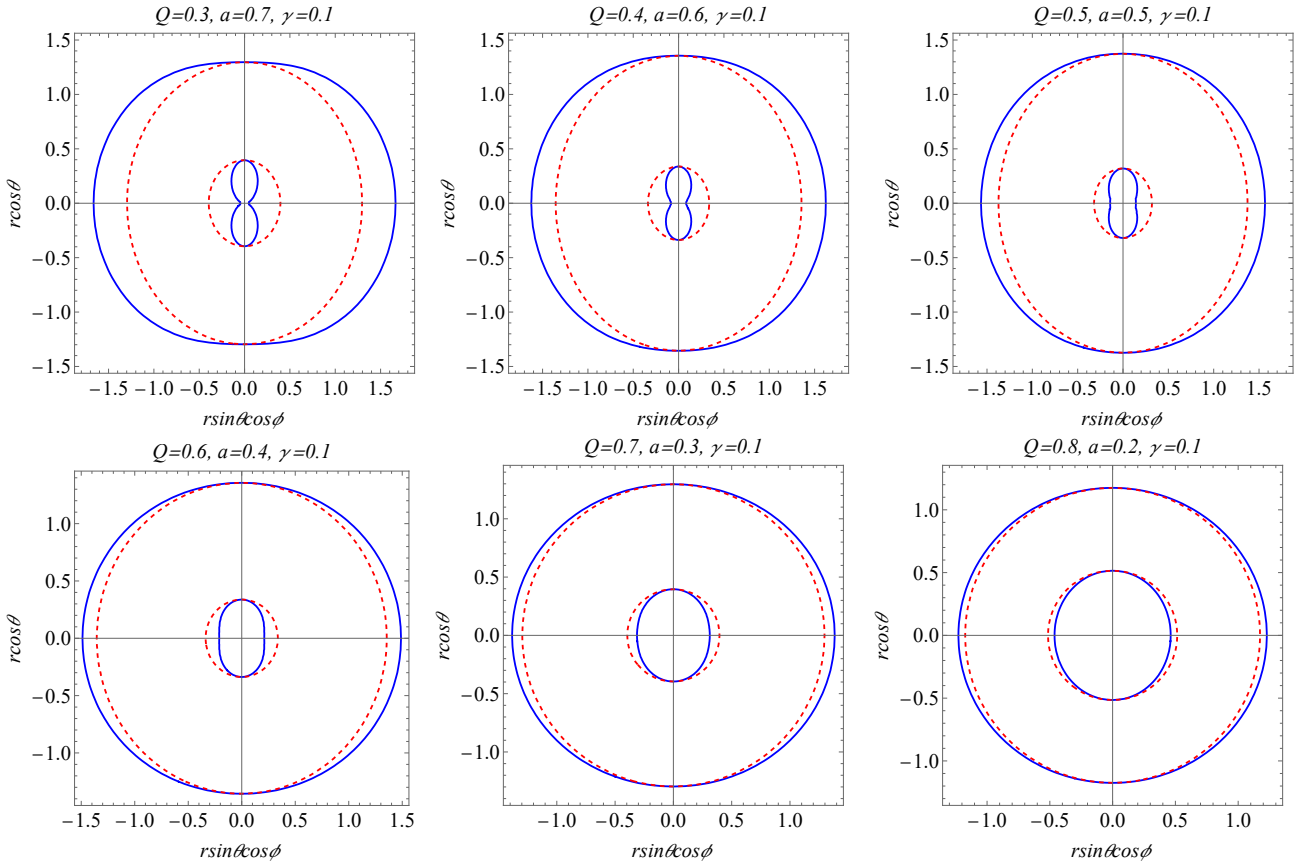

Figure 3.1: The variation of the shape of ergosphere of the rotating charged non-extremal BH in PFDM for the fixed PFDM parameter $\gamma = 0.1$

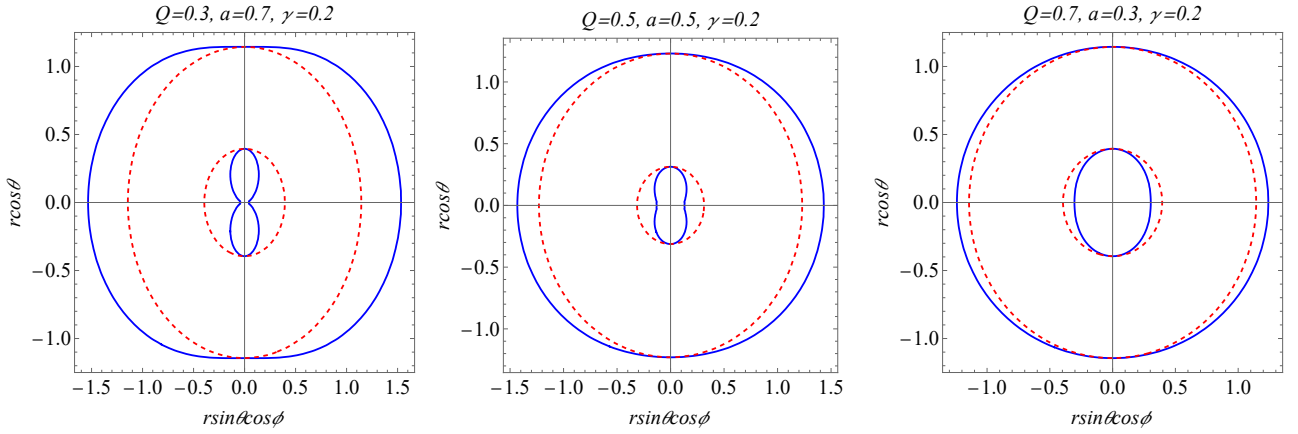

Figure 3.2: The variation of the shape of ergosphere of the rotating charged non-extremal BH in PFDM for the fixed PFDM parameter $\gamma = 0.2$

3.3 Particle acceleration near charged rotating black hole in perfect fluid dark matter

In this section, we want to study the charged rotating BH in PFDM as a particle accelerator. For this, we are going to consider the collision of two particles near the horizon and evaluate the exact expression for the center-of-mass energy produced by the collision for two cases: an extremal and non-extremal BH. To solve the geodesic equation for a timelike particle around charged rotating BH in PFDM we use constants of motions, such as P_t and P_ϕ:

$$\begin{aligned} P_t &= g_{tt}\dot{t} + g_{t\phi}\dot{\phi} = -E \\ P_\phi &= g_{\phi\phi}\dot{\phi} + g_{t\phi}\dot{t} = L \end{aligned} \tag{3.8}$$

Here, E and L are the energy and the angular momentum of the particle, respectively. Let's consider the motion at $\theta = \pi/2$, which means that $\dot{\theta} = 0$. By utilizing the expressions for the generalized momenta of the particle (3.8) and the normalization condition $u_\mu u^\mu = -m^2$ we get the following equation of motion:

$$\dot{t} = \frac{1}{r^2}\left[\frac{(a^2+r^2)}{\Delta}(E(a^2+r^2) - aL) + a(L - aE)\right], \tag{3.9}$$

$$\dot{\phi} = \frac{1}{r^2}\left[\frac{a^2}{\Delta}(E(a^2+r^2) - aL) + (L - aE)\right], \tag{3.10}$$

$$\dot{r} = \pm\frac{\sqrt{(aL - (a^2+r^2)E)^2 - \Delta(m^2r^2 + (L-aE)^2)}}{r^2} \tag{3.11}$$

The + and − signs in the radial velocity $\dot{r}$ indicate the outgoing and incoming geodesics, respectively. It is useful to derive the expression for the effective potential in order to acquire more information about the character of the motion

of the particle. With the help of (3.11) and the following expression:

$$\frac{1}{2}\dot{r}^2 + V_{eff} = 0, \tag{3.12}$$

it is not difficult to find the effective potential in the form:

$$V_{eff} = -\frac{(aL - (a^2 + r^2)E)^2 - \Delta(m_0^2 r^2 + (L - aE)^2)}{2r^4} \tag{3.13}$$

The solutions for $V'_{eff}(r) = 0$ and $V''_{eff}(r) = 0$ determine the innermost stable circular orbit of the particle. The Fig. (3.3) shows the ISCO radius versus γ, Q and a parameters. It is clear from the diagrams that the ISCO radius decreases with the growth of all parameters (γ, Q, and a) while making it possible to go closer to the BH.

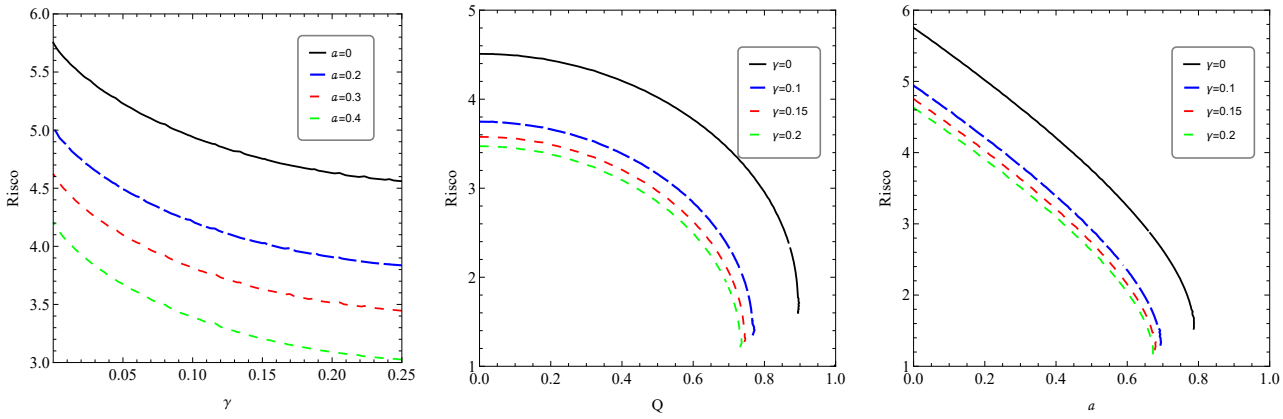

Figure 3.3: The variation of the innermost stable circular orbits for different parameters such as charge Q, PFDM parameter γ and rotating parameter a

Near horizon collision

Now our goal is to determine the ultrahigh-energy produced by the collision of two particles near the horizon of the rotating charged black hole in PFDM. Here, for simplicity, we assume that particles have the same mass m_0 and different four velocities u_1 and u_2, respectively. The CM energy E_{cm} of collision between two particles at the radial coordinate r is given by the following expression [152]:

$$E_{cm} = m_0\sqrt{2}\sqrt{1 - g_{\mu\nu}u_1^{\mu}u_2^{\nu}} \tag{3.14}$$

By substituting (3.9-3.11) into the equation (3.14) we get the following expression:

$$\frac{E_{cm}^2}{2m_0^2} = -\frac{K}{r^2\Delta} \tag{3.15}$$

where

$$\begin{aligned}\mathcal{K} = &\left(a^2 - aL_1 + r^2\right)\left(a^2 - aL_2 + r^2\right) + \Delta\left(r^2 - (a - L_1)(a - L_2)\right) \\ &- \sqrt{\left(a^2 - aL_1 + m_0^2r^2\right)^2 - \Delta\left((a - L_1)^2 + r^2\right)} \\ &\times \sqrt{\left(a^2 - aL_2 + m_0^2r^2\right)^2 - \Delta\left((a - L_2)^2 + r^2\right)}\end{aligned} \tag{3.16}$$

In order to get the ultrahigh-energy we need the particle to approach the BH with the critical angular momentum L_{cr}. We can get the critical value of the angular momentum L_{cr} from the condition $\dot{r} = 0$, when $r \longrightarrow r_h^E$. So, the expression for the critical angular momentum L_{cr} is:

$$L_{cr} = \frac{(a^2 + (r_h^E)^2)E}{a} \tag{3.17}$$

The limiting values of the angular momentum along with the corresponding spin parameters and the horizons for the extremal and nonextremal charged rotating BH in PFDM are presented in the Tab. (3.1) and Tab. (3.2), respectively. Fig. (3.4) illustrates the collision energy for an extremal BH at fixed PFDM parameter $\gamma = 0.2$ for different values of charge Q. In this case, the CM energy diverges sharply close to the region of the horizon. On the other hand, in Fig. (3.5) the collision energy diverges beyond the radius of the event horizon and maybe even finite at some values for Q.

Table 3.1: Limiting cases for angular momentum for an extremal BH

Q	a_E	L_{min}	L_{max}
0.2	0.836371	-3.40392	1.53746
0.3	0.805926	-3.36789	1.53350
0.4	0.761261	-3.31489	1.53152
0.5	0.699655	-3.24148	1.53774
0.6	0.61605	-3.14123	1.56787
0.7	0.499517	-3.00021	1.67339
0.8	0.315463	-2.77392	1.94426

Table 3.2: Limiting cases for angular momentum for a non-extremal BH

Q	a	r_-	r_+	L_{min}	L_{max}
0.2	0.8	0.537845	0.996355	-3.38472	1.82852
0.3	0.7	0.39476	1.14429	-3.31002	2.02628
0.4	0.6	0.331881	1.21029	-3.22286	2.13517
0.5	0.5	0.313006	1.23025	-3.12092	2.20061
0.6	0.4	0.331881	1.21029	-3.00059	2.23378
0.7	0.3	0.39476	1.14429	-2.85571	2.23662
0.8	0.2	0.537845	0.996355	-2.67415	2.20285

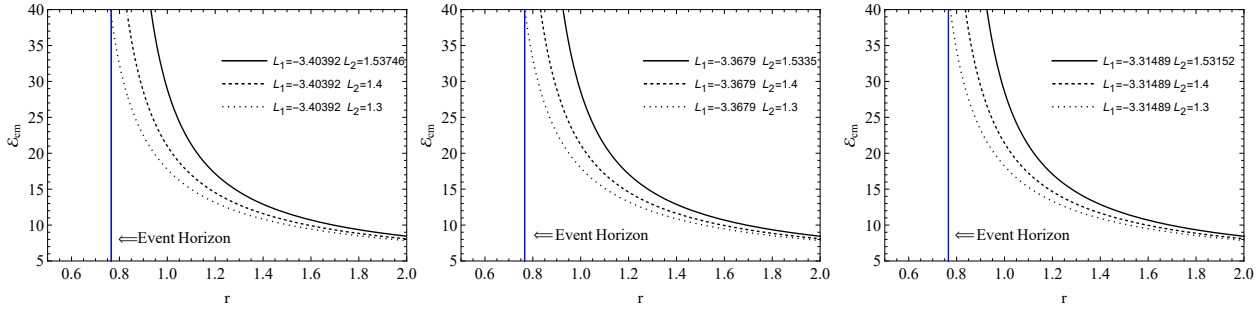

Figure 3.4: The center-of-mass energy E_{cm} dependence of the radial coordinate r for an extremal BH for $\gamma = 0.2$ and various $Q = 0.2; 0.3; 0.4$ values respectively, with $r_h^E = 0.765747$

3.4 Thermodynamics

In this part of our work, we discuss the thermodynamics of the charged rotating BH in PFDM. The event horizon of BH for the given metric is obtained

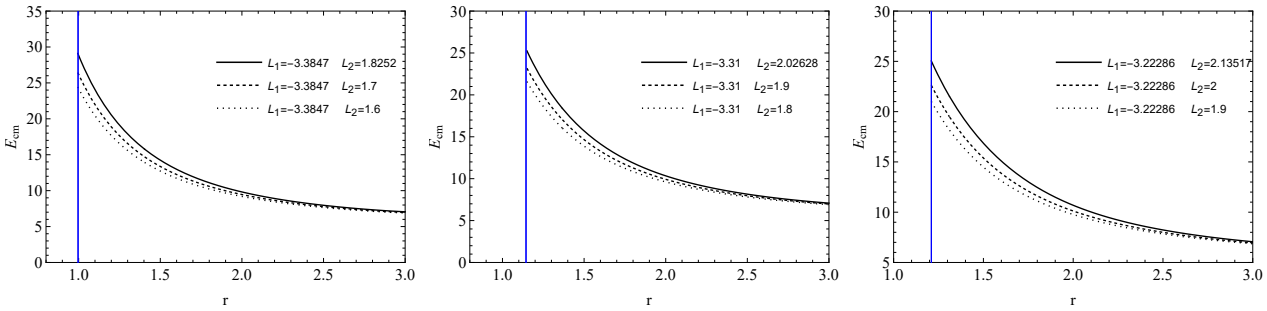

Figure 3.5: The center-of-mass energy E_{cm} dependence of the radial coordinate r for a non-extremal BH for $\gamma = 0.2$ and various $Q = 0.2; 0.3; 0.4$ values respectively.

by condition "$\Delta = 0$":

$$r_h^2 + a^2 - 2Mr + Q^2 + \gamma r_h \ln \frac{r_h}{\gamma} = 0. \tag{3.18}$$

It can be easily noticed that it has two horizons: the inner one r_- and the outer one r_+, which depend on the PFDM parameter γ. Using the condition for the BH event horizon (3.18) we can derive the BH mass M, which is equivalent to the enthalpy H:

$$H = \frac{1}{2}[r_h + \frac{(a^2 + Q^2)}{r_h} + \gamma ln \frac{r_h}{\gamma}]. \tag{3.19}$$

The graphical analysis of the enthalpy relation (3.19) is given in Fig. (3.6). It is clear from the plots that enthalpy decreases in the beginning and the rise of γ does not matter for it. However, it starts to increase from $r_h = 0.5$ when γ parameter increases. Whereas, when the spin parameter a and charge Q rise the enthalpy differs close to the BH and goes up becoming indifferent to parameter changes far away from the BH.

Now, in order to derive the expression for the entropy S of the BH we need to find the area of the event horizon A using the metric (3.6) with the following expression [57]:

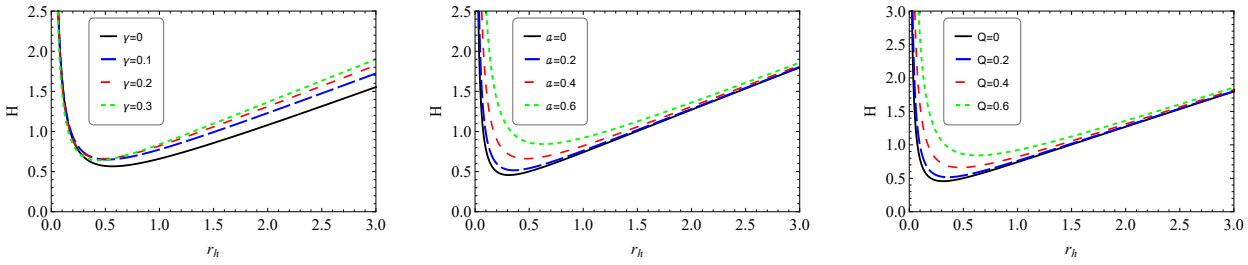

Figure 3.6: Enthalpy variation with horizon radius for different parameters of γ, a and Q. Here in the left panel: $a = 0.3$, $Q = 0.3$; in the middle panel: $\gamma = 0.2$, $Q = 0.4$ and in the right panel: $a = 0.3$,$\gamma = 0.2$

$$A = \int_0^{2\pi} \int_0^{\pi} \sqrt{g_{\theta\theta} g_{\phi\phi}} d\theta d\phi \tag{3.20}$$

At the horizon $\Delta = 0$, therefore $g_{\theta\theta}$ and $g_{\phi\phi}$ are expressed as: $g_{\theta\theta} = \rho^2$, $g_{\phi\phi} = \sin^2\theta[r^2 + a^2 + \frac{a^2 \sin^2\theta}{\rho^2}(2Mr - Q^2 - \gamma r \ln\frac{r}{\gamma})$. Putting these expressions in the Eq. (3.20) and doing some calculations, we arrive at the following final expression:

$$A = 4\pi(r_h^2 + a^2). \tag{3.21}$$

Now, it is easy to find the Bekenstein-Hawking entropy S, which has the form as [58]:

$$S = \frac{A}{4} = \pi(r_h^2 + a^2) \tag{3.22}$$

The next step is to calculate the angular velocity of the BH Ω at the horizon of the BH. For this, we will use the formulae for the angular velocity:

$$\Omega = -\frac{g_{t\phi}}{g_{\phi\phi}}. \tag{3.23}$$

Finding $g_{t\phi}$ and $g_{\phi\phi}$ from the metric (3.6) and using the expressions in (3.7), we find the angular velocity at horizon ($\Delta = 0$)in the equatorial plane ($\theta = \pi/2$) in the following form:

$$\Omega = \frac{a}{r_h^2 + a^2}. \tag{3.24}$$

The quantities: horizon area A, entropy S and angular velocity Ω do not explicitly depend on M, a, Q, γ, where $r_h = f(M, a, Q, \gamma)$.

Fig. (3.7) represents the radial dependence of the angular velocity for the alteration of parameters. The angular velocity Ω of the BH does not change much with the shift in the γ and decreases with increasing radius. While we see a decline in the angular velocity when the rotational parameter a and charge Q go up.

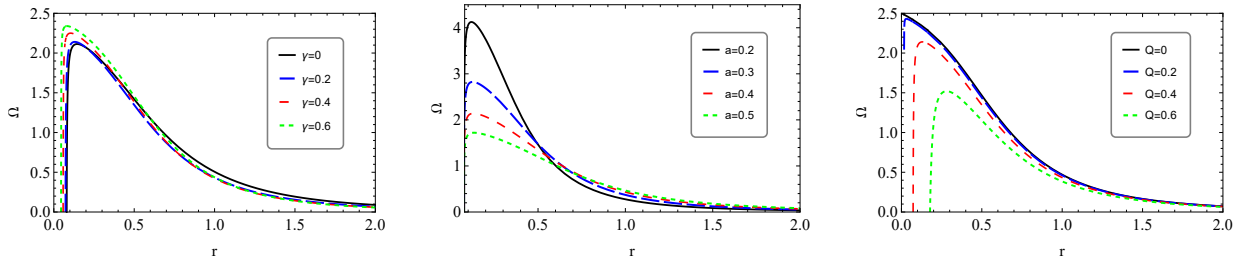

Figure 3.7: The variation of the angular velocity for different parameters. Here, in the left panel: $a = Q = 0.4$, in the middle: $\gamma = 0.2$, $Q = 0.4$ and in the right panel: $\gamma = 0.2$,$a = 0.4$.

It is time to compute Hawking's temperature T for the rotating BH which is defined as follows:

$$T = \frac{k}{2\pi} = \frac{\sqrt{G'_{tt} g^{rr\prime}}}{4\pi}. \tag{3.25}$$

Here, surface gravity k for the rotating BH has been derived in the work and has the form [57, 119]:

$$k = \frac{\sqrt{G'_{tt} g^{rr\prime}}}{2}, \tag{3.26}$$

where $G_{tt} = g_{tt} + 2g_{t\phi}\Omega - g_{\phi\phi}\Omega^2$ and $g^{rr} = 1/g_{rr}$. Here we have found the expression for Hawking's temperature with the mass of the black hole as a function of radius of horizon $M = M(r_h)$ from the condition for the event horizon ($\Delta = 0$, see Eq.3.7). As is seen from the left diagram for different values of the rotational parameter a the temperature drops when the spin of the black hole a increases. The right diagram for different γ values illustrates the growth of the Hawking's temperature

when PFDM parameter increases. So, the presence of the dark matter increases the surface gravity of the black hole, resulting in the increase of the temperature of the BH.

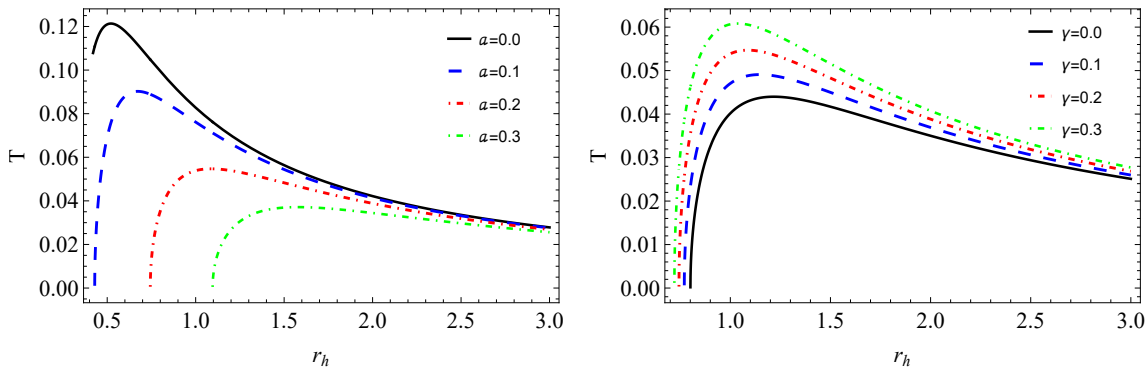

Figure 3.8: The dependence of Hawking's Temperature on horizon radius for different values of rotating parameter a (left panel: $\gamma = 0.2$, $Q = 0.4$) and PFDM parameter γ (right panel: $a = 0.2$, $Q = 0.4$). Note, that we have taken a mass of the BH as a function og radius of horizon here $M = M(r_h)$.

Now, it is time to define the thermodynamic variable - Gibbs free energy of the BH with the following definition [58, 120]:

$$G = M - TS \tag{3.27}$$

Here M, T, S stand for the enthalpy, Haking's temperature, and entropy of the BH. The variation of the Gibbs free energy for parameters (γ, Q, a) is given in Fig. (3.9). From the Fig. (3.9 (b)), we can see that the presence of the PFDM parameter leads to significant changes in the Gibbs free energy, namely the rise of the PFDM parameter results in the increase of the value of Gibbs free energy. The same situation occurs with the change of charge Q (a). However, the opposite case takes place with rotational parameter a (c).

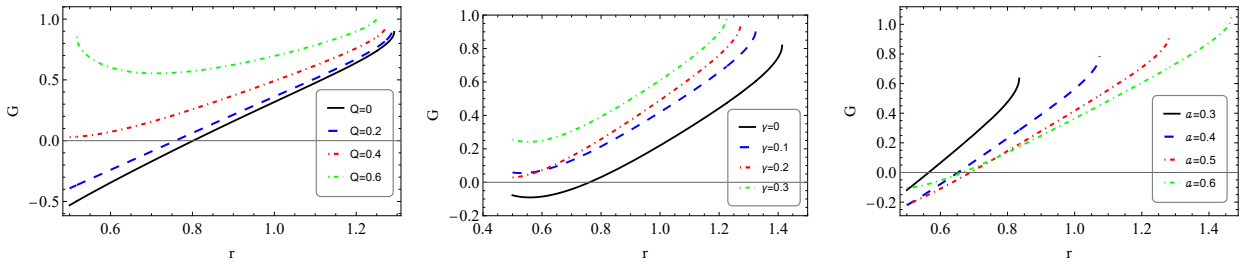

Figure 3.9: The radial dependence of Gibbs free energy for different parameters such as: PFDM parameter γ, charge Q and rotating parameter a

3.5 Thermal fluctuations

This section examines how simple logarithmic, second-order, and higher order corrections affect the Helmholtz free energy, internal energy, enthalpy, and Gibbs free energy of the rotating BH geometry under consideration with PFDM. As such, we determine the mathematical representation of the system's corrected entropy using the partition function, which is defined as [153–155]

$$R(\xi) = \int_0^\infty \rho(E)\exp(-\xi E)dE, \tag{3.28}$$

where $\rho(E)$ represents the density state with average energy E. Using the inverse Laplace transformation of the previously established function, we can get the density state, which is expressed as

$$\rho(E) = \frac{1}{2i\pi}\int_{-i\infty+\xi_0}^{i\infty+\xi_0}\exp(\xi E)R(\xi)d\xi = \frac{1}{2i\pi}\int_{-i\infty+\xi_0}^{i\infty+\xi_0}\exp(\tilde{S}(\xi))d\xi, \tag{3.29}$$

here the exact corrected expression of entropy is $\tilde{S}(\xi) = \beta E + \ln Z(\xi)$ with $\xi > 0$. By considering Taylor series expansion about ξ_0, we get

$$\tilde{S}(\xi) = S + \frac{1}{2}(\xi-\xi_0)^2\frac{\partial^2\tilde{S}(\xi)}{\partial\xi^2}\Big|_{\xi=\xi_0} + O(\xi-\xi_o)^2. \tag{3.30}$$

The following relations are verified for the equilibrium entropy S, i.e., $\frac{\partial^2 S}{\partial\xi^2} > 0$ and $\frac{\partial S}{\partial\xi} = 0$. By using Eq.(3.30) in (3.29), we get

$$\rho(E) = \frac{1}{2\pi i}\exp(S)\int d\xi\exp\left(\frac{1}{2}(\xi-\xi_0)^2\frac{\partial^2\tilde{S}(\xi)}{\partial\xi^2}\right). \tag{3.31}$$

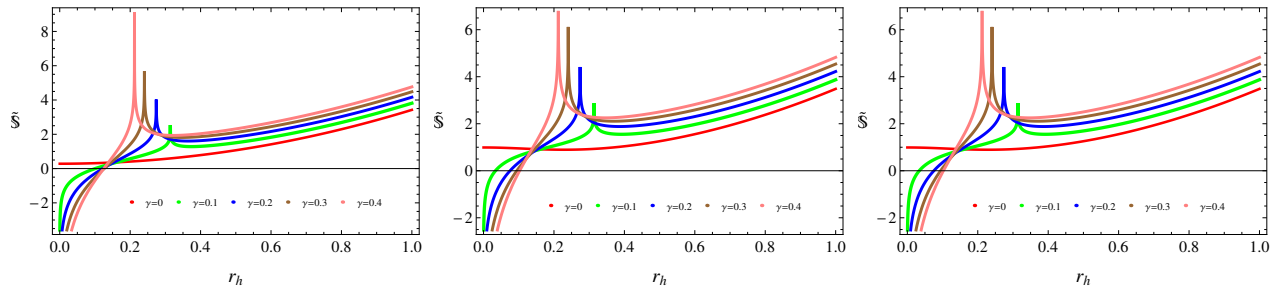

Figure 3.10: Corrected entropy versus r_h for different values of γ with $\chi = 0.2, \eta = 0$ (first plot), $\chi = 0, \eta = 0.2$ (second plot), $\chi = 0.2 = \eta$ (third plot) for $m = 0.2, Q = 0.2, a = 0.3$.

Further, it yields [153–155]

$$\rho(E) = \frac{1}{\sqrt{2\pi}} \exp(S)\Big(\Big(\frac{\partial^2 \tilde{S}(\xi)}{\partial \xi^2}\Big)\Big|_{\xi=\xi_0}\Big)^{-\frac{1}{2}}, \tag{3.32}$$

which leads to

$$\tilde{S} = S - \frac{1}{2}\ln(S\mathbb{T}^2) + \frac{\eta}{S}. \tag{3.33}$$

With the exception of the component $\frac{1}{2}$, which heightens the impact of correction terms on the entropy of BH, we are free to make use of a more inclusive parameter denoted by χ without losing generality. The respective expression of corrected entropy can be written as [155]

$$\tilde{S} = S - \chi\ln(S\mathbb{T}^2) + \frac{\eta}{S}. \tag{3.34}$$

By considering alternative correction parameter values χ and η, we obtain uncorrected entropy if $\eta,\ \chi \to 0$, simple logarithmic corrections if $\eta \to 0,\ \chi \to 1$, second order correction terms if $\eta \to 1,\ \chi \to 0$, higher orders correction terms if $\eta,\ \chi \to 1$.

Fig. (3.10) explains the graphical behavior of corrected entropy of rotating BH with PFDM for SLCs, SOCs, HOCs with suitable values of physical parameters. These plots express that the rate of fluctuation of the BH entropy increases as the PFDM parameter (γ) increases. It is also noted that there is no fluctuation

for the choice of rotating charged BH ($\gamma = 0$). In this figure, the first plot represents the behavior of corrected entropy for second-order correction terms, the second plot expresses the effects of simple logarithmic corrections and higher-order correction terms are discussed in the third plot. The corrected entropy shows the maximums fluctuations behavior for the choice of second-order correction terms. It should be pointed out that in all circumstances, the entropy of the system is seen to be steadily growing across the entirety of the domain under consideration for larger BHs. It should be noted that the graph of the charged rotating BH corrected entropy is rising steadily (the red curves), but the results of the charged rotating BH with PFDM corrected expression fluctuate for lower BHs and rise steadily for larger ones.

Now, check the other thermodynamic parameters under the influence of thermal fluctuations using the expression for the corrected entropy. The modified law of BH thermodynamics can be written as follows when there are fluctuations in temperature: [155, 156]

$$dM = \mathcal{T} d\tilde{S} + \Omega dJ + \Phi dQ, \tag{3.35}$$

where $\mathcal{T}$, Ω and Φ are denoted the corrected Hawking temperature, angular momentum the conjugate quantity where Q is a new thermodynamic variable. The relations can be used to derive these potential functions:

$$\mathcal{T} = \left(\frac{\partial M}{\partial \tilde{S}}\right)_Q, \quad \Omega = \left(\frac{\partial M}{\partial J}\right)_Q \quad \Phi = \left(\frac{\partial M}{\partial Q}\right)_{\mathbb{T}}.$$

The modification of the first law of BH thermodynamics is verified when the preceding expressions are substituted in Eq. (3.35), which suggests that the presence of thermal fluctuations strengthens the dependability of the first law of BH thermodynamics. In Figs. (3.11)-(3.14), we analyze the effects of second-order, simple logarithmic, and higher-order correction terms on the Helmholtz free

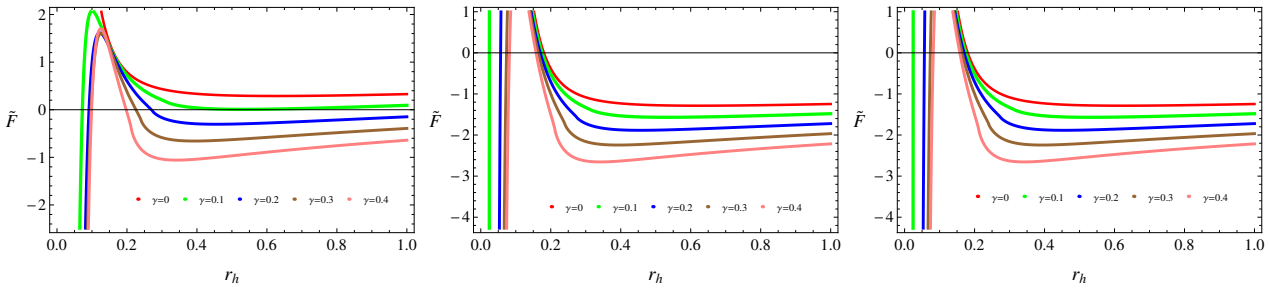

Figure 3.11: Corrected Helmholtz free energy versus r_h for different values of γ with $\chi = 0.2, \eta = 0$ (first plot), $\chi = 0, \eta = 0.2$ (second plot), $\chi = 0.2 = \eta$ (third plot) for $m = 0.2, Q = 0.2, a = 0.3$.

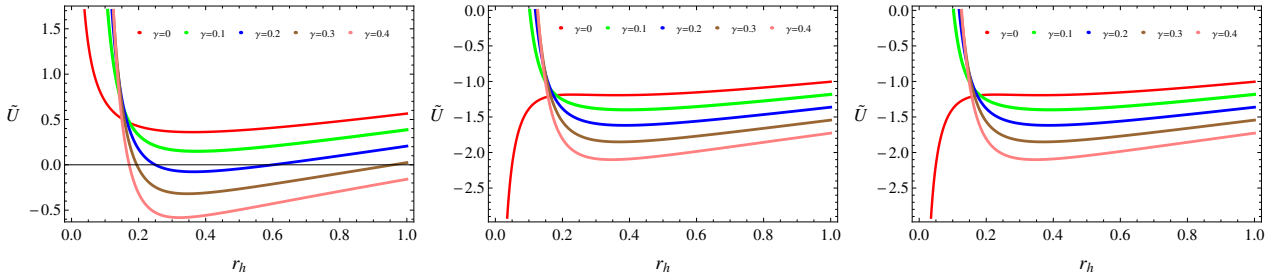

Figure 3.12: Corrected internal energy versus r_h for different values of γ with $\chi = 0.2, \eta = 0$ (first plot), $\chi = 0, \eta = 0.2$ (second plot), $\chi = 0.2 = \eta$ (third plot) for $m = 0.2, Q = 0.2, a = 0.3$.

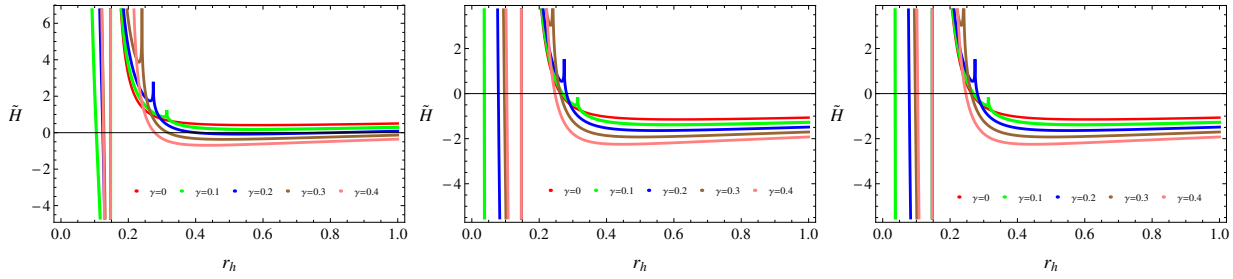

Figure 3.13: Corrected enthalpy versus r_h for different values of γ with $\chi = 0.2, \eta = 0$ (first plot), $\chi = 0, \eta = 0.2$ (second plot), $\chi = 0.2 = \eta$ (third plot) for $m = 0.2, Q = 0.2, a = 0.3$.

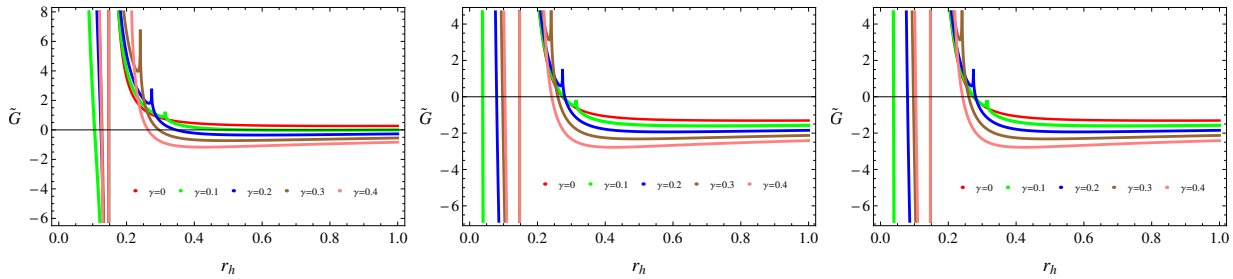

Figure 3.14: Corrected Gibbs free free energy r_h for different values of γ with $\chi = 0.2, \eta = 0$ (first plot), $\chi = 0, \eta = 0.2$ (second plot), $\chi = 0.2 = \eta$ (third plot) for $m = 0.2, Q = 0.2, a = 0.3$.

energy, internal energy, enthalpy, and Gibbs free energy of the charged rotating BH considered with and without PFDM.

- Fig. (3.11) is used to explain the graphical behavior of corrected form of Helmholtz free energy for different choices of χ and η with suitable physical parameters. It is found that for smaller BHs Helmholtz free energy increases and then decreases after the fluctuations. Without the PFDM parameter, it shows positive behavior for the case of second-order correction terms while it represents negative behavior as γ increases positively (first plot of Fig. (3.11)). For simple logarithmic (second plot of Fig. (3.11)) and higher-order correction terms (third plot of Fig. (3.11)), it represents the completely negative behavior after the fluctuations.

- Fig. (3.12) indicates the effects of the corrections terms on the internal energy of the BHs considered. It is found that the internal energy is maximum for the smaller BHs while it decreases for larger BHs. As the PFDM parameter increases, the internal energy of the system also decreases. Shows negative behavior for logarithmic and higher-order corrections terms.

- Fig. (3.13) represents that the corrected form of enthalpy fluctuates for the smaller BHs while for the larger BHs it shows a smooth increasing behavior. It also represents that the charged rotating BH enthalpy is maximum as compared to charged rotating PFDM BH.

- Fig. (3.14) explains the effects of the correction terms on the Gibbs free energy of the BH geometry considered. It is found that the Gibbs free energy fluctuates for the smaller BHs and represents the maximum behavior for the charged rotating BH without PFDM. For second-order and higher-order correction terms, the Gibbs free energy represents the negative behavior for

larger BHs.

It is found that the corrected thermodynamical quantities of the charged-rotating PFDM BH are smaller than those of the charged-rotating BH without PFDM.

Phase transition

Another method of determining the thermodynamical stability of BH locally is to study the sign of specific heat $\mathbb{C}_{\mathbb{S}} = \frac{d\tilde{U}}{d\mathbb{T}}$. It is noted that BH is locally unstable for $\mathbb{C}_{\mathbb{S}} < 0$ and the point of the phase transition can be found at $\mathbb{C}_{\mathbb{S}} = 0$ and BH is locally stable if $\mathbb{C}_{\mathbb{S}} > 0$. The mathematical expression of specific heat is given as [155, 157]

$$\mathbb{C}_{\mathbb{S}} = \frac{2\left(\pi\left(a^2+r_h^2\right)\left(\gamma^2 r_h\left(2a^2+r_h^2\right)+A_9\right)+\eta r_h^2\left(a^2+Q^2-r_h(\gamma+r_h)\right)\right)}{\pi\left(a^2+r_h^2\right)^2\left(3a^2+3Q^2-r_h(2\gamma+r_h)\right)},$$

with

$$\begin{aligned}\mathbb{C}_{\mathbb{S}} &= \gamma\left(-r_h^2\left(a^2+2Q^2\right)-3a^2\left(a^2+Q^2\right)+\pi a^2 r_h^3+\pi r_h^5\right)- \\ &\quad -\pi r_h^2\left(a^2+r_h^2\right)\left(a^2+Q^2-r_h^2\right),\end{aligned}$$

The stability of the system under thermodynamic fluctuations is now discussed using three different cases of correction terms with different values of Q and γ through the graphical behavior of specific heat (Fig. (3.15)). It is worth noting that the specific heat indicates a stable structure for BHs of a certain size, but an unstable design for BHs that are significantly larger. For every value of charge, the graphical behavior of the specific heat of the charged rotating BH without PFDM shows maximum stable configurations. The stability of the charged rotating BH decreases as the PFDM parameter increases. By increasing the charge of the geometry, the specific heat of the system also increases. The cases of correction terms considered show a similar behavior for every value of χ, η.

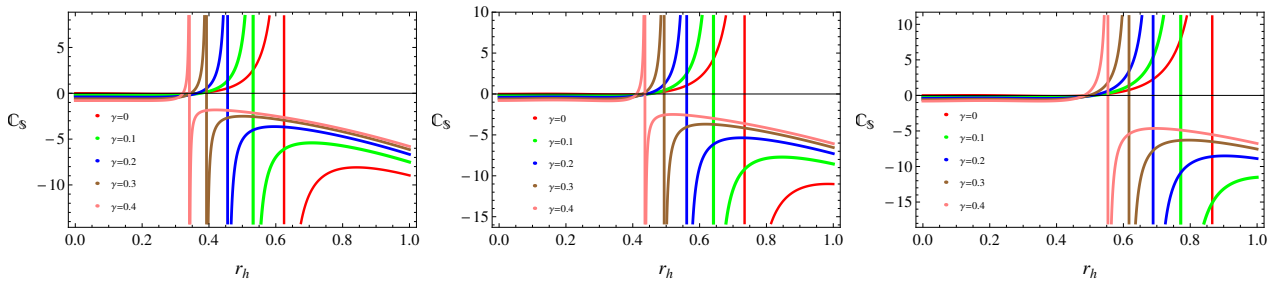

Figure 3.15: Corrected specific heat versus r_h for different values of γ with $Q = 0.2$ (first plot), $Q = 0.3$ (second plot), $Q = 0.4$ (third plot) for $m = 0.2, Q = 0.2, a = 0.3, \chi = 0.2, \eta = 0.2$.

3.6 Conclusion

There are several observational parameters to study properties of BH but there is no exact data in which only charge or rotational parameters of BHs are discussed. Here, we have tried to theoretically analyze the charged rotating BH in the presence of PFDM and investigated the following:

First, we have discussed the borders for horizons and ergosphere region of this BH. It is necessary to mention that we have calculated an extremal BH for a certain critical value of the rotational parameter $a = a_E$, where the two radii of the horizons have coincided. The ergosphere region of the present BH is provided graphically in Fig. (3.1) and Fig. (3.2) for the different choices of the parameters involved.

We have studied the influence of PFDM parameters on horizons and ergosphere region for two cases: an extremal and non-extremal BH. We take the behavior of the shape of these regions graphically. We find that the PFDM parameter γ shortens the border for both the horizon and ergosphere regions, almost merging into one region.

Fig. (3.3) has described the ISCO radius versus γ, Q and a involved model parameters. The ISCO radius has been observed to decrease within the scope of all parameters (γ, Q and a).

We have studied the thermodynamic characteristics of this BH in PFDM and have discovered that the increase in γ results in an increase in the enthalpy H and the Gibbs free energy G. In contrast, the temperature of the BH decreases with growth γ.

The effect of the PFDM parameter γ on the ISCO radius has also been discussed in the work, namely, with increasing γ the ISCO radius decreases.

We have studied the collision of two identical massive particles near the horizon of the BH and studied the behavior of the CM energy for an extremal and nonextremal case.

The effect of second-order, simple logarithmic, and higher-order correction terms on the Helmholtz free energy, internal energy, enthalpy, and Gibbs free energy of the charged rotating BH with and without PFDM have been observed, which can be checked from Figs. (3.11)-(3.14).

It is worth noting that the specific heat indicates a stable structure for BHs of a certain size but an unstable design for BHs that are significantly larger, which has also been confirmed from Fig. (3.15).

Conclusion

The following conclusions were presented based on research carried out on the topic of 'Thermodynamic and Energetic Processes Around Compact Objects in Modified Theories of Gravity' for the Doctor of Philosophy (PhD) dissertation:

1. For the first time, it has been demonstrated that the horizon structure, ergosphere geometry, and extremality conditions in modified gravity spacetimes (4D Einstein–Gauss–Bonnet, Simpson–Visser, and perfect fluid dark matter models) depend systematically on additional gravitational parameters—revealing a direct link between "black hole hair" and observable spacetime features.

2. For the first time, it has been shown that the innermost stable circular orbit (ISCO) undergoes parameter-dependent shifts in these frameworks, providing a new diagnostic tool to test modified gravity using accretion disk observations.

3. For the first time, it has been derived that the Banados–Silk–West (BSW) particle acceleration mechanism can be significantly enhanced in modified gravity, with explicit critical angular momentum conditions obtained for black holes surrounded by dark matter or nonlinear electromagnetic fields.

4. For the first time, it has been found that logarithmic and higher-order quantum corrections to black hole entropy lead to new thermodynamic phase

transitions and modified stability criteria, especially in the presence of perfect fluid dark matter.

5. For the first time, it has been established that modified gravity parameters govern not only spacetime geometry but also the dynamics of spinning particles and thermodynamic behavior—creating a unified, observationally testable framework to constrain alternative theories of gravity.

Bibliography

[1] M. Bañados, J. Silk, and S. M. West, "Kerr Black Holes as Particle Accelerators to Arbitrarily High Energy," *Phys. Rev. Lett.*, vol. 103, no. 11, p. 111102, Sep. 2009.

[2] T. Jacobson and T. P. Sotiriou, "Spinning Black Holes as Particle Accelerators," *Physical Review Letters*, vol. 104, no. 2, p. 021101, Jan. 2010.

[3] K. Lake, "Particle Accelerators inside Spinning Black Holes," *Phys. Rev. Lett.*, vol. 104, no. 21, p. 211102, May 2010.

[4] S.-W. Wei, Y.-X. Liu, H.-T. Li, and F.-W. Chen, "Particle collisions on stringy black hole background," *Journal of High Energy Physics*, vol. 2010, p. 66, Dec. 2010.

[5] O. B. Zaslavskii, "Acceleration of particles by nonrotating charged black holes?" *Soviet Journal of Experimental and Theoretical Physics Letters*, vol. 92, no. 9, pp. 571–574, Nov. 2010.

[6] ——, "Acceleration of particles as a universal property of rotating black holes," *Phys. Rev. D*, vol. 82, no. 8, p. 083004, Oct. 2010.

[7] P.-J. Mao, R. Li, L.-Y. Jia, and J.-R. Ren, "Acceleration of particles in Einstein-Maxwell-dilaton black holes," *Chin. Phys. C*, vol. 41, no. 6, p. 065101, Jun. 2017.

[8] S.-W. Wei, Y.-X. Liu, H.-T. Li, and F.-W. Chen, "Particle collisions on stringy black hole background," *Journal of High Energy Physics*, vol. 2010, p. 66, Dec. 2010.

[9] Y. Li, J. Yang, Y.-L. Li, S.-W. Wei, and Y.-X. Liu, "Particle acceleration in Kerr-(anti-)de Sitter black hole backgrounds," *Class. Quant. Grav.*, vol. 28, no. 22, p. 225006, Nov. 2011.

[10] J. Yang, Y.-L. Li, Y. Li, S.-W. Wei, and Y.-X. Liu, "Particle collisions in the lower dimensional rotating black hole space-time with the cosmological constant," *arXiv e-prints*, p. arXiv:1202.4159, Feb. 2012.

[11] A. Abdujabbarov, B. Ahmedov, and B. Ahmedov, "Energy extraction and particle acceleration around a rotating black hole in Hořava-Lifshitz gravity," *Phys, Rev. D*, vol. 84, no. 4, p. 044044, Aug. 2011.

[12] A. A. Grib and Y. V. Pavlov, "On particle collisions near rotating black holes," *Grav. Cosmol.*, vol. 17, no. 1, pp. 42–46, Jan. 2011.

[13] A. A. Grib, Y. V. Pavlov, and O. F. Piattella, "High Energy Processes in the Vicinity of the Kerr's Black Hole Horizon," *Int. J. Mod. Phys. A*, vol. 26, no. 22, pp. 3856–3867, Jan. 2011.

[14] A. A. Grib and Y. V. Pavlov, "On particle collisions in the gravitational field of the Kerr black hole," *Astropart. Phys.*, vol. 34, no. 7, pp. 581–586, Feb. 2011.

[15] M. Patil and P. S. Joshi, "Naked singularities as particle accelerators," *Phys. Rev. D*, vol. 82, no. 10, p. 104049, Nov. 2010.

[16] M. Patil, P. S. Joshi, and D. Malafarina, "Naked singularities as particle accelerators. II." *Phys. Rev. D*, vol. 83, no. 6, p. 064007, Mar. 2011.

[17] M. Patil and P. Joshi, "Kerr naked singularities as particle accelerators," *Class. Quant. Grav.*, vol. 28, no. 23, p. 235012, Dec. 2011.

[18] M. Patil, P. S. Joshi, M. Kimura, and K.-i. Nakao, "Acceleration of particles and shells by Reissner-Nordström naked singularities," *Phys. Rev. D*, vol. 86, no. 8, p. 084023, Oct. 2012.

[19] T. Harada and M. Kimura, "Collision of two general geodesic particles around a Kerr black hole," *Phys. Rev. D*, vol. 83, no. 8, p. 084041, Apr. 2011.

[20] C.-Q. Liu, "Collision of Two General Geodesic Particles around a Kerr—Newman Black Hole," *Chin. Phys. Lett.*, vol. 30, no. 10, p. 100401, Oct. 2013.

[21] C. Liu, S. Chen, C. Ding, and J. Jing, "Particle acceleration on the background of the Kerr-Taub-NUT spacetime," *Phys. Lett. B*, vol. 701, no. 3, pp. 285–290, Jul. 2011.

[22] T. Harada and M. Kimura, "Black holes as particle accelerators: a brief review," *Class. Quant. Grav.*, vol. 31, no. 24, p. 243001, Dec. 2014.

[23] S. G. Ghosh, P. Sheoran, and M. Amir, "Rotating Ayón-Beato-García black hole as a particle accelerator," *Phys. Rev. D*, vol. 90, no. 10, p. 103006, Nov. 2014.

[24] M. Amir and S. G. Ghosh, "Rotating Hayward's regular black hole as particle accelerator," *Journal of High Energy Physics*, vol. 2015, p. 15, Jul. 2015.

[25] A. Naveena Kumara, C. L. A. Rizwan, K. Hegde, M. S. Ali, and K. M. Ajith, "Rotating 4D Gauss-Bonnet black hole as a particle accelerator," *Annals of Physics*, vol. 434, p. 168599, Nov. 2021.

[26] G. Z. Babar, F. Atamurotov, S. Ul Islam, and S. G. Ghosh, "Particle acceleration around rotating Einstein-Born-Infeld black hole and plasma effect on gravitational lensing," *Phys. Rev. D*, vol. 103, no. 8, p. 084057, Apr. 2021.

[27] F. Hejda, J. Bičák, and O. B. Zaslavskii, "Extraction of energy from an extremal rotating electrovacuum black hole: Particle collisions along the axis of symmetry," *Phys. Rev. D*, vol. 100, no. 6, p. 064041, Sep. 2019.

[28] K. Karshiboev, F. Atamurotov, A. Övgün, A. Abdujabbarov, and E. Karimbaev, "Particle dynamics and thermodynamical analysis of the rotating ModMax black holes," *New Astronomy*, vol. 109, p. 102200, Jul. 2024.

[29] A. Nosirov, F. Atamurotov, G. Rakhimova, and A. Abdujabbarov, "Particle acceleration and thermodynamics of the rotating Simpson-Visser black hole," *Eur. Phys. J. Plus*, vol. 138, no. 9, p. 846, Sep. 2023.

[30] O. B. Zaslavskii, "Schwarzschild black hole as particle accelerator of spinning particles," *EPL (Europhysics Letters)*, vol. 114, no. 3, p. 30003, May 2016.

[31] S. Fernando, "Spinning dilaton black hole in 2 + 1 dimensions as a particle accelerator," *Mod. Phys. Lett. A*, vol. 32, no. 13, p. 1750074, Apr. 2017.

[32] J. An, "Naked Singularity as Accelerator for Spinning Particle," *arXiv e-prints*, p. arXiv:1710.09880, Oct. 2017.

[33] F. Atamurotov, S. Shaymatov, P. Sheoran, and S. Siwach, "Charged black hole in 4D Einstein-Gauss-Bonnet gravity: Particle motion, plasma effect on weak gravitational lensing and centre-of-mass energy," *J. Cosmol. A. P.*, vol. 2021, no. 08, p. 045, 2021.

[34] U. Papnoi and F. Atamurotov, "Rotating charged black hole in 4 D Einstein-Gauss-Bonnet gravity: Photon motion and its shadow," *Phys. Dark Univ.*, vol. 35, p. 100916, Mar. 2022.

[35] M. Gürses, T. ç. Şişman, and B. Tekin, "Comment on "Einstein-Gauss-Bonnet Gravity in Four-Dimensional Spacetime"," *Phys. Rev. Lett.*, vol. 125, no. 14, p. 149001, Oct. 2020.

[36] P. Cañate and S. E. P. Bergliaffa, "Novel exact magnetic black hole solution in four-dimensional extended scalar-tensor-Gauss-Bonnet theory," *Phys. Rev. D*, vol. 102, no. 10, p. 104038, Nov. 2020.

[37] P. Cañate, J. Sultana, and D. Kazanas, "Gravitational analog of the canonical acoustic black hole in Einstein–scalar–Gauss–Bonnet theory," *Classical and Quantum Gravity*, vol. 38, no. 12, p. 125002, Jun. 2021.

[38] D. Glavan and C. Lin, "Einstein-Gauss-Bonnet Gravity in Four-Dimensional Spacetime," *Phys. Rev. Lett.*, vol. 124, no. 8, p. 081301, Feb. 2020.

[39] R. A. Konoplya and A. F. Zinhailo, "Quasinormal modes, stability and shadows of a black hole in the 4D Einstein-Gauss-Bonnet gravity," *Eur. Phys. J. C*, vol. 80, no. 11, p. 1049, Nov. 2020.

[40] M. Guo and P.-C. Li, "The innermost stable circular orbit and shadow in the novel $4D$ Einstein-Gauss-Bonnet gravity," *arXiv e-prints*, p. arXiv:2003.02523, Mar. 2020.

[41] P. G. S. Fernandes, "Charged black holes in AdS spaces in 4D Einstein Gauss-Bonnet gravity," *Phys. Lett. B*, vol. 805, p. 135468, Jun. 2020.

[42] S.-W. Wei and Y.-X. Liu, "Testing the nature of Gauss-Bonnet gravity by four-dimensional rotating black hole shadow," *European Physical Journal Plus*, vol. 136, no. 4, p. 436, Apr. 2021.

[43] D. D. Doneva and S. S. Yazadjiev, "Relativistic stars in 4D Einstein-Gauss-Bonnet gravity," *JCAP*, vol. 2021, no. 5, p. 024, May 2021.

[44] S. G. Ghosh and S. D. Maharaj, "Radiating black holes in the novel 4D Einstein-Gauss-Bonnet gravity," *Phys. Dark Univ.*, vol. 30, p. 100687, Dec. 2020.

[45] S. G. Ghosh, D. V. Singh, R. Kumar, and S. D. Maharaj, "Phase transition of AdS black holes in 4D EGB gravity coupled to nonlinear electrodynamics," *Annals of Physics*, vol. 424, p. 168347, Jan. 2021.

[46] R. Kumar, S. U. Islam, and S. G. Ghosh, "Gravitational lensing by charged black hole in regularized 4D Einstein-Gauss-Bonnet gravity," *Eur. Phys. J. C*, vol. 80, no. 12, p. 1128, Dec. 2020.

[47] S. G. Ghosh, A. Kumar, and D. V. Singh, "Anti-de Sitter Hayward black holes in Einstein-Gauss-Bonnet gravity," *Phys. Dark Univ.*, vol. 30, p. 100660, Dec. 2020.

[48] R. Kumar and S. G. Ghosh, "Rotating black holes in 4D Einstein-Gauss-Bonnet gravity and its shadow," *JCAP*, vol. 2020, no. 7, p. 053, Jul. 2020.

[49] M. Azreg-Aïnou, "Generating rotating regular black hole solutions without complexification," *Phys. Rev. D*, vol. 90, no. 6, p. 064041, Sep. 2014.

[50] ——, "From static to rotating to conformal static solutions: rotating imperfect fluid wormholes with(out) electric or magnetic field," *Eur. Phys. J. C*, vol. 74, p. 2865, May 2014.

[51] R. P. Kerr, "Gravitational field of a spinning mass as an example of algebraically special metrics," *Phys. Rev. Lett.*, vol. 11, pp. 237–238, 1963.

[52] R. M. Wald, "The Thermodynamics of Black Holes," *Living.Rev.Rel.*, vol. 4, no. 1, p. 6, Jul. 2001.

[53] W. Israel, "Event Horizons in Static Vacuum Space-Times," *Phys. Rev.*, vol. 164, pp. 1776–1779, Dec. 1967.

[54] S. W. Hawking, "Particle creation by black holes," *Commun. Math. Phys*, vol. 43, no. 3, pp. 199–220, Aug. 1975.

[55] J. D. Bekenstein, "Black Holes and Entropy," *Phys. Rev. D*, vol. 7, no. 8, pp. 2333–2346, Apr. 1973.

[56] K. Murata and J. Soda, "Hawking radiation from rotating black holes and gravitational anomalies," , vol. 74, no. 4, p. 044018, Aug. 2006.

[57] S. H. Hendi, S. Hajkhalili, M. Jamil, and M. Momennia, "Stability and phase transition of rotating Kaluza-Klein black holes," *Eur. Phys. J. C*, vol. 81, no. 12, p. 1112, Dec. 2021.

[58] S. Mahapatra and I. Banerjee, "Rotating hairy black holes and thermodynamics from gravitational decoupling," *Phys. Dark Univ.*, vol. 39, p. 101172, Feb. 2023.

[59] F. W. Dyson, A. S. Eddington, and C. Davidson, "A Determination of the Deflection of Light by the Sun's Gravitational Field, from Observations Made at the Total Eclipse of May 29, 1919," *Philosophical Transactions of the Royal Society of London Series A*, vol. 220, pp. 291–333, Jan. 1920.

[60] B. Patla and R. J. Nemiroff, "Gravitational Lensing Characteristics of the Transparent Sun," *Astrophys. J*, vol. 685, no. 2, pp. 1297–1303, Oct. 2008.

[61] A. Einstein, "Zur allgemeinen Relativitätstheorie," *Sitzungsberichte der Königlich Preussischen Akademie der Wissenschaften*, pp. 778–786, Jan. 1915.

[62] C. M. Will, "The Confrontation between General Relativity and Experiment," *Living Reviews in Relativity*, vol. 9, no. 1, p. 3, Mar. 2006.

[63] B. P. Abbott, LIGO Scientific Collaboration, and Virgo Collaboration, "Observation of Gravitational Waves from a Binary Black Hole Merger," *Phys. Rev. Lett.*, vol. 116, no. 6, p. 061102, Feb. 2016.

[64] K. Akiyama and et al. (Event Horizon Telescope Collaboration), "First M87 Event Horizon Telescope Results. I. The Shadow of the Supermassive Black Hole," *Astrophys. J.*, vol. 875, no. 1, p. L1, Apr 2019.

[65] K. Akiyama and et al., "First Sagittarius A* Event Horizon Telescope Results. I. The Shadow of the Supermassive Black Hole in the Center of the Milky Way," *Astrophys. J. Lett*, vol. 930, no. 2, p. L12, May 2022.

[66] C. Bambi, "Testing the space-time geometry around black hole candidates with the analysis of the broad Kα iron line," *Phys. Rev. D*, vol. 87, no. 2, p. 023007, Jan. 2013.

[67] Z. Li, L. Kong, and C. Bambi, "Testing the Nature of the Supermassive Black Hole Candidate in SgrA* with Light Curves and Images of Hot Spots," *The Astrophysical Journal*, vol. 787, no. 2, p. 152, Jun. 2014.

[68] T. Johannsen and D. Psaltis, "Testing the No-hair Theorem with Observations in the Electromagnetic Spectrum. I. Properties of a Quasi-Kerr Spacetime," *The Astrophysical Journal*, vol. 716, no. 1, pp. 187–197, Jun. 2010.

[69] ——, "Testing the No-hair Theorem with Observations in the Electromagnetic Spectrum. II. Black Hole Images," *The Astrophysical Journal*, vol. 718, no. 1, pp. 446–454, Jul. 2010.

[70] A. Simpson and M. Visser, "Astrophysically viable Kerr-like spacetime – into the eye of the storm," *arXiv e-prints*, p. arXiv:2112.04647, Dec. 2021.

[71] F. Sarikulov, F. Atamurotov, A. Abdujabbarov, and B. Ahmedov, "Shadow of the Kerr-like black hole," *Eur. Phys. J. C*, vol. 82, no. 9, p. 771, Sep. 2022.

[72] A. Simpson and M. Visser, "Regular Black Holes with Asymptotically Minkowski Cores," *Universe*, vol. 6, no. 1, p. 8, Dec. 2019.

[73] T. Berry, A. Simpson, and M. Visser, "Photon Spheres, ISCOs, and OSCOs: Astrophysical Observables for Regular Black Holes with Asymptotically Minkowski Cores," *Universe*, vol. 7, no. 1, p. 2, Dec. 2020.

[74] F. Atamurotov, F. Sarikulov, V. Khamidov, and A. Abdujabbarov, "Gravitational weak lensing of Schwarzschild-like black hole in presence of plasma," *European Physical Journal Plus*, vol. 137, p. 567, May 2022.

[75] M. Bañados, J. Silk, and S. M. West, "Kerr Black Holes as Particle Accelerators to Arbitrarily High Energy," *Physical Review Letters*, vol. 103, no. 11, p. 111102, Sep. 2009.

[76] A. Jawad, F. Ali, M. Jamil, and U. Debnath, "Dynamics of Particles Around a Regular Black Hole with Nonlinear Electrodynamics," *Communications in Theoretical Physics*, vol. 66, no. 5, p. 509, Nov. 2016.

[77] S. Hussain and M. Jamil, "Timelike geodesics of a modified gravity black hole immersed in an axially symmetric magnetic field," *Phys. Rev. D*, vol. 92, no. 4, p. 043008, Aug. 2015.

[78] G. Z. Babar, M. Jamil, and Y.-K. Lim, "Dynamics of a charged particle around a weakly magnetized naked singularity," *International Journal of Modern Physics D*, vol. 25, no. 2, p. 1650024, Dec. 2016.

[79] A. Zakria and M. Jamil, "Center of mass energy of the collision for two general geodesic particles around a Kerr-Newman-Taub-NUT black hole," *Journal of High Energy Physics*, vol. 2015, p. 147, May 2015.

[80] I. Brevik and M. Jamil, "Black holes in the turbulence phase of viscous rip cosmology," *International Journal of Geometric Methods in Modern Physics*, vol. 16, no. 2, p. 1950030, Jan. 2019.

[81] S. Chen, M. Wang, and J. Jing, "Chaotic motion of particles in the accelerating and rotating black holes spacetime," *Journal of High Energy Physics*, vol. 2016, no. 9, p. 82, Sep. 2016.

[82] K. Hashimoto and N. Tanahashi, "Universality in chaos of particle motion near black hole horizon," *Phys. rev. D*, vol. 95, no. 2, p. 024007, Jan. 2017.

[83] W. Han, "Chaos and dynamics of spinning particles in Kerr spacetime," *General Relativity and Gravitation*, vol. 40, no. 9, pp. 1831–1847, Sep. 2008.

[84] R. M. Wald, "Black hole in a uniform magnetic field," *Phys. Rev. D.*, vol. 10, pp. 1680–1685, Sep. 1974.

[85] A. N. Aliev and N. Özdemir, "Motion of charged particles around a rotating black hole in a magnetic field," *Mon. Not. R. Astron. Soc.*, vol. 336, pp. 241–248, Oct. 2002.

[86] Z. Stuchlík, J. Schee, and A. Abdujabbarov, "Ultra-high-energy collisions of particles in the field of near-extreme Kehagias-Sfetsos naked singularities and their appearance to distant observers," *Phys. Rev. D*, vol. 89, no. 10, p. 104048, May 2014.

[87] A. Abdujabbarov and B. Ahmedov, "Test particle motion around a black hole in a braneworld," *Phys. Rev. D*, vol. 81, no. 4, p. 044022, Feb. 2010.

[88] A. Abdujabbarov, B. Ahmedov, and A. Hakimov, "Particle motion around black hole in Hořava-Lifshitz gravity," *Phys.Rev. D*, vol. 83, no. 4, p. 044053, Feb. 2011.

[89] A. A. Abdujabbarov, B. J. Ahmedov, S. R. Shaymatov, and A. S. Rakhmatov, "Penrose process in Kerr-Taub-NUT spacetime," *Astrophys Space Sci*, vol. 334, pp. 237–241, Aug. 2011.

[90] Z. Stuchlík and M. Kološ, "Acceleration of the charged particles due to chaotic scattering in the combined black hole gravitational field and asymptotically uniform magnetic field," *European Physical Journal C*, vol. 76, p. 32, Jan. 2016.

[91] J. Kovář, O. Kopáček, V. Karas, and Z. Stuchlík, "Off-equatorial orbits in strong gravitational fields near compact objects II: halo motion around magnetic compact stars and magnetized black holes," *Classical and Quantum Gravity*, vol. 27, no. 13, p. 135006, Jul. 2010.

[92] J. Kovář, P. Slaný, C. Cremaschini, Z. Stuchlík, V. Karas, and A. Trova, "Electrically charged matter in rigid rotation around magnetized black hole," *Phys. Rev. D*, vol. 90, no. 4, p. 044029, Aug. 2014.

[93] F. de Felice and F. Sorge, "Magnetized orbits around a Schwarzschild black hole," *Classical and Quantum Gravity*, vol. 20, pp. 469–481, Feb. 2003.

[94] F. de Felice, F. Sorge, and S. Zilio, "Magnetized orbits around a Kerr black hole," *Classical and Quantum Gravity*, vol. 21, pp. 961–973, Feb. 2004.

[95] J. Rayimbaev, A. Abdujabbarov, M. Jamil, and W.-B. Han, "Dynamics of magnetized particles around Einstein-Æther black hole with uniform magnetic field," *Nuclear Physics B*, vol. 966, p. 115364, May 2021.

[96] A. Abdujabbarov, J. Rayimbaev, B. Turimov, and F. Atamurotov, "Dynamics of magnetized particles around 4-D Einstein Gauss-Bonnet black hole," *Physics of the Dark Universe*, vol. 30, p. 100715, Dec. 2020.

[97] B. Narzilloev, J. Rayimbaev, S. Shaymatov, A. Abdujabbarov, B. Ahmedov, and C. Bambi, "Can the dynamics of test particles around charged stringy black holes mimic the spin of Kerr black holes?" *Physical Review D*, vol. 102, no. 4, p. 044013, Aug. 2020.

[98] J. Vrba, A. Abdujabbarov, M. Kološ, B. Ahmedov, Z. Stuchlík, and J. Rayimbaev, "Charged and magnetized particles motion in the field of generic singular black holes governed by general relativity coupled to nonlinear electrodynamics," *Phys.Rev.D*, vol. 101, no. 12, p. 124039, Jun. 2020.

[99] O. B. Zaslavskii, "Acceleration of particles as a universal property of rotating black holes," *Phys. Rev. D*, vol. 82, no. 8, p. 083004, Oct. 2010.

[100] ——, "Energetics of particle collisions near dirty rotating extremal black holes: Banados-Silk-West effect versus Penrose process," *Phys. Rev. D*, vol. 86, no. 8, p. 084030, Oct. 2012.

[101] ——, "Acceleration of particles near the inner black hole horizon," *Phys. Rev. D*, vol. 85, no. 2, p. 024029, Jan. 2012.

[102] G. Z. Babar, F. Atamurotov, S. Ul Islam, and S. G. Ghosh, "Particle acceleration around rotating einstein-born-infeld black hole and plasma effect on gravitational lensing," *Phys. Rev. D*, vol. 103, p. 084057, Apr 2021. [Online]. Available: https://link.aps.org/doi/10.1103/PhysRevD.103.084057

[103] A. Tursunov, M. Kološ, A. Abdujabbarov, B. Ahmedov, and Z. Stuchlík, "Acceleration of particles in spacetimes of black string," *Phys. Rev. D*, vol. 88, no. 12, p. 124001, Dec. 2013.

[104] A. Abdujabbarov, F. Atamurotov, N. Dadhich, B. Ahmedov, and Z. Stuchlik, "Energetics and optical properties of 6-dimensional rotating black hole in pure Gauss-Bonnet gravity," *Eur. Phys. J. C*, vol. 75, no. 8, p. 399, 2015.

[105] V. P. Frolov and A. A. Shoom, "Motion of charged particles near a weakly magnetized Schwarzschild black hole," *Phys. Rev. D.*, vol. 82, no. 8, p. 084034, Oct. 2010.

[106] V. P. Frolov, "Weakly magnetized black holes as particle accelerators," *Phys. Rev. D.*, vol. 85, no. 2, p. 024020, Jan. 2012.

[107] A. Tursunov, M. Kološ, Z. Stuchlík, and D. V. Gal'tsov, "Radiation Reaction of Charged Particles Orbiting a Magnetized Schwarzschild Black Hole," *Astrophys. J*, vol. 861, no. 1, p. 2, Jul. 2018.

[108] A. Tursunov, B. Juraev, Z. Stuchlík, and M. Kološ, "Electric Penrose process: High-energy acceleration of ionized particles by nonrotating weakly charged black hole," *Phys. Rev. D*, vol. 104, no. 8, p. 084099, Oct. 2021.

[109] N. Dadhich, A. Tursunov, B. Ahmedov, and Z. Stuchlík, "The distinguishing signature of magnetic Penrose process," *Mon. Not. R. Astron. Soc*, vol. 478, no. 1, pp. L89–L94, Jul. 2018.

[110] S. W. Hawking, "Black holes in general relativity," *Commun. Math. Phys*, vol. 25, no. 2, pp. 152–166, Jun. 1972.

[111] J. M. Bardeen, B. Carter, and S. W. Hawking, "The four laws of black hole mechanics," *Commun. Math. Phys*, vol. 31, no. 2, pp. 161–170, Jun. 1973.

[112] S. W. Hawking, "Particle creation by black holes," *Commun. Math. Phys*, vol. 46, no. 2, pp. 206–206, Jun. 1976.

[113] M. R. R. Good and Y. C. Ong, "Particle spectrum of the Reissner-Nordström black hole," *Eur. Phys. J. C*, vol. 80, no. 12, p. 1169, Dec. 2020.

[114] Y. S. Myung, Y.-W. Kim, and Y.-J. Park, "Thermodynamics of regular black hole," *General Relativity and Gravitation*, vol. 41, no. 5, pp. 1051–1067, May 2009.

[115] K. Ghaderi and B. Malakolkalami, "Effects of quintessence on thermodynamics of the black holes," *Astrophys. Space. Sci.*, vol. 361, no. 5, p. 161, May 2016.

[116] M. B. Jahani Poshteh and R. B. Mann, "Thermodynamics of z =4 Hořava-Lifshitz black holes," *Phys. Rev. D*, vol. 103, no. 10, p. 104024, May 2021.

[117] R.-G. Cai, L.-M. Cao, and N. Ohta, "Thermodynamics of black holes in Hořava-Lifshitz gravity," *Phys. Lett. B*, vol. 679, no. 5, pp. 504–509, Sep. 2009.

[118] A. Ditta, X. Tiecheng, G. Mustafa, M. Yasir, and F. Atamurotov, "Thermal stability with emission energy and Joule-Thomson expansion of regular BTZ-like black hole," *Eur. Phys. J. C*, vol. 82, no. 8, p. 756, Aug. 2022.

[119] A. Fatima and K. Saifullah, "Thermodynamics of charged and rotating black strings," *Astrophys. Space. Sci.*, vol. 341, no. 2, pp. 437–443, Oct. 2012.

[120] D. V. Singh, S. Upadhyay, and M. S. Ali, "Rotating Lee-Wick black hole and thermodynamics," *International Journal of Modern Physics A*, vol. 37, no. 9, p. 2250049, Mar. 2022.

[121] G. Bertone and D. Hooper, "History of dark matter," *Reviews of Modern Physics*, vol. 90, no. 4, p. 045002, Oct. 2018.

[122] D. Huterer and D. L. Shafer, "Dark energy two decades after: observables, probes, consistency tests," *Reports on Progress in Physics*, vol. 81, no. 1, p. 016901, Jan. 2018.

[123] V. C. Rubin, J. Ford, W. K., and N. Thonnard, "Rotational properties of 21 SC galaxies with a large range of luminosities and radii, from NGC 4605 (R=4kpc) to UGC 2885 (R=122kpc)." *Astrophys. J.*, vol. 238, pp. 471–487, Jun. 1980.

[124] V. V. Kiselev, "Quintessence and black holes," *Classical and Quantum Gravity*, vol. 20, no. 6, pp. 1187–1197, Mar. 2003.

[125] Y. Zhang and Y. X. Gui, "Quasinormal modes of gravitational perturbation around a Schwarzschild black hole surrounded by quintessence," *Classical and Quantum Gravity*, vol. 23, no. 22, pp. 6141–6147, Nov. 2006.

[126] B. Toshmatov, Z. Stuchlík, and B. Ahmedov, "Rotating black hole solutions with quintessential energy," *European Physical Journal Plus*, vol. 132, no. 2, p. 98, Feb. 2017.

[127] S. Shaymatov, B. Ahmedov, Z. Stuchlík, and A. Abdujabbarov, "Effect of an external magnetic field on particle acceleration by a rotating black hole surrounded with quintessential energy," *International Journal of Modern Physics D*, vol. 27, no. 8, p. 1850088, Jan. 2018.

[128] K. Jusufi, M. Jamil, P. Salucci, T. Zhu, and S. Haroon, "Black hole surrounded by a dark matter halo in the M87 galactic center and its identification with shadow images," *Phys. Rev. D*, vol. 100, no. 4, p. 044012, Aug. 2019.

[129] R. G. Daghigh and G. Kunstatter, "The effect of dark matter spikes on galactic black hole ringdown waveforms and shadows," *arXiv preprint arXiv:2308.15682*, 2023.

[130] R. C. Pantig and A. Övgün, "Black hole in quantum wave dark matter," *Fortschritte der Physik*, vol. 71, no. 1, p. 2200164, 2023.

[131] D. Liu, Y. Yang, A. Övgün, Z.-W. Long, and Z. Xu, "Gravitational ringing and superradiant instabilities of the kerr-like black holes in a dark matter halo," *The European Physical Journal C*, vol. 83, no. 7, p. 565, 2023.

[132] R. C. Pantig and A. Övgün, "Dark matter effect on the weak deflection angle by black holes at the center of milky way and m87 galaxies," *The European Physical Journal C*, vol. 82, no. 5, p. 391, 2022.

[133] A. Övgün, "Evolving topologically deformed wormholes supported in the dark matter halo," *The European Physical Journal Plus*, vol. 136, no. 10, pp. 1–11, 2021.

[134] R. C. Pantig and A. Övgün, "Dehnen halo effect on a black hole in an ultra-faint dwarf galaxy," *Journal of Cosmology and Astroparticle Physics*, vol. 2022, no. 08, p. 056, 2022.

[135] R. G. Daghigh and G. Kunstatter, "Spacetime metrics and ringdown waveforms for galactic black holes surrounded by a dark matter spike," *The Astrophysical Journal*, vol. 940, no. 1, p. 33, 2022.

[136] M. Sharif and F. Javed, "Dynamics of the scalar shell in higher dimensions," *Annals of Physics*, vol. 416, p. 168146, 2020.

[137] ——, "Dynamical stability of gravastars covered with abg black holes," *Journal of Experimental and Theoretical Physics*, vol. 133, no. 4, pp. 439–448, 2021.

[138] F. Javed, "Stability and dynamics of scalar field thin-shell for renormalization group improved schwarzschild black holes," *The European Physical Journal C*, vol. 83, no. 6, p. 513, 2023.

[139] F. Javed, G. Mustafa, and A. Övgün, "Effect of scalar field on dynamical evolution of thin-shell with hairy schwarzschild black hole," *The European Physical Journal Plus*, vol. 138, no. 8, p. 706, 2023.

[140] F. Javed, A. Waseem, and B. Almutairi, "Quantum corrected charged thin-shell wormholes surrounded by quintessence," *The European Physical Journal C*, vol. 83, no. 9, p. 811, 2023.

[141] F. Javed, "Computational analysis of thin-shell with scalar field for class of new black hole solutions in metric-affine gravity," *Annals of Physics*, p. 169464, 2023.

[142] S. W. Hawking, "Black hole explosions?" *Nature*, vol. 248, no. 5443, pp. 30–31, Mar. 1974.

[143] F. Javed, G. Mustafa, S. Mumtaz, and F. Atamurotov, "Thermal analysis with emission energy of perturbed black hole in f (q) gravity," *Nuclear Physics B*, vol. 990, p. 116180, 2023.

[144] F. Javed, G. Fatima, S. Sadiq, and G. Mustafa, "Thermodynamics of charged black hole in symmetric teleparallel gravity," *Fortschritte der Physik*, p. 2200214, 2023.

[145] M. Yasir, X. Tiecheng, A. Ditta, R. Ali, and F. Atamurotov, "Thermodynamical analysis of acoustic Schwarzschild black hole," *New Astronomy*, vol. 105, p. 102106, Jan. 2024.

[146] A. Ditta, X. Tiecheng, R. Ali, F. Atamurotov, A. Mahmood, and S. Mumtaz, "Thermodynamic stability of the regular charged torus-like black hole," *Annals of Physics*, vol. 453, p. 169326, Jun. 2023.

[147] F. Javed, A. Basit, A. Caliskan, and E. Gudekli, "Thermal fluctuations, qnms and emission energy of charged-ads black hole with nonlinear electrodynamic," *Frontiers in Astronomy and Space Sciences*, vol. 10, p. 1174029.

[148] M. Yasir, X. Tiecheng, F. Javed, and G. Mustafa, "Thermal analysis and joule-thomson expansion of black hole exhibiting metric-affine gravity," *arXiv preprint arXiv:2305.13709*, 2023.

[149] A. Ditta, F. Javed, S. K. Maurya, and D. G. Mustafa, "Thermal stability and effects of thermal fluctuations on the static and spherically symmetric hairy black hole by gravitational decoupling," *Available at SSRN 4493573*.

[150] F. Atamurotov, U. Papnoi, and K. Jusufi, "Shadow and deflection angle of charged rotating black hole surrounded by perfect fluid dark matter," *Classical and Quantum Gravity*, vol. 39, no. 2, p. 025014, Jan. 2022.

[151] A. Das, A. Saha, and S. Gangopadhyay, "Investigation of circular geodesics in a rotating charged black hole in the presence of perfect fluid dark matter," *Classical and Quantum Gravity*, vol. 38, no. 6, p. 065015, Mar. 2021.

[152] M. Bañados, J. Silk, and S. M. West, "Kerr Black Holes as Particle Accelerators to Arbitrarily High Energy," *Phys. Rev. Lett*, vol. 103, no. 11, p. 111102, Sep. 2009.

[153] M. Sharif and A. G., "Phantom Energy Accretion by a Stringy Charged Black Hole," *Chinese Physics Letters*, vol. 29, no. 1, p. 010401, Jan. 2012.

[154] B. Pourhassan, K. Kokabi, and Z. Sabery, "Higher order corrected thermodynamics and statistics of Kerr-Newman-Gödel black hole," *Annals of Physics*, vol. 399, pp. 181–192, Dec. 2018.

[155] S. Gunasekaran, D. Kubizňák, and R. B. Mann, "Extended phase space thermodynamics for charged and rotating black holes and born-infeld vacuum polarization," *Journal of High Energy Physics*, vol. 2012, no. 11, pp. 1–43, 2012.

[156] A. Jawad and M. U. Shahzad, "Effects of thermal fluctuations on non-minimal regular magnetic black hole," *European Physical Journal C*, vol. 77, no. 5, p. 349, May 2017.

[157] B. Pourhassan, M. Dehghani, M. Faizal, and S. Dey, "Non-perturbative quantum corrections to a Born-Infeld black hole and its information geometry," *Classical and Quantum Gravity*, vol. 38, no. 10, p. 105001, May 2021.